cy 1

AMMRC MS 80-5

WORK-IN-PROGRESS PRESENTED AT THE ARMY SYMPOSIUM ON SOLID MECHANICS, 1980 - DESIGNING FOR EXTREMES: ENVIRONMENT, LOADING, AND STRUCTURAL BEHAVIOR

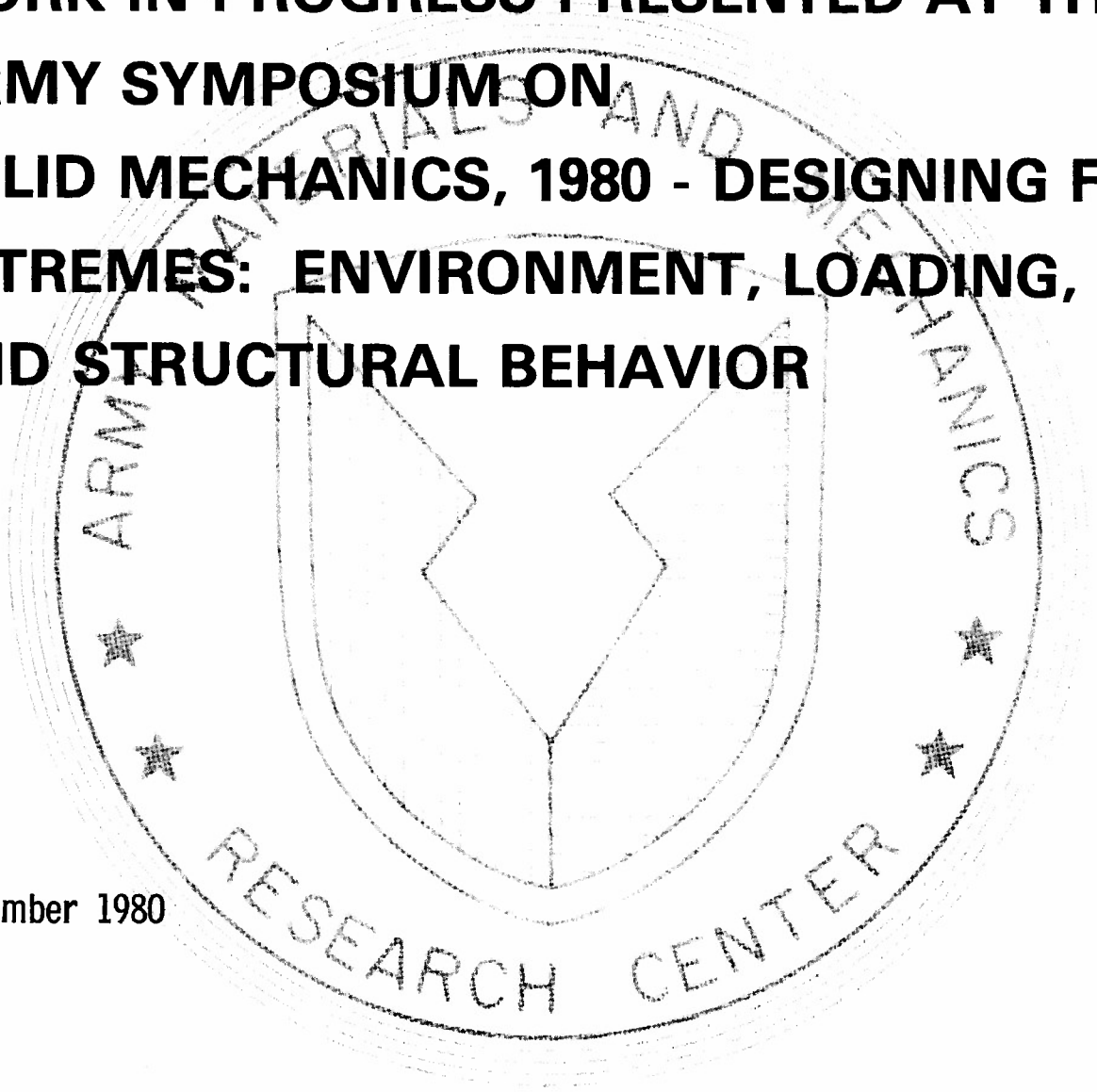

September 1980

ARMY MATERIALS AND MECHANICS RESEARCH CENTER
Watertown, Massachusetts 02172

The findings in this report are not to be construed as an official Department of the Army position, unless so designated by other authorized documents.

Mention of any trade names or manufacturers in this report shall not be construed as advertising nor as an official indorsement or approval of such products or companies by the United States Government.

DISPOSITION INSTRUCTIONS

Destroy this report when it is no longer needed.
Do not return it to the originator.

UNCLASSIFIED

SECURITY CLASSIFICATION OF THIS PAGE *(When Data Entered)*

REPORT DOCUMENTATION PAGE		READ INSTRUCTIONS BEFORE COMPLETING FORM
1. REPORT NUMBER AMMRC MS 80-5	2. GOVT ACCESSION NO.	3. RECIPIENT'S CATALOG NUMBER
4. TITLE *(and Subtitle)* Work-in-Progress presented at the Army Symposium on Solid Mechanics, 1980 - Designing for Extremes: Environment, Loading, and Structural Behavior		5. TYPE OF REPORT & PERIOD COVERED Final Report 6. PERFORMING ORG. REPORT NUMBER
7. AUTHOR*(s)*		8. CONTRACT OR GRANT NUMBER*(s)*
9. PERFORMING ORGANIZATION NAME AND ADDRESS Army Materials and Mechanics Research Center Watertown, Massachusetts 02172 DRXMR-T		10. PROGRAM ELEMENT, PROJECT, TASK AREA & WORK UNIT NUMBERS
11. CONTROLLING OFFICE NAME AND ADDRESS U. S. Army Materiel Development and Readiness Command, Alexandria, Virginia 22333		12. REPORT DATE September 1980 13. NUMBER OF PAGES 107
14. MONITORING AGENCY NAME & ADDRESS*(if different from Controlling Office)*		15. SECURITY CLASS. *(of this report)* Unclassified 15a. DECLASSIFICATION/DOWNGRADING SCHEDULE

16. DISTRIBUTION STATEMENT *(of this Report)*

Approved for public release; distribution unlimited.

17. DISTRIBUTION STATEMENT *(of the abstract entered in Block 20, if different from Report)*

18. SUPPLEMENTARY NOTES

19. KEY WORDS *(Continue on reverse side if necessary and identify by block number)*

(See Reverse Side)

20. ABSTRACT *(Continue on reverse side if necessary and identify by block number)*

Work-in-Progress presented at the Army Symposium on Solid Mechanics, 1980 - Designing for Extremes: Environment, Loading, and Structural Behavior, held at Bass River (Cape Cod), Massachusetts, 29 September through 2 October 1980.

DD FORM 1 JAN 73 1473 EDITION OF 1 NOV 65 IS OBSOLETE

UNCLASSIFIED

SECURITY CLASSIFICATION OF THIS PAGE *(When Data Entered)*

Block No. 19

KEY WORDS

Acceleration
Adhesives
Aircraft
Airframes
Aluminum Alloys
Ballistics
Ceramic Materials
Collisions
Composite Materials
Computerized Simulation
Confidence Level
Copper
Corrosion
Crack Propagation
Cracks
Crashes
Crash Resistance
Defects (Materials)
Displacements
Dynamic Response
Dynamics
Energy Absorbers
Environments
Explosives
Fabrication
Failure
Fatigue (Materials)
Fighter Aircraft
Fragmentation
Fuselages
Gunfire
Guns
Helicopters
High Temperature
Impact
Intertia
Intensity
Joining
Joints
Kinetic Energy
Landing Gear
Life (Durability)
Lightweight
Loads (Forces)
Materials
Measurement
Mechanics
Metals
Mines (Ordnance)
Models
Moisture
Nondestructive Testing
Plastic Properties
Plates
Predictions
Pressure
Probability
Projectiles
Protection
Reliability
Rotating Bands
Rotor Blades
Shaped Charges
Shear Properties
Shelters
Ships
Shock (Mechanics)
Spectra
Statistical Analysis
Strain (Mechanics)
Strain Rate
Strength (General)
Stress Corrosion
Stresses
Structural Properties
Structural Response
Structures
Survival (General)
Telemeter Systems
Temperatures
Thermal Stresses
Threats
Time Dependence
Titanium
Transients
Vibration
Vulnerability
Weapon Systems

PREFACE

This document contains extended abstracts of presentations made within the Work-In-Progress Sessions of the Army Symposium on Solid Mechanics, 1980. These sessions were comprised of a series of brief presentations and discussions of current (but not necessarily complete) research relating to the theme of the conference: "Designing for Extremes: Environment, Loading, and Structural Behavior." This meeting was held at Bass River (Cape Cod), Massachusetts on 29 September through 2 October 1980. The proceedings of this symposium and the opening session addresses presented at this meeting are published in companion documents, Army Materials and Mechanics Research Center, Manuscript Series Reports: AMMRC MS 80-4 and 80-6, dated September 1980.

We acknowledge the contributions of the authors cited in the table of contents and also the clerical staff of the Mechanics and Engineering Laboratory and the Technical Reports Office of the Army Materials and Mechanics Research Center for their unflagging efforts in the preparation and printing of numerous symposium materials.

PREVIOUS DOCUMENTS IN THIS SYMPOSIA SERIES*

Proceedings of the Army Symposium on Solid Mechanics, 1968,
AMMRC MS 68-09, September 1968, AD 675 463

Proceedings of the Army Symposium on Solid Mechanics, 1970 -
Lightweight Structures,
AMMRC MS 70-5, December 1970, AD 883 455L

Proceedings of the Army Symposium on Solid Mechanics, 1972 -
The Role of Mechanics in Design - Ballistic Problems,
AMMRC MS 73-2, September 1973, AD 772 827

Proceedings of the Army Symposium on Solid Mechanics, 1974:
The Role of Mechanics in Design - Structural Joints,
AMMRC MS 74-8, September 1974, AD 786 543

Work-In-Progress Presented at the Army Symposium on Solid Mechanics, 1974:
The Role of Mechanics in Design - Structural Joints,
AMMRC MS 74-9, September 1974, AD 786 524

Stress Analysis of Structural Joints and Interfaces -
A Selective Annotated Bibliography
by M. M. Murphy and E. M. Lenoe,
AMMRC MS 74-10, September 1974, AD 786 520

Proceedings of the Army Symposium on Solid Mechanics, 1976 -
Composite Materials: The Influence of Mechanics of Failure on Design,
AMMRC MS 76-2, September 1976, AD A029 735

Work-In-Progress Presented at the Army Symposium on Solid Mechanics, 1976 -
Composite Materials: The Influence of Mechanics of Failure on Design,
AMMRC MS 76-3, September 1976, AD A029 736

Proceedings of the Army Symposium on Solid Mechanics 1978 -
Case Studies on Structural Integrity and Reliability
AMMRC MS 78-3, September 1978, AD A059 834/2G1

Ongoing Case Studies Presented at the Army Symposium on Solid Mechanics, 1978 -
Case Studies on Structural Integrity and Reliability
AMMRC MS 78-4, September 1978, AD A059 605/6G1

* These documents may be ordered from the National Technical Information Service, U. S. Department of Commerce, Springfield, VA 22161

SYMPOSIUM COMMITTEE

E. M. LENOE, Chairman, AMMRC
J. F. MESCALL, Vice Chairman, AMMRC
R. J. MORRISSEY, Coordinator, AMMRC

TECHNICAL PAPERS AND PROGRAM

J. ADACHI, Chairman, AMMRC
F. I. BARATTA, AMMRC
L. BERKE, NASA-Lewis Research Center
C. I. CHANG, Naval Research Laboratory
H. D. CURCHACK, Harry Diamond Laboratories
G. A. DARCY, JR., AMMRC
T. S. DESISTO, AMMRC
C. M. ELDRIDGE, Army Missile Command
J. FEROLI, Army Test and Evaluation Command
G. L. FILBEY, JR., Ballistic Research Laboratories
R. FOYE, Army Aviation R&D Command
C. E. FREESE, AMMRC
J. J. GASSNER, JR., AMMRC
A. J. GUSTAFSON, Army Aviation R&D Command
G. E. MADDUX, Air Force Flight Dynamics Laboratory
J. F. MESCALL, AMMRC
D. R. MULVILLE, Naval Research Laboratory
R. P. PAPIRNO, AMMRC
E. W. ROSS, JR., Army Natick R&D Command
E. SAIBEL, Army Research Office
T. SIMKINS, Army Armament R&D Command
J. H. SMITH, National Bureau of Standards
D. M. TRACEY, AMMRC
G. WILLIAMSON, Army Construction Engineering Research Laboratory

WORK IN PROGRESS SESSION

G. E. MADDUX, Co-Chairman, Air Force Flight Dynamics Laboratory
R. P. PAPIRNO, Co-Chairman, AMMRC

CONTENTS

*Not presented orally due to time limitations.

ON DESIGN FOR 23MM HE INVULNERABILITY IN COMPOSITE HELICOPTER TAILBOOM

D. G. HARDING
Engineer

D. J. TOTO
Engineer
Boeing Vertol Company
P.O. Box 16858
Philadelphia, Pennsylvania 19142

An all-composite 23mm HE survivable airframe was designed and tested for a helicopter in the 6,000-pound gross weight class. Prior work showed the tailboom to be the largest, most critical part. Several programs have been conducted to define the failure mechanics and means of hardening conventional aluminum tailboom structures. There were also several programs involving the construction and testing of different composite tailbooms. Where these are weight competitive with aluminum structures they have proved to be vulnerable to 23mm HE hits.

The failure modes involved in metal and composites are distinctly different.

Metal booms fail from broaching of the skin by the fuse and base fragments with attendant tearing due to the forward directed blast pressure acting on this damaged area.

Composites on the other hand fail along the line of damage from the peripheral fragments then tear from this damage along the axis due to the internal blast and/or pressure so that the structure splits in two.

A series of tests were conducted on lightweight Kevlar honeycomb sandwich structures with filament wound Kevlar crack stoppers applied at intervals along the length. The tests demonstrated that the typical minimum weight structure could be protected for only 5 pounds of additional weight and small cost.

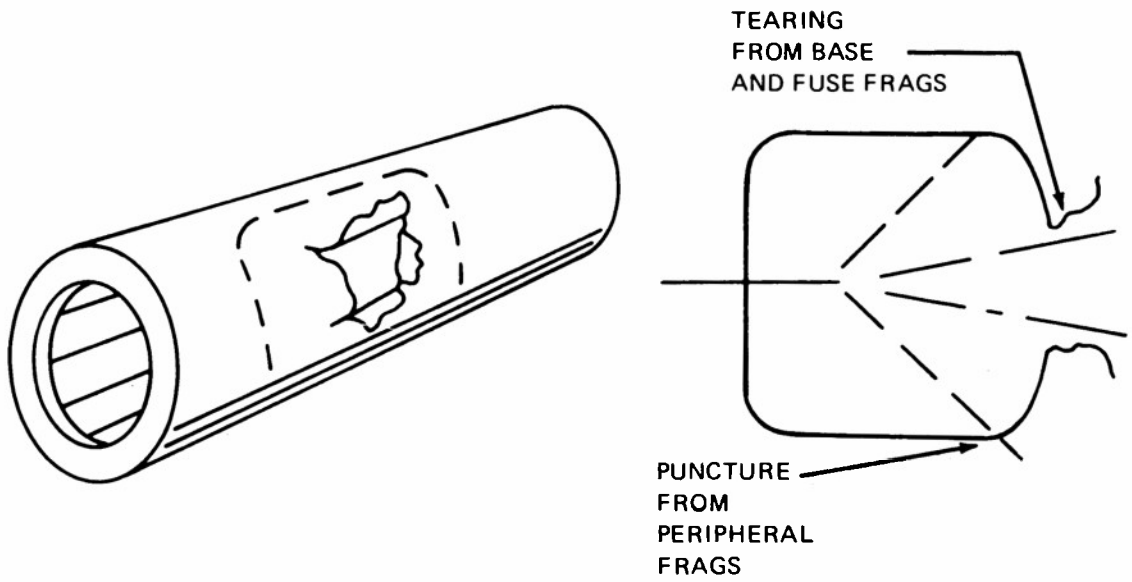

Metallic Failure Mode Due to 23mm HEI.

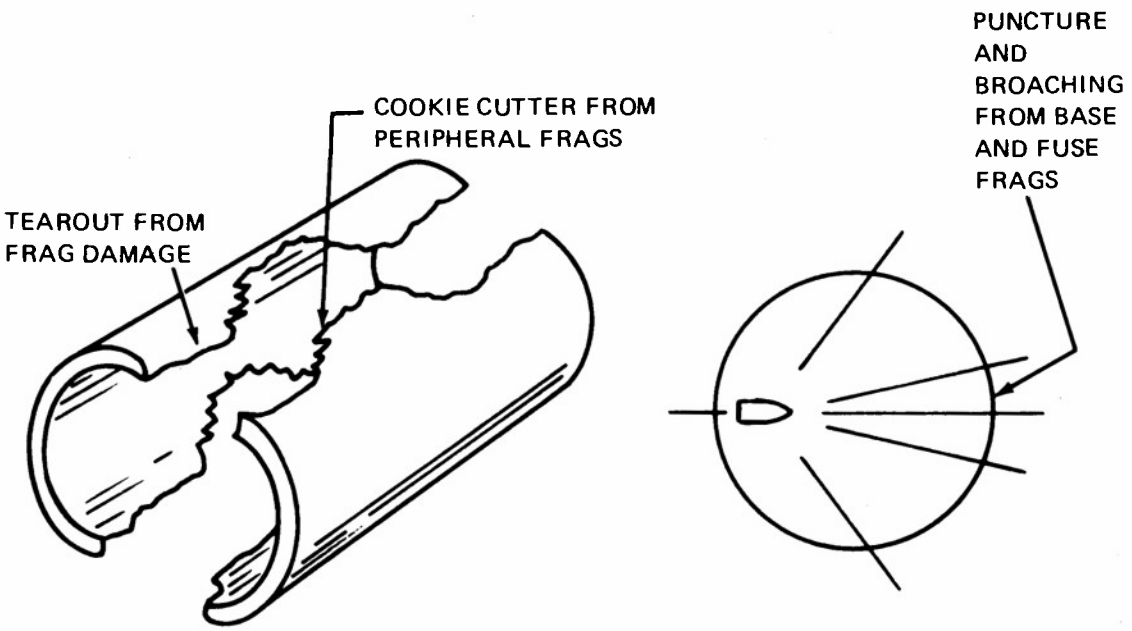

Composite Failure Mode Due to 23mm HEI Impact.

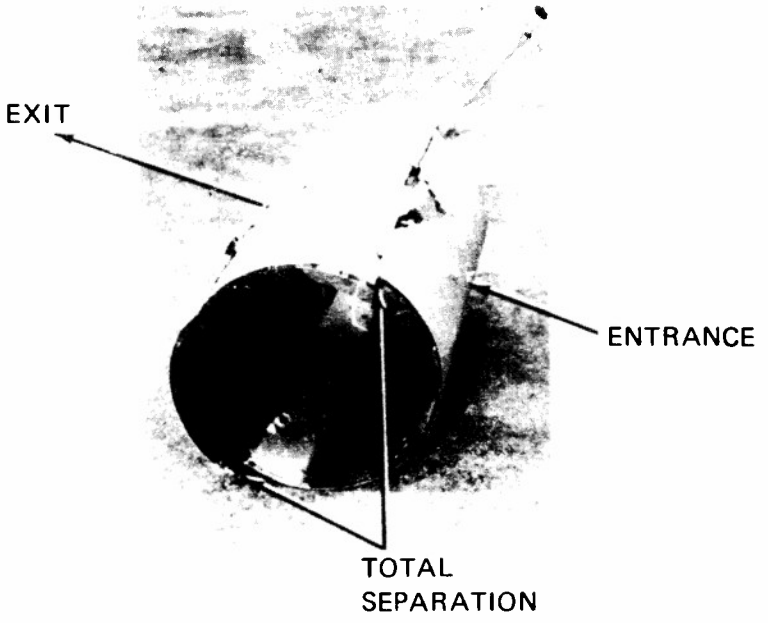

UNPROTECTED COMPOSITE
STRUCTURE 23MM HEI-T TEST

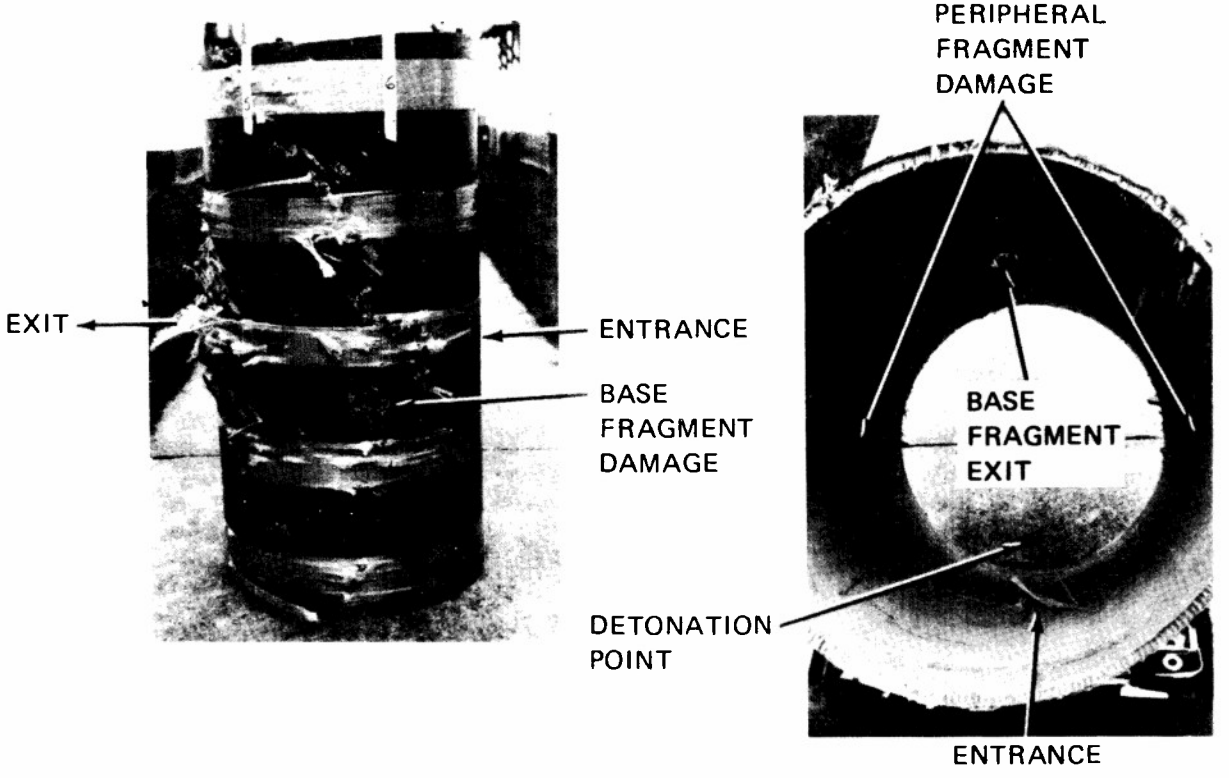

23MM Tailboom Protection Verification Test.

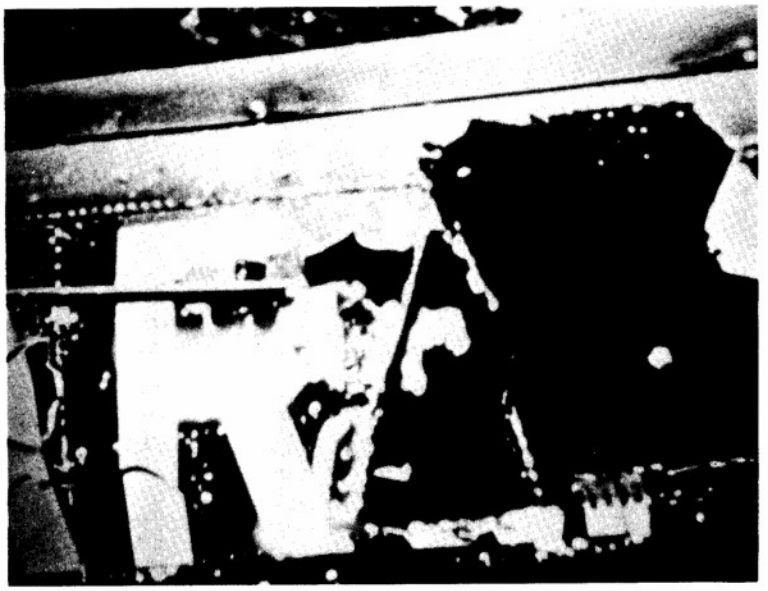

Exit Damage to Tailboom

FABRICATION METHODS AND STRENGTH DATA FOR 600°F (588°K) GRAPHITE CLOTH POLYIMIDE COMPOSITES*

C. A. Vollersen
Group Engineer
Lockheed Missiles and Space Company
P.O. Box 504
Sunnyvale, California 94086

EXTENDED ABSTRACT

The objective of this work was to develop simple, reliable methods of fabricating composite structures to be utilized at temperatures up to 600°F (588°K). The first step in this program was the creation of fabrication methods. The conventional autoclave techniques involves heating the facility gas to the highest temperature of the cure cycle. To provide simpler, safer options alternative methods were investigated. The most attractive of these involved the use of electrically heated tools. By inserting electrical resistance heaters into close tolerance holes in the tool, very accurate thermal control of the cure cycle can be exercised.

Several advantages accrue from this method. By allowing the pressurizing gas to enter at room temperature and using an insulating layer under the bag, the bag temperature can be held to less than 380°F (450°K). This is important when complex, highly curved parts are to be fabricated. Conventional bagging materials with enough elongation to accomodate radical contours are not suitable for production use at 600°F (588°K). The energy saving in not requiring a large fan to move the pressurized gas within the confines of the autoclave is significant. The thermal variance over the part is reduced since heat transfer from the resistance heaters is considerably more uniform and efficient than that from a heated gas. As a typical example of this method, a tool for fabricating test panels is shown in Fig. 1.

Cure cycle development of the material is reviewed in some detail. CELION 6000 fibers woven into 24 x 24 8HS cloth, impregnated with LARC-160 addition polimide resin, was the prepreg used. The layup of the panels and the cure cycle utilized are described. A critical consideration for this material type is the imidization temperature and successful removal of the volatiles generated during this phase. A second important element is the time at which the pressure is applied. The rationale behind the optimum choices are outlined.

Conventional glass epoxy tabs and adhesives were obviously inadequate for 600°F (588°K) testing. Thin tabs made of the same material as the panels were bonded to them using an epoxy phenolic adhesive. This was demonstrated to be entirely satisfactory for the short duration static strength tests. Modifications to the test fixtures to produce the high temperature enviornment are explained.

Test data is presented to illustrate the effect of temperature up to 600°F (588°K) on Flexural, Shear, Tension and Compression.

*This work was supported by the Missile Systems Independent Development Funding.

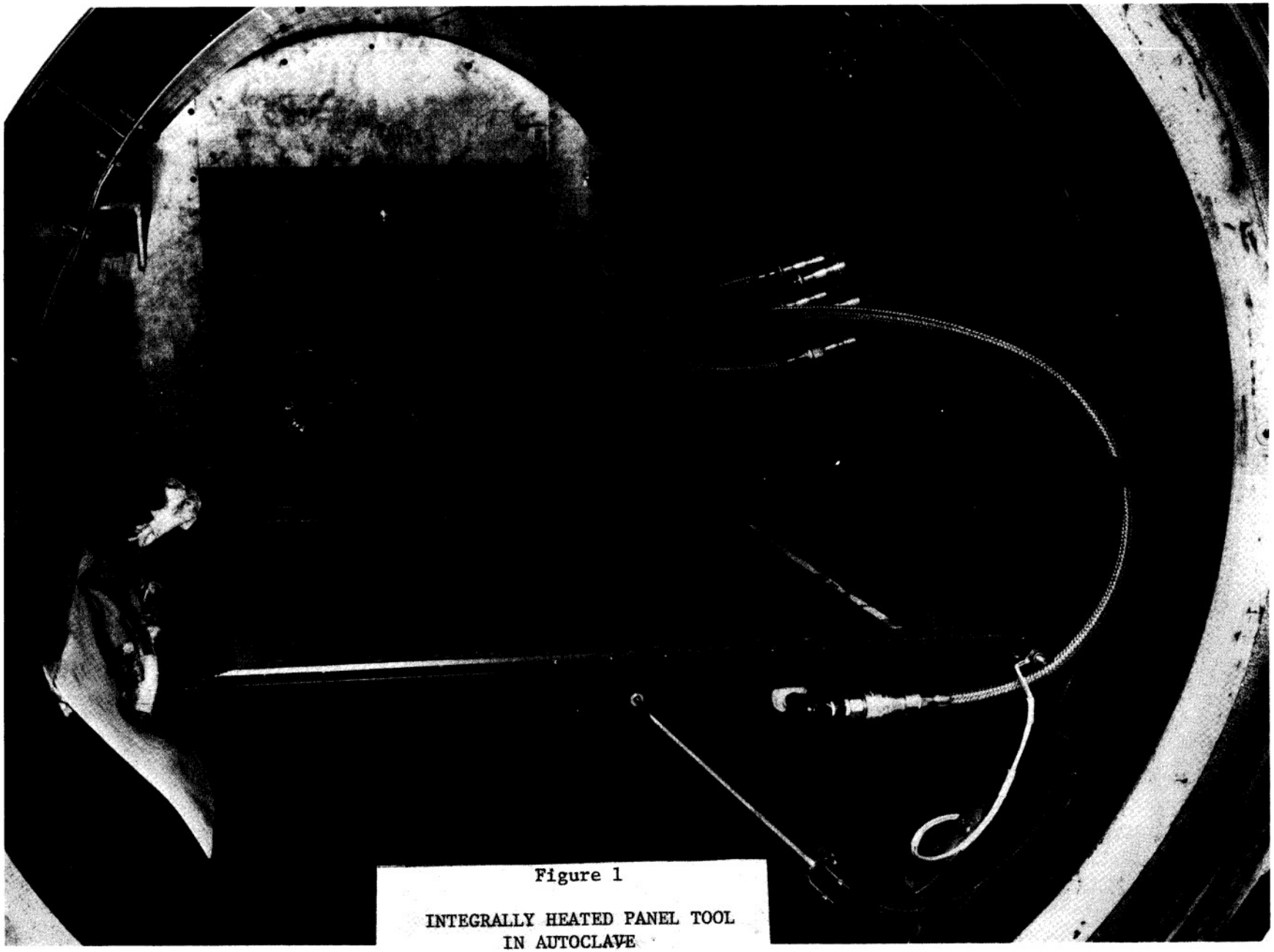

Figure 1

INTEGRALLY HEATED PANEL TOOL
IN AUTOCLAVE

LIGHTWEIGHT COMPOSITE STRUCTURES FOR THE INTERMEDIATE WATER DEPTH MINE SYSTEM

W.D. Humphrey
Program Manager IR & D
Brunswick Corporation
Lincoln, Nebraska

Ed Johnson
Senior Engineer
Naval Surface Weapons Center
White Oak, Maryland

Abstract

Trends in enemy naval capabilities have created a need for advanced mines and torpedoes. These weapon systems are volume and/or weight limited and are required to be positively buoyant in certain configurations. Launch platform restraints and delivery requirements present formidable structural problems in the design of mines and torpedo shell structures. Environments during deployment, as well as increasing depth regimes resulting from deeper operational requirements, demand that lighter, stronger structures be developed to achieve the desired system performance. Additionally, the deliverable payload, which includes warhead, electronics, sensors, power sources, and propulsion, is increasing as weapons systems become more sophisticated.

It has long been recognized that composite materials offer the potential of achieving lighter weight, hull-type structures than are possible using conventional homogeneous metals. This fact results from the ability to orient fiber reinforcement to react specific loads and from the inherently high specific properties (strength and modulus) of composite materials. Work has been in progress for approximately 12 years to design and fabricate advanced lightweight composite sandwich structures for underwater applications.

Effort is currently underway by Brunswick Corporation, Lincoln, Nebraska, under contract with the Naval Surface Weapons Center, White Oak, Maryland, to develop this technology. This effort addresses the combined effects of environment, fabrication methods, and reliability of glass epoxy sandwich cylinders for the Intermediate Water Depth Mine System.

Work to date has screened several resin systems for suitability to, and mechanical strengths for, underwater applications. Two resin systems were selected for winding with S-901 fiberglass roving and for evaluation of mechanical properties in a variety of composite specimens.

One resin system was then selected for fabricating honeycomb/composite cylinders for static and cyclic external pressure tests. Additional cylinders evaluated five different RF shielding techniques wound into a composite structure. Testing indicated that near equivalency to an all aluminum cylinder was achieved with one candidate technique.

Using these results, a full scale (21 inch diameter) component representative of a typical Intermediate Water Depth Mine was designed utilizing a unique mid-

cylinder metallic penetration. Two prototypes are currently being fabricated and will then be evaluated by NSWC and other government agencies. These tests will include electromagnetic radiation (HERO), vibration, and external pressure environments.

ON THE USE OF STATIC CONTACT LAW IN IMPACT ANALYSIS OF COMPOSITE LAMINATES

T. WANG
Graduate Assistant

C. T. SUN
Professor
School of Aeronautics and Astronautics
Purdue University
West Lafayette, Indiana 47907

ABSTRACT

Composite laminates are susceptible to damage due to impacts of foreign objects. In the case that the object is relatively rigid and small, the damage may be confined to a small area containing the contact zone. The damage obviously depends on the total force between the object and the target composite. An accurate account of the contact force is necessary in the attempts to quantify the impact damage.

Direct measurement of the dynamic contact force is not an easy task in view of the wide range of impact velocities and other parameters. The objective of this paper is to determine the law of contact statically and then use it in the dynamic impact analysis.

The law of contact between a spherical indentor and a graphite/epoxy composite laminate was established by a static indentation test. For the loading process, the contact force F is expressed in the form

$$F = k\,\alpha^{3/2} \tag{1}$$

where α is the indentation depth and k is a coefficient depending on the material properties. As a significant amount of permanent deformation would occur, the unloading process is given by

$$F = F_M \left[\frac{\alpha - \alpha_0}{\alpha_M - \alpha_0}\right]^{2.5} \tag{2}$$

where F_M is the contact force at the indentation depth α_M at which unloading begins; and α_0 is the depth of the permanent crater after the contact.

The law of contact as represented by Eqs (1) and (2), was incorporated in a beam finite element program for dynamic analyses. Such program can be used to calculate the time history of the contact force and the dynamic deformation at any point in the beam. In addition, it can be used for estimating the energy imparted from the striking sphere to the target composite as well as the energy dissipated at the impact zone.

The validity of the static law of contact as given by Eqs. (1) and (2) was examined experimentally. The response strain history at the point of a

composite beam after impact was measured and compared with the finite element solution. It is believed that if the static law of contact is adequate for dynamic impact, then the finite element account of the subsequent dynamic response should agree with the experimental result.

Beam-like specimens of width 1 in. (25.4 mm) and thickness 0.1 in. (2.54 mm) were cut from a graphite/epoxy laminate. Two types of lay-up were considered, namely $[0/\ 45/\ 0/\ -45/\ 0]_{2s}$ and $[90/\ 45/\ 90/\ -45/\ 90]_{2s}$. The projectiles were steel balls with diameters of 0.25 in. and 0.5 in., respectively. Bending strains were picked up at the point of 1.5 in. from the point of impact.

Figure 1 shows the experimental result and the finite element solution for the bending strain at 1.5 in. from the point of impact in a $[90/\ 45/\ 90/\ -45/\ 90]_{2s}$ graphite/epoxy composite beam. The impact velocity was 124.3 in./sec. (3.1 m/sec.). The 0.5 in. diameter steel ball was used. The agreement between the finite element solution and the experimental result appears to be excellent for the first 300 μ seconds before the reflected waves arrive.

Similar results for a higher impact velocity, 1194.3 in./sec. (30.34 m/sec.), are shown in Fig. 2. The steel ball used in this case has a diameter of 0.25 in. (6.35 mm). Again, the finite element solution is in excellent agreement with the experimental data. The excellent result obtained from the finite element program with the static contact law can be considered as a strong indication that the contact law established statically is suitable for dynamic impact up to a rather high impact velocity.

In the case of beams with $[0/\ 45/\ 0/\ -45/\ 0]_{2s}$ laminates, the finite element solution is not as good when compared with the experimental data as shown in Fig. 3. The discrepancy could be caused by strong plate bending effects in such specimens which have a much larger bending rigidity in the longitudinal direction than that in the transverse direction. As a result, it would take longer time for waves to propagate across the width of the specimen and make it behave like a beam. For a more accurate analysis, plate finite elements should be employed.

Acknowledgment - This research project was sponsored by National Aeronautics and Space Administration, Lewis Research Center under Grant No. NSG3185.

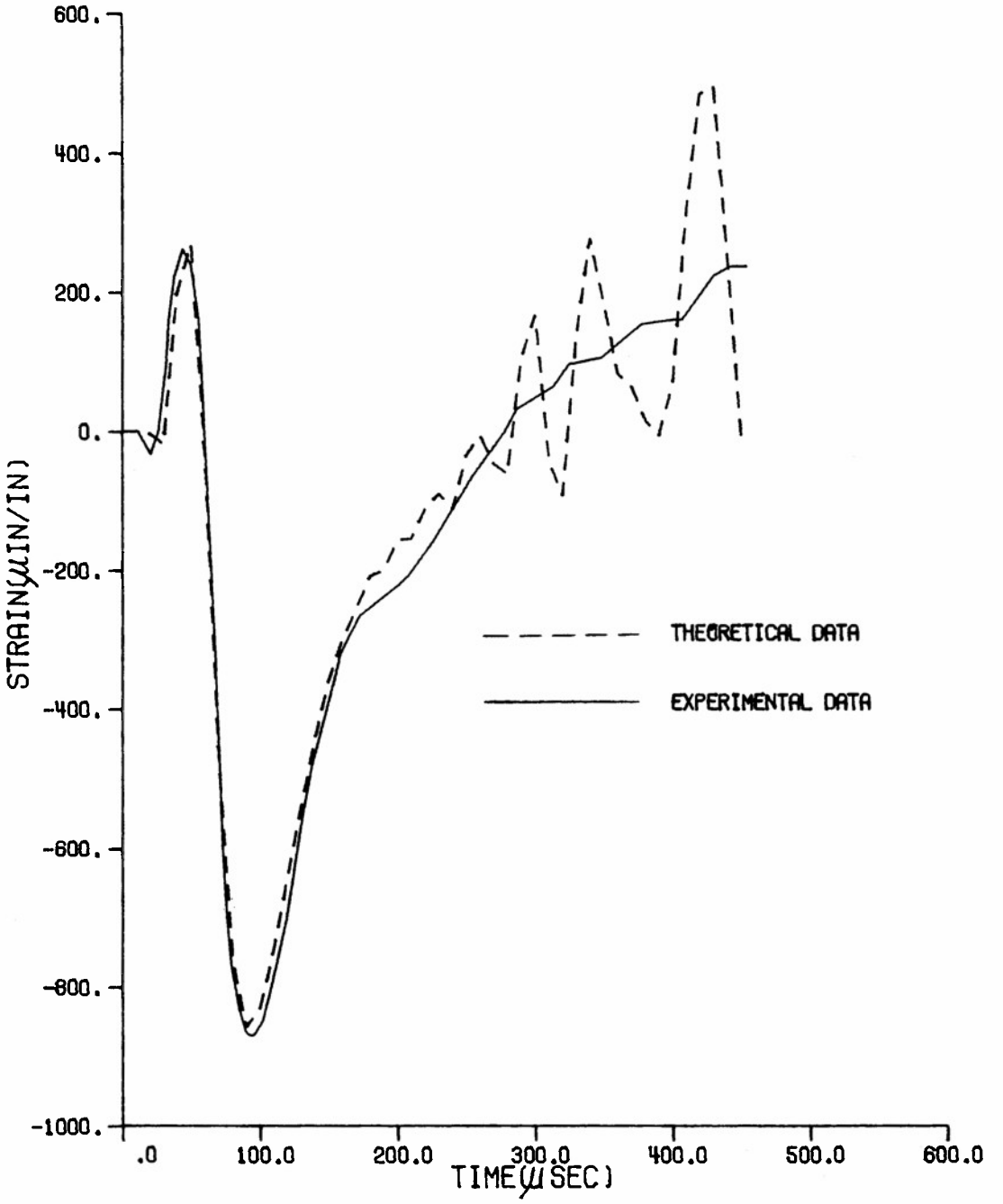

Fig. 1 Bending strain at 1.5 in. (38.1 mm) from the impact point in a $[90/45/90/-45/90]_{2s}$ composite beam subjected to impact of a steel ball of 0.5 in. (12.7 mm) in diameter with velocity 124.30 in./sec. (3.16 m/sec.). The beam was clamped at both ends with a span of 15 in. (381 mm).

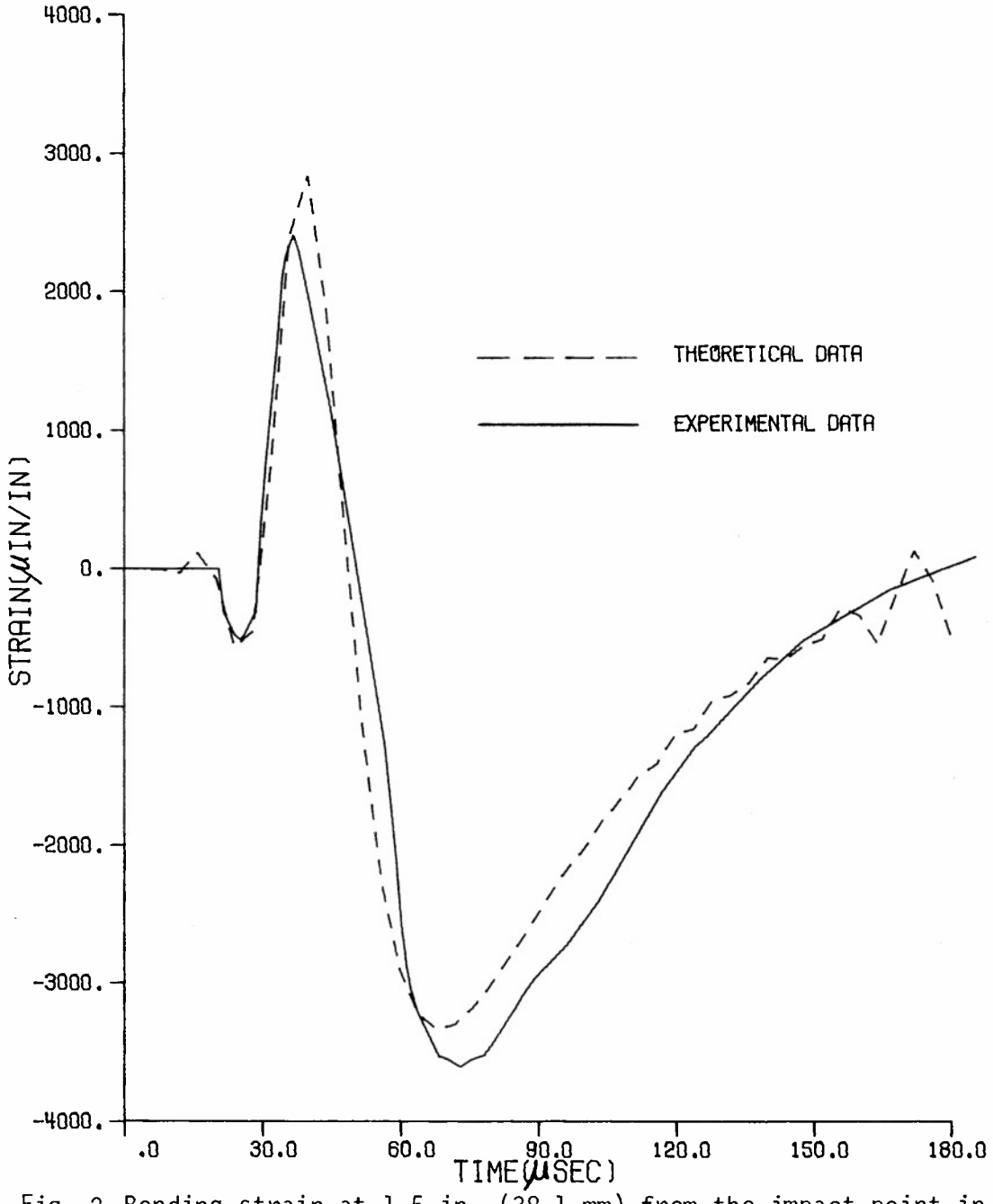

Fig. 2 Bending strain at 1.5 in. (38.1 mm) from the impact point in a $[90/45/90/-45/90]_{2s}$ composite beam subjected to impact of a steel ball of 0.25 in. (6.35 mm) in diameter with velocity 1194.3 in./sec. (30.34 m/sec.). The span between the two clamped ends is 14 in. (355.6 mm).

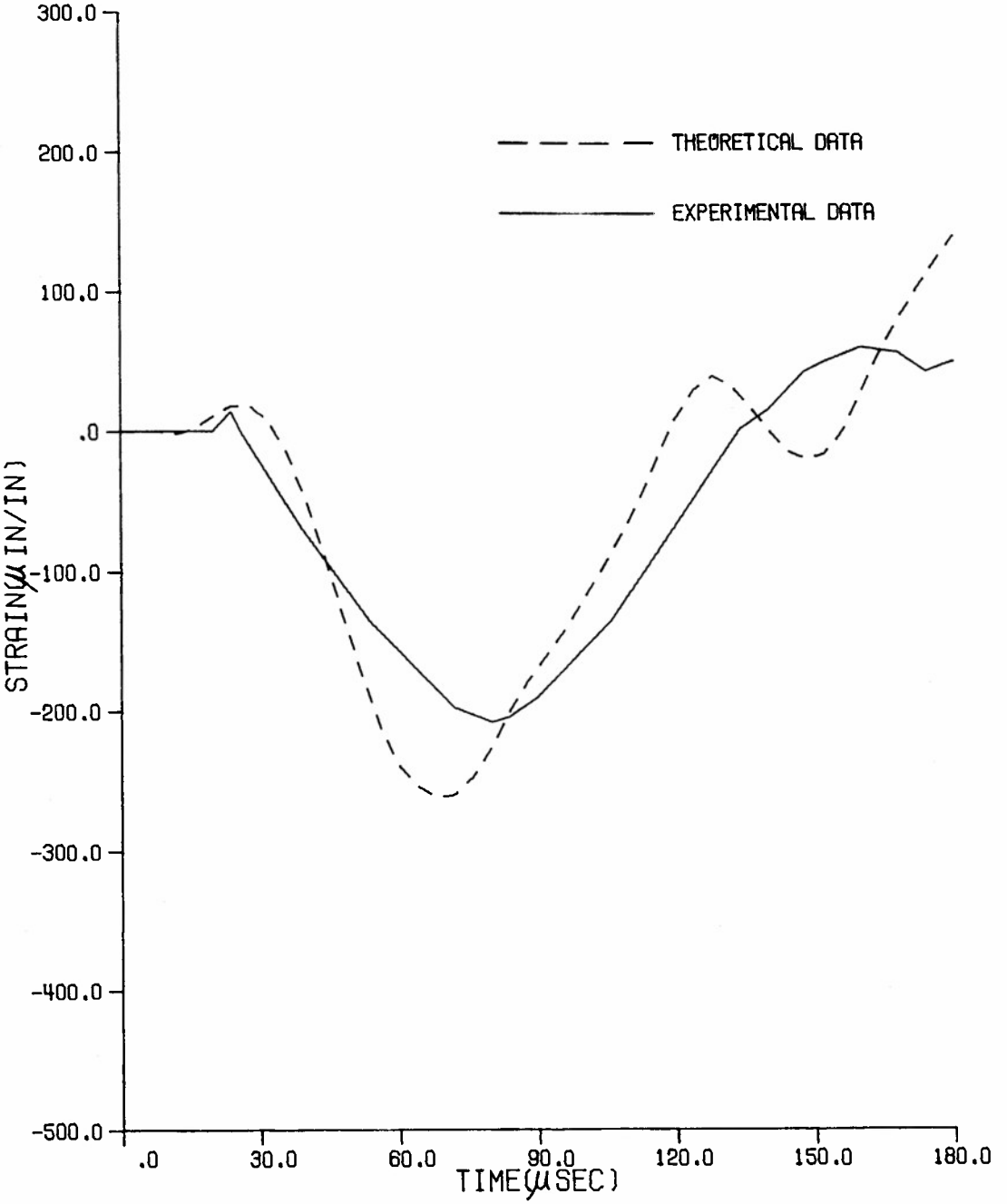

Fig. 3 Bending strain at 1.5 in. (38.1 mm) from the impact point in a $[0/45/0/-45/0]_{2s}$ composite beam subjected to impact of a steel ball of 0.5 in. (12.7 mm) in diameter with velocity 87.9 in./sec. (2.23 m/sec.). The span between the clamped ends is 9 in. (228.6 mm).

SHEAR PROPERTIES OF POLYIMIDE ADHESIVES AT VARIOUS TEMPERATURES

J. R. VINSON
H. Fletcher Brown Professor of Mechanical and Aerospace Engineers

R. TSCHIRSCHNITZ
Laboratory Supervisor, Mechanical & Aerospace Engineering
University of Delaware
Newark, Delaware 19711

DONALD L. SKOUMAL
Lead Engineer, Structures Division
Boeing Aerospace Company
Seattle, Washington 98124

ABSTRACT

In composite material structures, one of the primary limitations in minimizing structural weight is the joining of various structural components. In composite structures joining is largely limited to employing adhesive bonding (1) or mechanical fasteners (2), such as bolts or rivets, or possibly a combination of the two. Since mechanical fastening requires intermittent load paths, resulting in large stress concentration, as well as the cutting of fibers to make the necessary holes, adhesive bonding is considered more desirable for joining composite structural components to either other composite or metallic structural components.

Concerning various adhesive systems, in order to design, analyze and optimize bonded structures (3-13) it is necessary to know the mechanical properties of the adhesives in both shear and tension. Furthermore, it is necessary to know these properties for each temperature and moisture level to which the structure will be subjected, because the adhesives today are polymeric, and therefore subjected to "hygrothermal" effects, i.e. the deterious effects of combined high moisture and high temperature (8,10,11).

Unfortunately, not many of the moderate temperature adhesives, which are mostly epoxies, have been to characterized. However, a few dozen have been characterized to some extent (11-13,15,16). One of the reasons for this lack of material property data is the lack of standardization of a suitable shear and tension test piece configuration. However, more and more, the thick adherend shear test specimen is being accepted as the means to obtain shear properties because of the constancy of the shear across most of the length of the joint in this test configuration (11-13,15,16).

There is an increasing need for adhesives to operate at higher temperatures than attainable with epoxy adhesives, which are largely limited to less than 300°F. Thus, polyimide adhesives are being developed for this purpose. Not only do they have promising material properties at high temperatures, but they appear to be less sensitive to hygrothermal effects than are the epoxy adhesives.

Shear stress strain curves are being measured by the authors on a polyimide adhesive joining stainless steel adherends at room temperature, +550°F, and -250°F.

Two conditions are being measured: the as cured/post cured, and specimens conditioned at 600°F for 125 hours, prior to testing. The thick adherend test specimen is being used, the loads being measured by a load cell, the displacements being measured through an LVDT capable of these temperatures. Mean values for all properties as well as standard deviations are being obtained.

The result will be useful information for designing, analyzing and optimizing adhesive bonded joints using polyimide adhesives under these extreme temperature conditions. Such data is not presently available.

Included below are several publications of the authors on the joining of composite structures.

REFERENCES

1. Vinson, J. R., "On the State of Technology in Adhesively Bonded Joints," to be presented at the ASME Aerospace Division Conference, San Francisco, August 1980 (This contains dozens of references of the work of numerous authors).

2. Vinson, J. R., "On the State of Technology Regarding the Use of Mechanical Fasteners in Composite Material Structures," AFOSR TR 78-1278 (This contains dozens of references of the work of numerous authors).

3. Renton, W. J. and Vinson, J. R., "On the Behavior of Bonded Joints in Composite Materials," Journal of Engineering Fracture Mechanics, Vol. 7, pp. 41-60, 1975.

4. Renton, W. J. and Vinson, J. R., "Fatigue Behavior of Bonded Joints in Composite Material Structures," AIAA Journal of Aircraft, Vol. 12, No. 5, pp. 442-447, May 1975.

5. Renton, W. J. and Vinson, J. R., "Fatigue Response of Anisotropic Adherend Bonded Joints," Proceedings of the U.S. Army Symposium on Solid Mechanics, AMMRC-74-8, September 1974.

6. Renton, W. J. and Vinson, J. R., "The Efficient Design of Adhesive Bonded Joints," Journal of Adhesion, Vol. 7, pp. 175-193, 1975.

7. Renton, W. J. and Vinson, J. R., "On Improvement in Structural Efficiency of Single Lap Bonded Joints," Proceedings of the Fourth Army Materials Technology Conference-Advances in Joining Technology, 1975.

8. Wetherhold, R. C. and Vinson, J. R., "An Analytic Model for Bonded Joint Analysis in Composite Structures Including Hygrothermal Effects," AJTM Fourth Conference on Composite Materials, 1976, AFOSR TR 78-1337.

9. Renton, W. J. and Vinson, J. R., "Analysis of Adhesively Bonded Joints Between Panels of Composite Materials," Journal of Composite Materials, pp. 101-106, April, 1977.

10. Vinson, J. R. and Zumsteg, J. R., "Analysis of Bonded Joints in Composite Material Structures Including Hygrothermal Effects," AIAA Paper 79-0798.

11. Renton, W. J. and Vinson, J. R., "The Analysis and Design of Composite Material Bonded Joints Under Static and Fatigue Loads," AFOSR TR 73-1627, August, 1973.

12. Renton, W. J. and Vinson, J. R., "The Analysis Design of Anisotropic Bonded Joints, Report No. 2," AFOSR TR 75-0125, August, 1974.

13. Renton, W. J.; Flaggs, D. L. and Vinson, J. R., "The Analysis and Design of Composite Material Bonded Joints, Report No. 3," AFOSR TR, 1979.

14. Pipes, R. B.; Vinson, J. R. and Chou, T. W., "On the Hygrothermal Response of Laminated Composite Systems," Journal of Composite Materials, pp. 130-148, April 1976.

15. Renton, W. J. and Vinson, J. R., "Shear Property Measurements of Adhesives in Composite Material Bonded Joints," ASTM Special Technical Publication 580, pp. 119-132, 1975.

16. Flaggs, D. L. and Vinson, J. R., "Shear Properties of Promising Adhesives for Bonded Joints in Composite Materials Structures," AIAA Journal of Aircraft, January 1979.

TESTING TECHNIQUES FOR HIGH HEATING RATE EFFECT

KENNETH D. ROBERTSON
Mechanical Engineer

SHUN-CHIN CHOU
Mechanical Engineer
Ballistic Missile Defense Materials Program Office
Army Materials and Mechanics Research Center
Watertown, Massachusetts 02172

EXTENDED ABSTRACT

The behavior of certain materials under stress is affected by the combination of a rapid temperature rise in conjunction with a high strain rate. Materials characterized by metallurgical processes which involve finite times, such as precipitation hardening, display this type of behavior. The object of this investigation was to determine the behavior of two materials, aluminum and MAR-M200 under these conditions. Quantities of interest in this study are the elastic modulus, yield strength, ultimate strength, and maximum elongation.

To implement this investigation, a rapid heating device was designed and built; a rapid and accurate temperature sensor was selected, and a unique strain measuring device was designed and is currently being built. The special requirements and operating characteristics of each of these subsystems is the subject of this report.

A heating device was required which would heat a specimen (1/4" diameter x 1" length) from room temperature to $2000^{o}F$ in one second, sense when the desired temperature was reached and shut off. To accomplish this, a resistance heating device was designed and assembled. It consisted of a variac, step-down transformer, relays, cabling, electrodes, and special specimen grips.

In resistance heating, the heating rate $\Delta T/\Delta t$ is proportional to the energy dissipated in the specimen, thus $V^2/R \alpha$ specimen mass x specific heat x $\Delta T/\Delta t$. Consequently, the voltage across the specimen controls the heating rate. This voltage is set by a variac in series with a step-down transformer. Maximum power to the variac was 240 V at 20 A. This was stepped down to 10 V at 480 A. In practice considerably less power was generally required.

Relays, under computer control, were used to activate and de-activate the rapid heating device. Special welding cables #4/0 were used as cabling. Loads were applied through special aluminum oxide inserts in the specimen grips which also served to isolate the specimen thermally and electrically.

The rapid temperature changes involved in this study required a temperature sensor that could respond full-scale in 50ms or less. Thermocouples

will generally not respond this fast, require attachment, and can be influenced by the heating current. We chose an optical pyrometer to measure temperature. Full-scale response of this instrument ($350^{o}F$ - $3000^{o}F$) was of the order of 20ms.

Strain measurement at high temperature has always been a problem; but when combined with high strain rate, it becomes a serve limitation. Accurate strain measurements are required to determine elastic modulus values; yet, large strain measurements are required to determine maximum elongation. Present strain gage technologies are limited to temperatures below $1500^{o}F$. Temperatures in these tests could exceed this limit. To measure strains accurately and quickly, a unique optical extensometer has been developed. This extensometer employs a shutter system formed by sliding matching gratings across one another to interrupt or transmit light and a light sensor to measure light intensity. Resolution is of the order of .0002 in/in.

Tests will be conducted in a medium strain rate machine. A computer will be used to control the test and sample variables.

MECHANICAL RESPONSE OF REACTION BONDED SILICON NITRIDE SPRINGS AT ELEVATED TEMPERATURES

JOSEPH R. PETERS
Research Mechanical Engineer
Army Materials and Mechanics Research Center
Watertown, Mass. 02172

The elevated temperature working limits of most energy conversion devices are being continually extended. There are many examples wherein heat exchangers, combustors and other high-temperature components must be attached, securely positioned and aligned under various preloading conditions such as in the stacking of gas turbine components. An area that has not received sufficient attention is the potential utilization of structural ceramics in such applications. Thus the objective of this study is to investigate ceramic springs for high temperature service.

The determination of strength, relaxation, creep and other physical characteristics of ceramic materials at high temperatures is necessary if structural ceramics are to be used in high temperature ($1800^{o}F$-$2500^{o}F$, $980^{o}C$-$1370^{o}C$) applications.

Preliminary designs for ceramic springs have been completed and reaction bonded silicon nitride springs from two different manufacturers were ordered. Ten RBSN springs have been received from one manufacturer, the second manufacturer attempted to make the springs but gave up the attempt due to difficulties he encountered. (For spring details see Figure 1.)

Apparatus will be described for obtaining material characteristics of ceramic springs which will involve:

a. Simple load/deflection data
b. Creep
c. Relaxation
d. Fatigue

for the temperature range between $1800^{o}F$-$2500^{o}F$ ($980^{o}C$-$1370^{o}C$).

Data that has been generated up to the time of the symposium will also be presented.

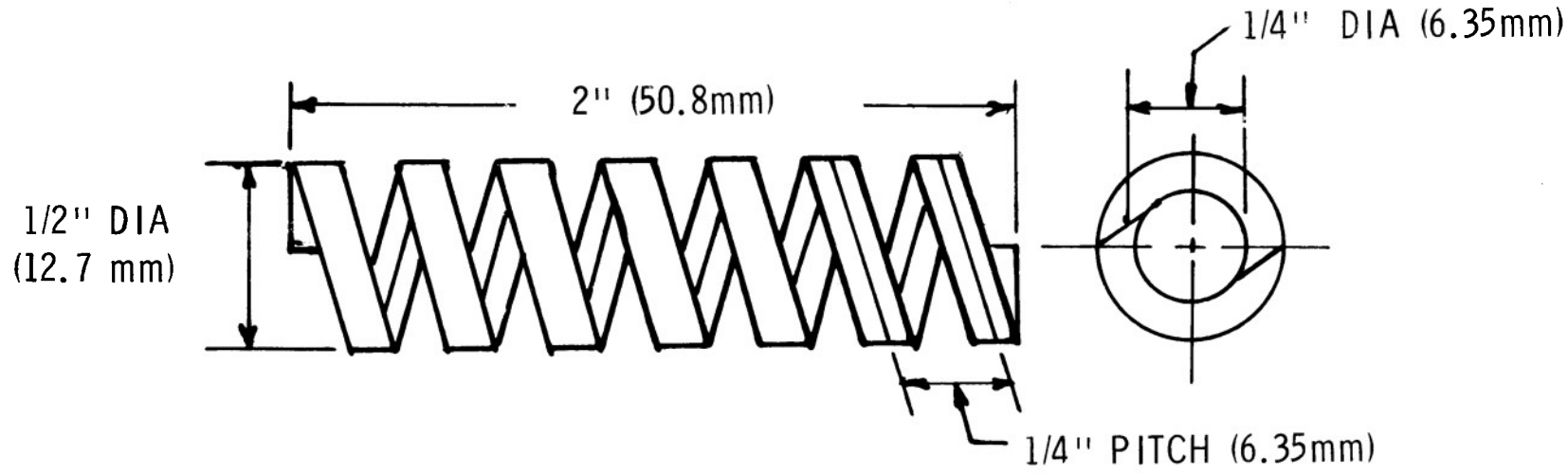

NOTES:

1. TOLERANCE ± 0.005" (0.127mm)
2. USE 1/8" x 1/8" (3.18 x 3.18mm) SQUARE STOCK
3. HELIX ANGLE 15^{0}

FIGURE 1 - DETAILS OF CERAMIC SPRING
MATERIAL: REACTION BONDED SILICON NITRIDE

INFERENCE PROCEDURES FOR DETERMINING LIFE TIME ESTIMATES OF ADVANCED MATERIALS AT ELEVATED TEMPERATURES

DONALD NEAL
Mathematician

EDWARD LENOE
Supervisory Mechanical Engineer

DONALD MASON
Engineering Aid
Army Materials and Mechanics Research Center
Watertown, Massachusetts 02172

EXTENDED ABSTRACT

An improved procedure for treatment of so-called censored data has been developed and life-time estimates made for proof tested ceramic rotor hubs, for fatigue sensitive composite helicopter components and in development of quality assurance control of powder metallurgically produced turbine engine discs. These represent various situations of structures to perform under extreme environmental conditions and analytical procedures to aid in achieving required component capability.

Two and three parameter Lognormal, Weibull and Gamma functions represent the candidate statistic models. These functions are examined for best representation of data in order to provide flexibility in the fitting process. The functional parameters are obtained from the maximum likelihood (M.L.) method. This method provides a superior representation of the cyclic fatigue data as compared to the more conventional procedures. The M.L. method can also provide the desired confidence limits for the parameter and reliability determinations associated with the given data set. The inadequacies associated with the method of moments, graphical procedures, etc., in obtaining the functional parameters is recognized from the arbitrariness of the functional representation of the data. The acceptability of these methods is acutely data dependent.

The need for considering all data including censored data is established. Both lower and upper bound censored data are considered as they relate to proof testing and run-outs respectively. An improved probability of failure computation can be obtained when the total data set is represented. Partial probability ranking procedures tend to introduce substantial errors in the extrapolation process necessary in obtaining minimum life-time estimates. By including censored data, one can provide a more complete understanding of the materials capabilities.

The results of combining the M.L. method with the inclusion of censored data are compared with conventional procedures in obtaining both structural reliability and material probability of failure computations. The comparison indicates a substantial nonconservative estimate of failure probabilities can occur if threshold stress values are obtained from proof testing without consideration of the censored data. Application of the M.L. procedure provided an improvement in the functional representation of data.

RECENT TEST RESULTS ON ENERGY ABSORPTION CHARACTERISTICS OF DIFFERENT CYLINDER DESIGNS

W. T. HODGES
U. S. Army R&T Laboratories (AVRADCOM)
NASA Langley Research Center
Hampton, VA 23665

R. L. FOYE
U. S. Army R&D Laboratory HQ (AVRADCOM)
NASA Ames Research Center
Moffett Field, CA 94035

ABSTRACT

The ability of landing gear and fuselage structure to absorb kinetic energy (and thereby attenuate the deceleration forces on aircraft occupants in a potentially survivable crash) is a significant design consideration of fixed and rotary winged vehicles. The same considerations are also important in automotive and railroad car design. The unyielding character of most composite materials has given cause to question the ability of structures made from these materials to provide the same level of protection as conventional aluminum construction. The current FAA certification specifications for transport aircraft require that this aspect of the crashworthiness of composite fuselage structure be demonstrated to be equivalent to conventional aluminum construction. The U. S. Army has had comprehensive crashworthiness requirements in all its recent helicopter designs without distinction to the materials of construction.

Our understanding of the crash energy absorption characteristics of metal construction leaves much to be desired. Composites are understood even less. In some instances composites have been shown to be excellent energy absorbers but in other instances, when the structures have not been designed with that factor in mind, composites have not compared well with metals. A series of tests were recently reported by the authors in which various composite material/design concepts, typical of lightly loaded fuselage construction, were used in the fabrication of cylindrical shell specimens which were subsequently crushed in compression as a means of observing and measuring the energy absorption capacity of the design concepts. These tests provided a practical basis for comparing the various composite construction concepts to that of aluminum. However, in photos of full scale airframe drop tests it

can clearly be seen that a significant portion of the available energy is absorbed by skin shearing, away from the point of impact, as well as compaction of the fuselage structure at the point of impact. For this reason several of the previous design concepts were tested in a torsion loading machine to induce shear deformations in the cylindrical specimens.

This talk will describe the material/design concepts, the test specimens, the test method and the results. The pertinent features and differences in the response of the various design concepts will be discussed and compared to the compression loading results. The specimens were all designed to the same strength and stiffness requirements which were typical of helicopter fuselage design.

These tests compared fiberglass, Kevlar, graphite and hybrids, in the form of sandwich and stiffened skin construction, to the traditional all-aluminum concepts (Figure 1). All the tests were run at slow strain rates. The shear energy absorption characteristics of all the materials were very different from what they exhibited under compression loading and the results were much more complex and difficult to interpret. However, some of the conclusions from compression tests remained valid. Namely, honeycomb sandwich construction appears to offer greater energy absorption capacity than stiffened skin construction and, in the absence of crash energy absorption criteria, composites tend to have significantly lower absorption capacity than aluminum construction.

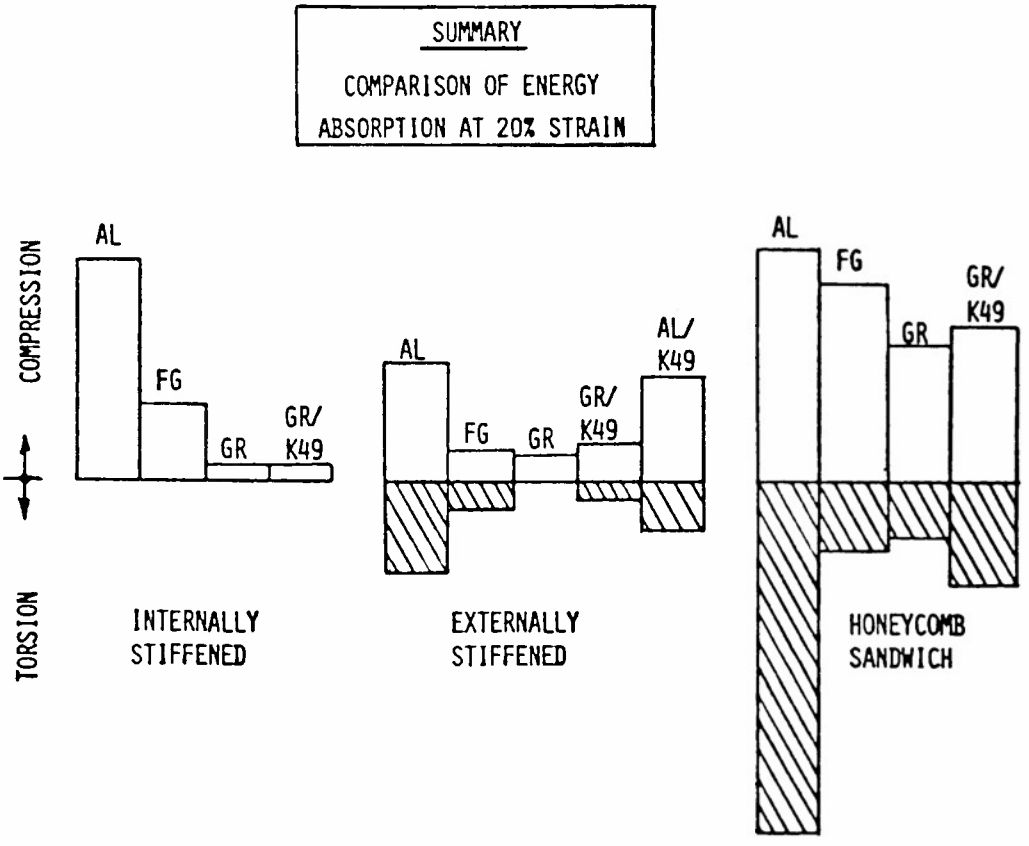

THE DEVELOPMENT OF A RATIONAL METHODOLOGY FOR THE ANALYSIS OF IMPACT FORCE, RESPONSE, AND DAMAGES DUE TO COLLISION OF VEHICLES

DR. P. Y. CHANG
Principal Research Scientist
HYDRONAUTICS, Incorporated
7210 Pindell School Road
Laurel, Maryland 20810

EXTENDED ABSTRACT

Collisions involving two ships and/or ships and offshore structures have been a major cause of loss of property and pollution. Even minor damage can cause significant losses in productivity. For these reasons, certain protective structures are desirable to reduce damage in the event of such collisions.

The reliability of any protective structure depends on the accurate prediction of the impact load and the resistance capacity of the structure. However, such accurate prediction is very difficult by the existing analytical methods. In case of a collision, both the impact force and the geometry of the two structures change rapidly. The elastic and plastic, linear and nonlinear responses of the two structures subjected to dynamic forces which are the function of the responses and motions of the two structures are involved. The destruction, crushing, and rupture of the structural members also occur. This is a very complicated problem and, so far as we know, no existing methods nor computer program can solve this problem explicitly.

For the design of protection barriers for nuclear merchant ships, the international maritime community has relied on scale model collision experiments. The experimental approach to this problem is not satisfactory, because of the instrumentation difficulties and the scale factor problems. In the past few years, the author has gradually synthesized a rational method for this problem, using the nonlinear finite element analysis, experimental data, analytical methods, and the collapse theorems.

The development of the methodology was supported by the U.S. Maritime Administration and GKSS of Germany, mainly for nuclear ships. The results are also applicable to other ships and offshore constructions and should be useful to other types of structures.

The historical background, the currently used methods, and the extensive experimental programs carried out by the German investigators will be reviewed briefly. The general procedure, theoretical background, and the method of computation will be discussed in detail. The analytical results and the correlation with experimental data will also be presented.

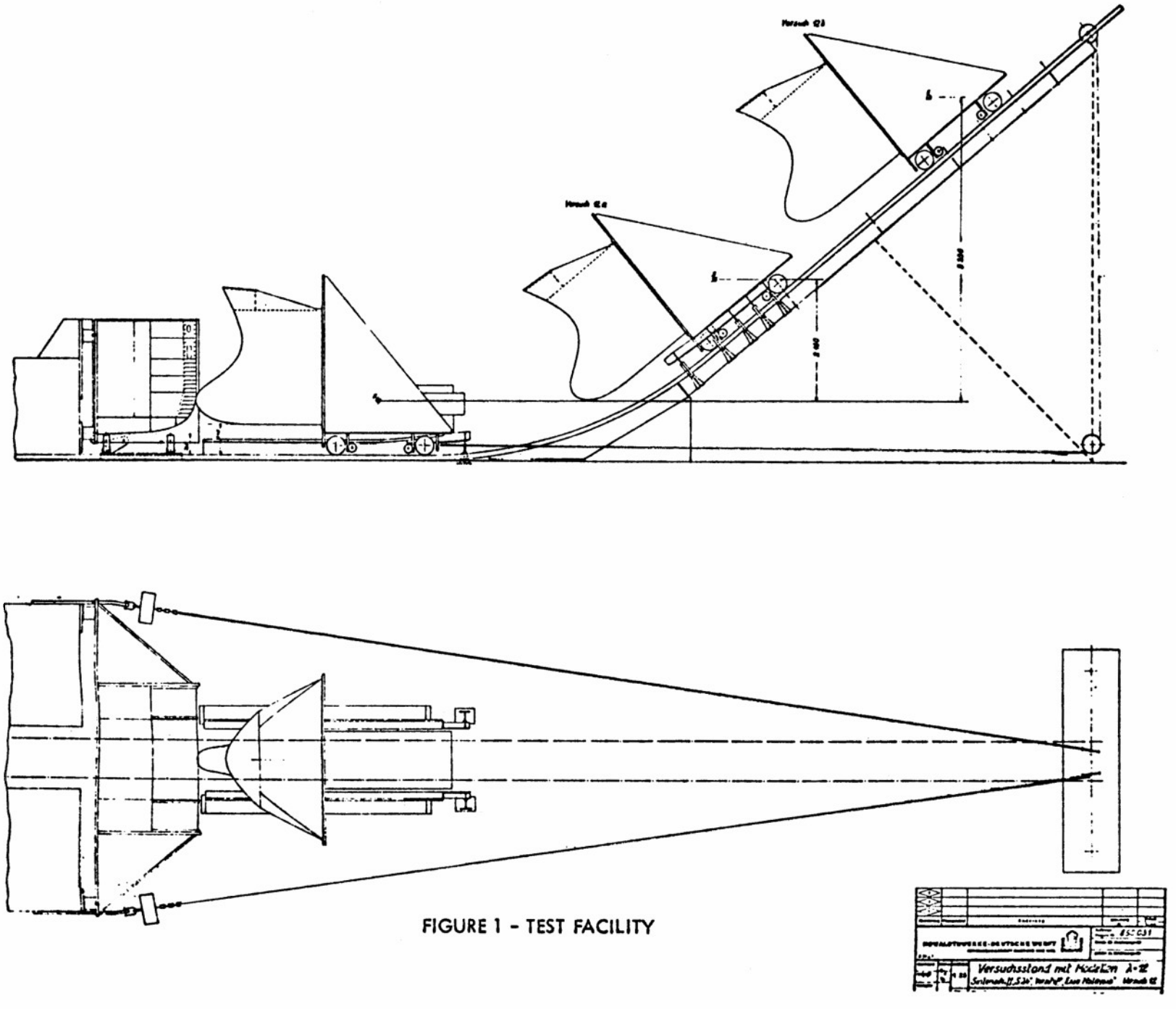

FIGURE 1 - TEST FACILITY

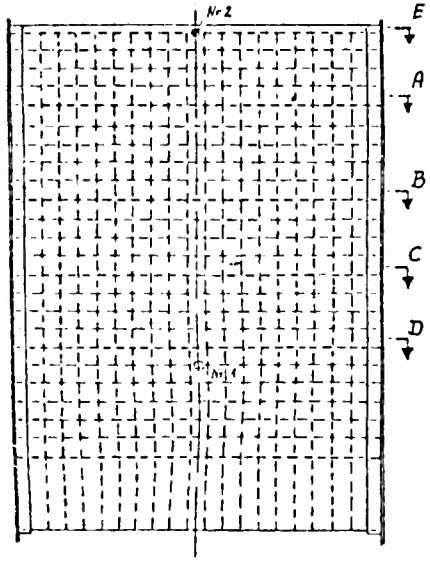

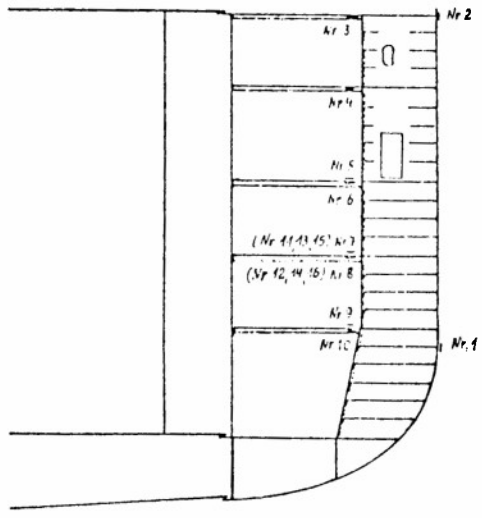

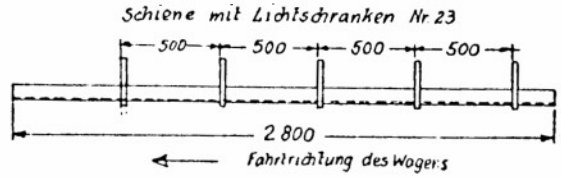

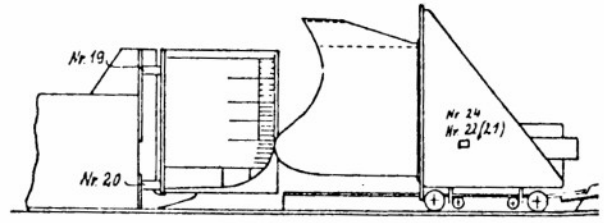

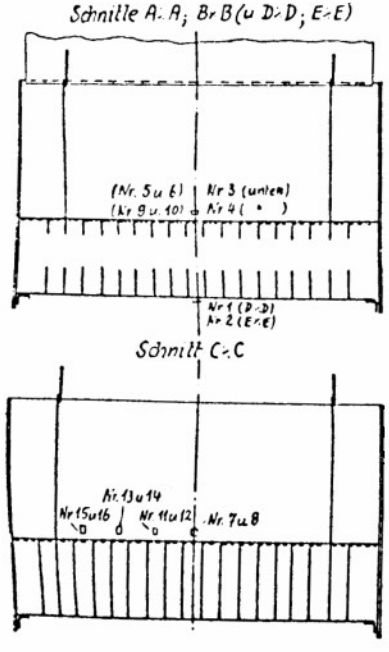

Nr.	Art der Meßstelle		Lage	Bemerkung
1	1 DMS	5/120 PA	Außenhaut in 5. Deck	1. Auftreffpunkt
2	1 DMS	" "	Außenhaut 4. Deck	2 Auftreffpunkt
3	1 DMS	10/120 LS 11	Mitte 1. Deck unten	
4	1 DMS	" "	Mitte 2. Deck unten	
5	1 DMS	" "	Mitte 3. Deck oben	
6	1 DMS	" "	Mitte 3. Deck unten	
7	1 DMS	" "	Mitte 4. Deck oben	
8	1 DMS	" "	Mitte 4. Deck unten	
9	1 DMS	" "	Mitte 5. Deck oben	
10	1 DMS	" "	Mitte 5. Deck unten	
11	1 DMS	" "	4. Deck oben	
12	1 DMS	" "	4. Deck unten	
13	1 DMS	" "	4. Deck oben	
14	1 DMS	" "	4. Deck unten	
15	1 DMS	" "	4. Deck oben	
16	1 DMS	" "	4. Deck unten	
17	1 Kraftmeßdose	RA/500M	Widerlag/Bügeln links ob	
18	1 Kraftmeßdose	" " "	" " links unt	
19	1 Kraftmeßdose	" " "	" " rechts ob	
20	1 Kraftmeßdose	" " "	" " rechts unt	
21	1 Beschleunig'aufnehmer		Wagen-O Stb-Seite	HBM / B1M/170
22	1 Beschleunig'aufnehmer		Wagen-O Bb-Seite	HBM / B12/1000
23	6 Gabellichtschranken		links der Bahn	2 Zungen, 250 m Abst
24	1 Beschleunig'aufnehmer		Wagen-O Bb-Seite	HBM B1M gefiltert

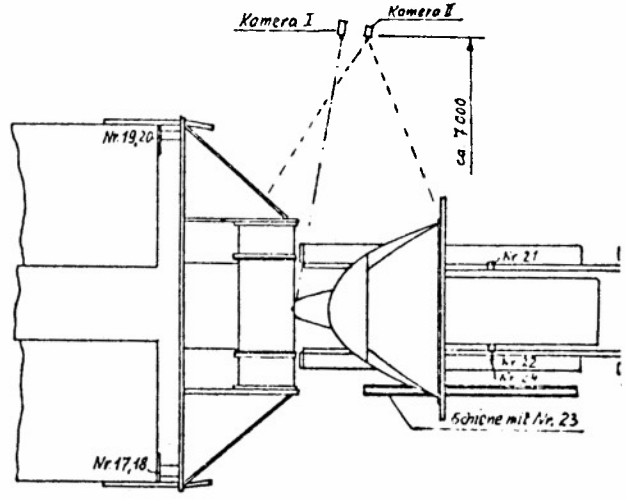

FIGURE 2 – LOCATIONS OF MEASUREMENTS

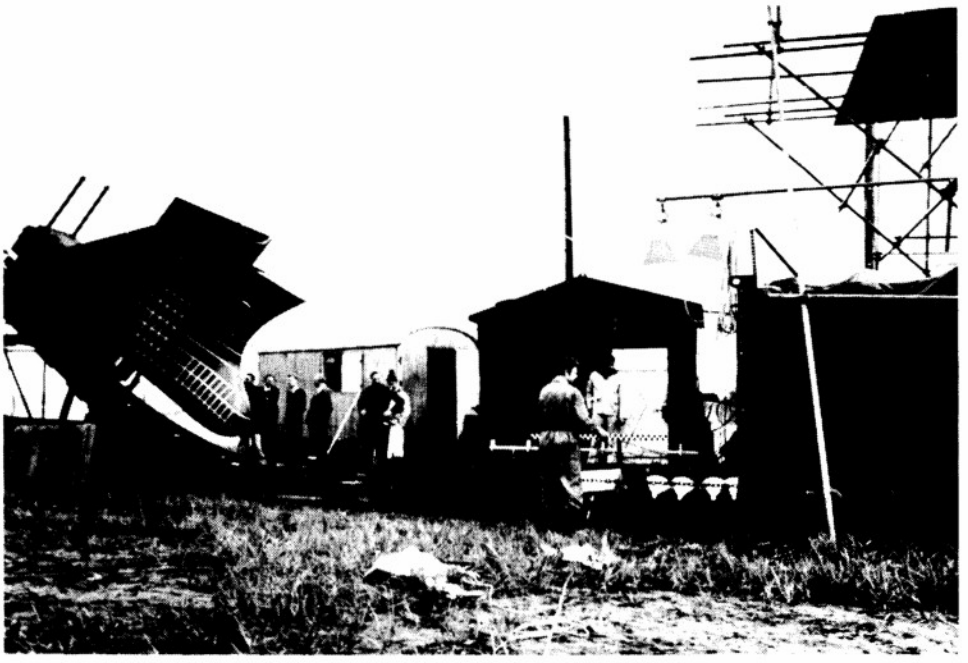

FIGURE 3a - TEST FACILITIES

FIGURE 3b - THE STRIKING BOW AND CARRIER

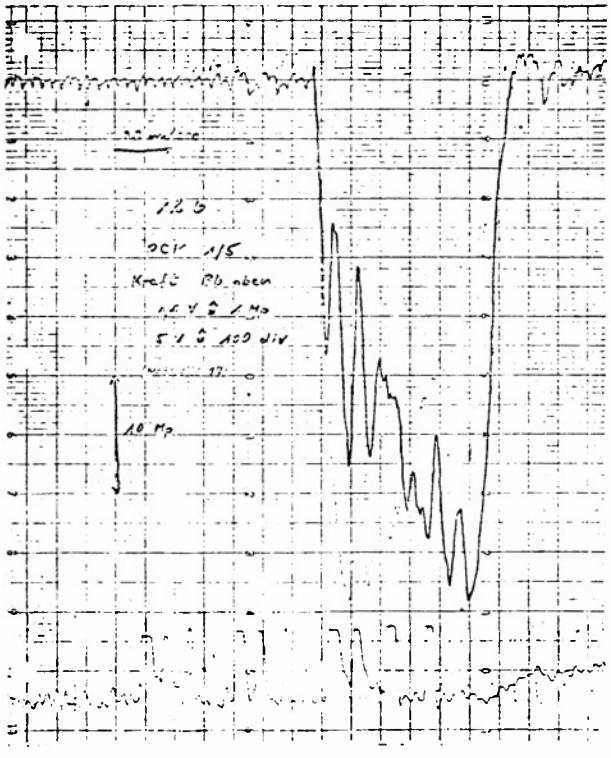

FIGURE 4 - COLLISION IMPACT FORCE FROM MODEL TEST

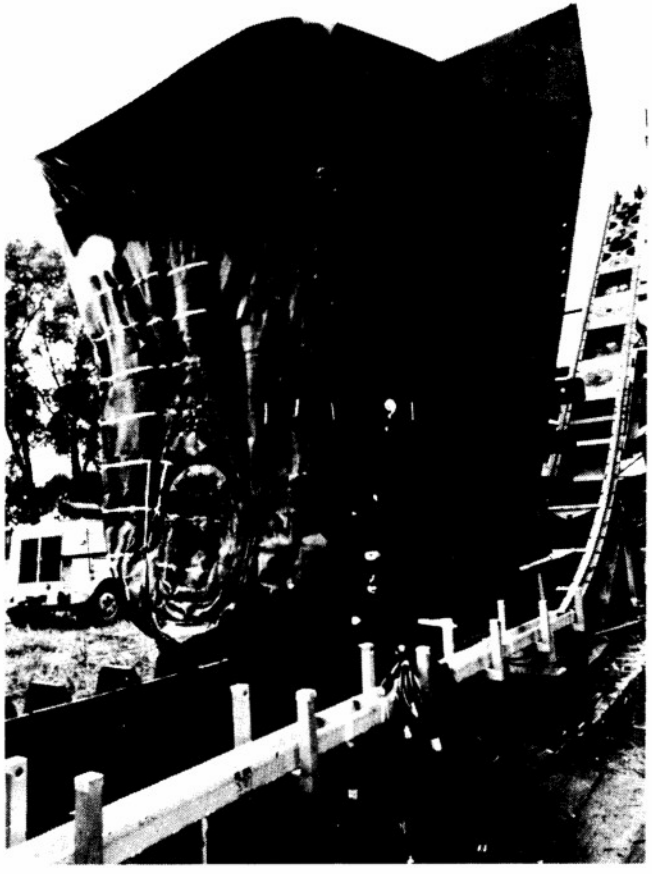

FIGURE 5a - BOW AFTER COLLISION

FIGURE 5b - BARRIER AFTER COLLISION

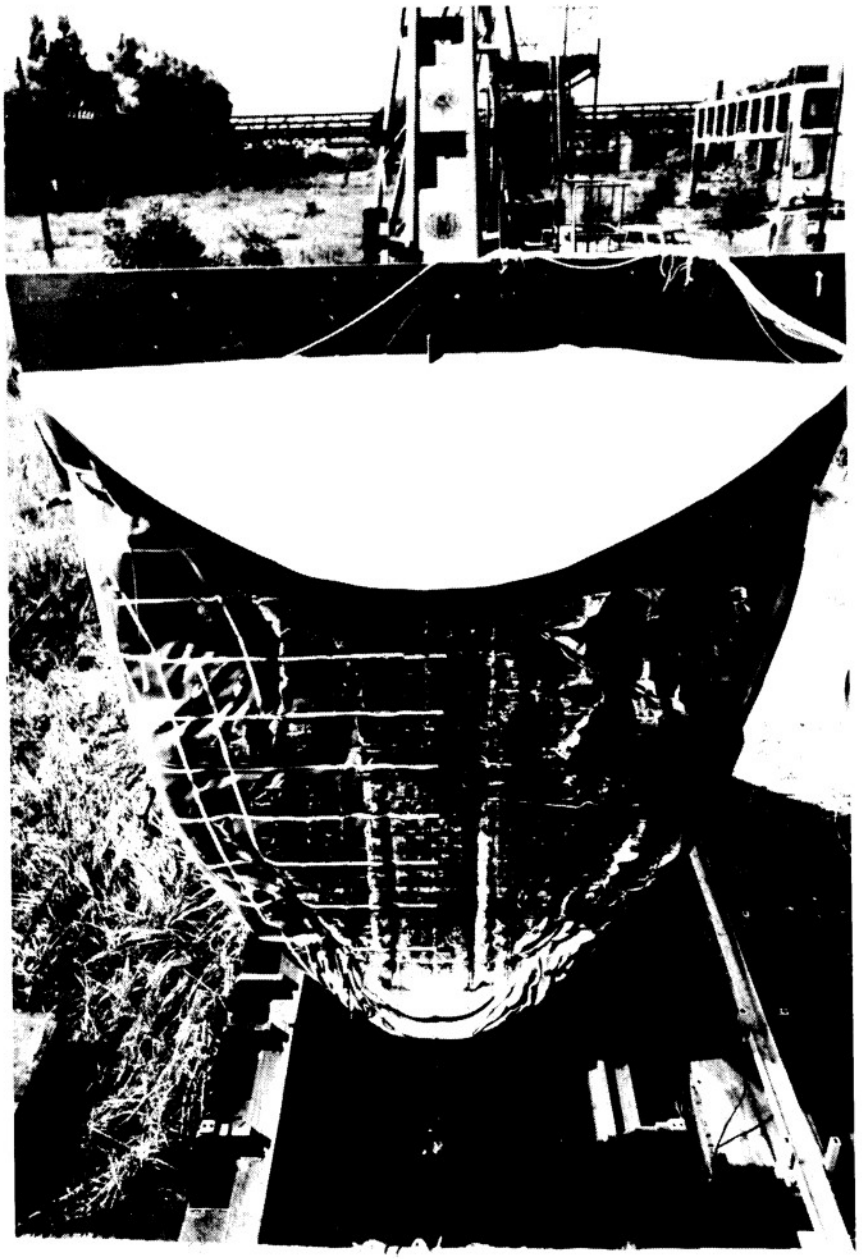

FIGURE 6a - BOW MODEL AFTER TEST NO. 9

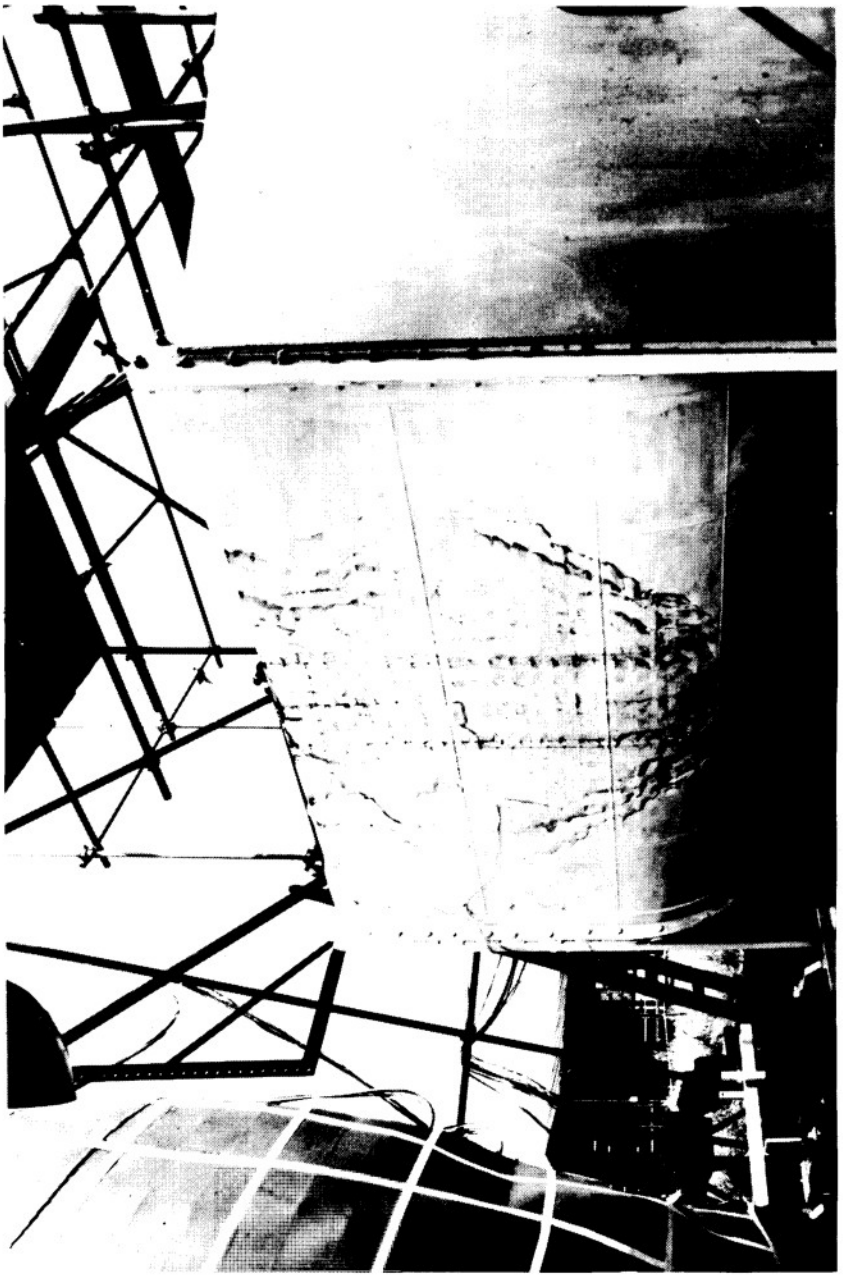

FIGURE 6b - BARRIER MODEL AFTER TEST NO. 9

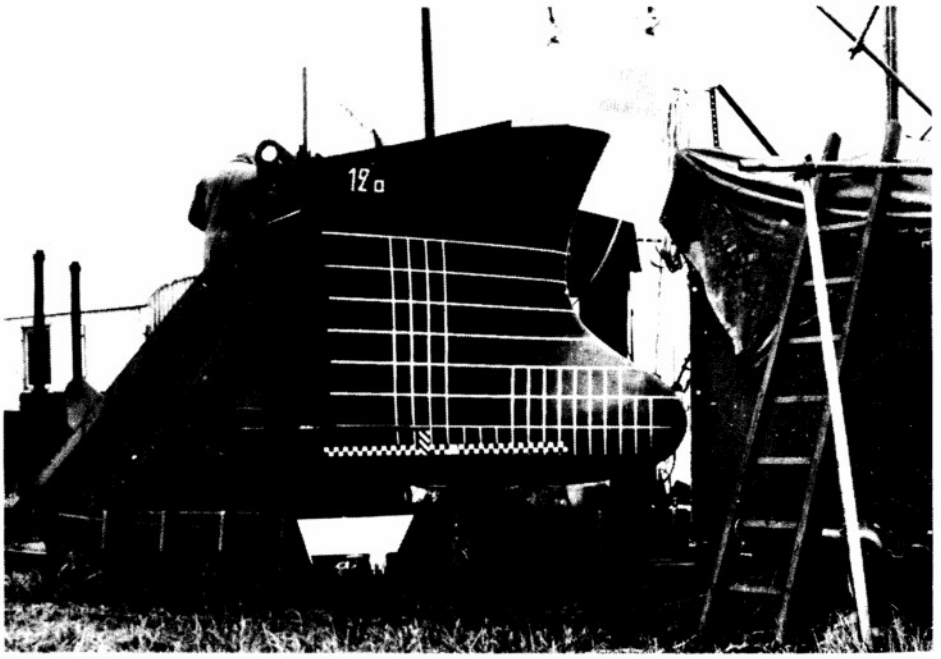

FIGURE 7a - THE ESSO MALAYSIA BOW

FIGURE 7b - ESSO MALAYSIA BOW AFTER TEST

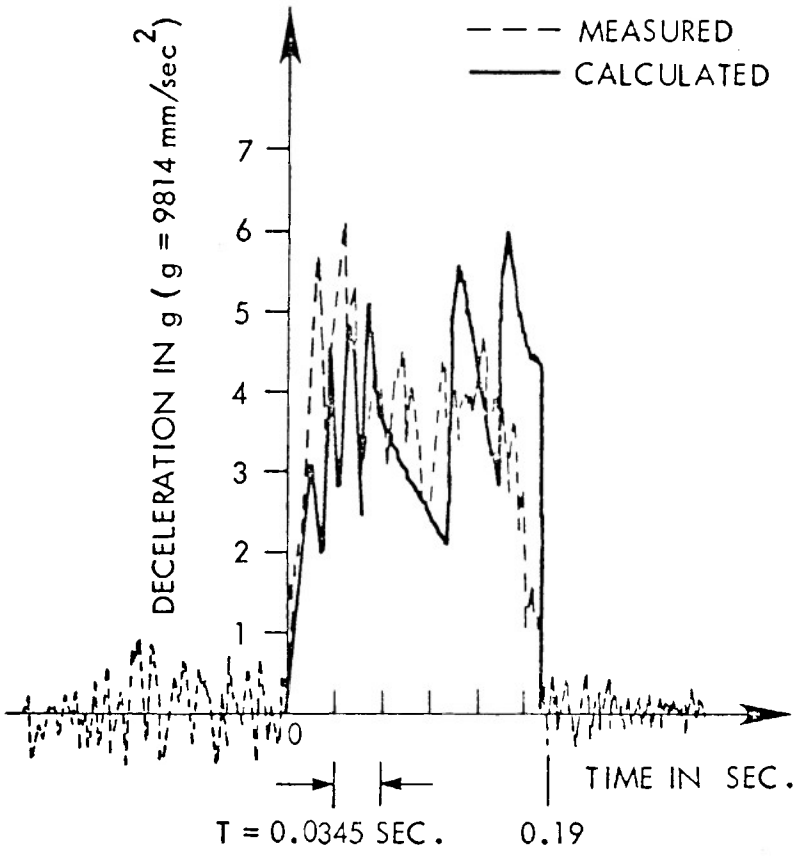

FIGURE 8 - TIME - ACCELERATION CURVE FOR "ESSO MALAYSIA" MODEL TESTS

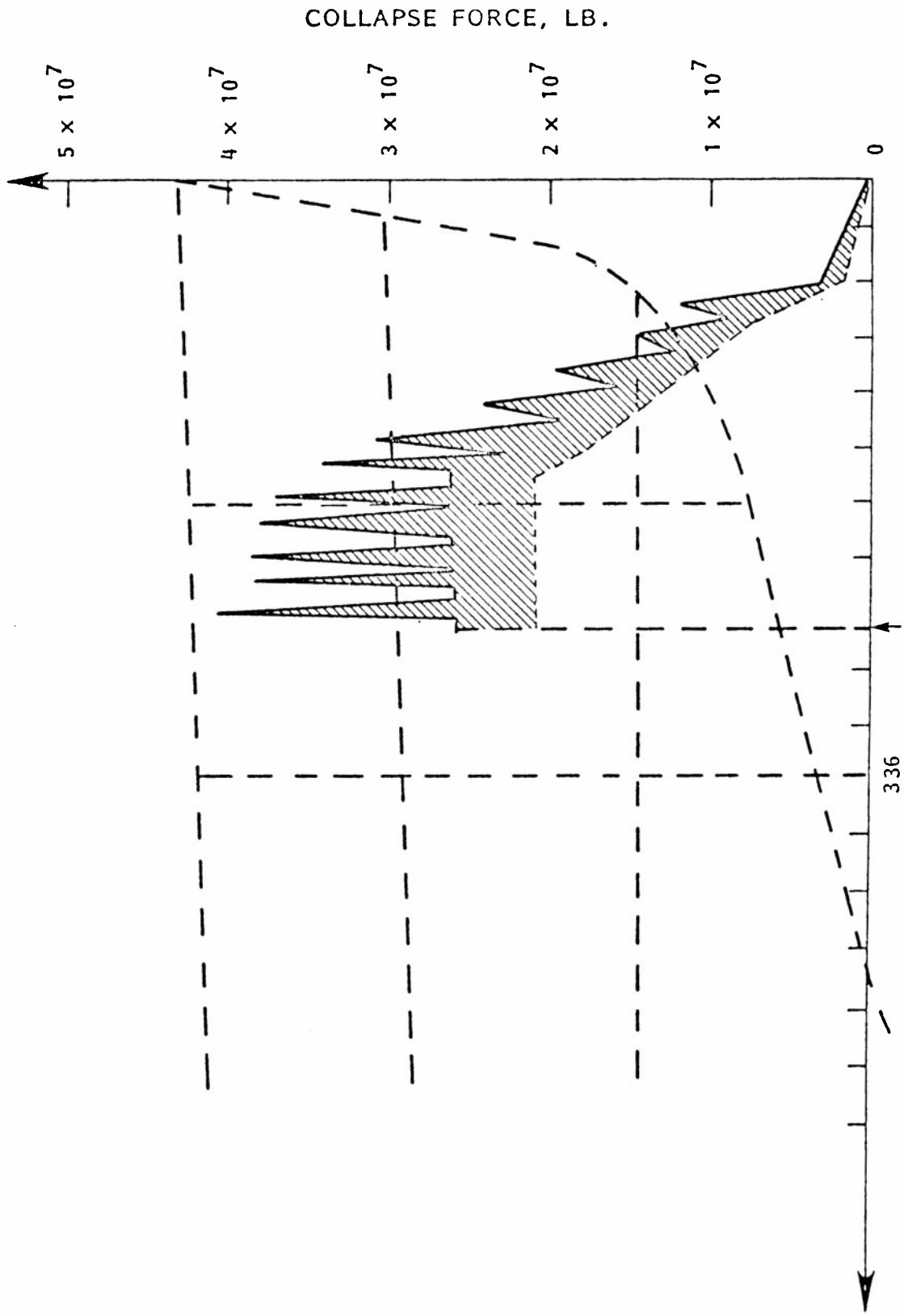

FIGURE 9 - MATHEMATICAL SIMULATION OF THE POLAR STAR STRUCTURAL RESPONSE, IMPACT VELOCITY = 344.64 in./sec

STRESS INTENSITY PREDICTION FOR A MULTIPLY-CRACKED, PRESSURISED GUN TUBE WITH RESIDUAL AND THERMAL STRESSES

A. P. PARKER
Mechanics and Engineering Laboratory
Army Materials and Mechanics Research Center
Watertown, Massachusetts 02172

C. P. ANDRASIC
Materials Branch
Royal Military College of Science
Shrivenham
Swindon
Wiltshire
England

ABSTRACT

1. INTRODUCTION

Fatigue crack growth arising from the cyclic pressurisation of gun tubes tends to produce a regular array of up to 50 equal-length, radial cracks emanating from the bore (1). A knowledge of the crack tip stress intensity factor, K, is necessary in order to predict the fatigue growth rate, and critical length of such cracks. It is common practice to produce a more advantageous stress distribution by a partial yielding (autofrettage) treatment of the cylinder prior to use.

Several solutions for the case of a cracked, pressurised thick cylinder are available (1), (2), (3), (4), (5). The solution for a finite pressurised thick cylinder with up to 40 radial cracks is due to Pu & Hussain (2), and employs Finite Element techniques with 12-noded, singular, isoparametric elements. The errors in this solution are estimated at 7%. More accurate solutions for up to 4 internal or external radial cracks were obtained by Tracy (5), using a modified mapping collocation (MMC) technique. The errors associated with MMC technique are estimated at less than 1%. An approximate solution, which employs a load relief factor (LRF) technique, has been obtained for the case of a pressurised, autofrettaged or thermally stressed tube (6). The errors associated with the LRF solution are estimated at 8-10%.

2. FORMULATION

Complex variable methods, due to Muskhelishvili (7) are utilized. Stresses and displacements within a body are represented in terms of complex stress functions. By employing a MMC technique as described by Tracy (5), the cracked ring segment in the physical (z) plane, Figure 1, is mapped from a rectangular region in the γ (parameter) plane. Traction-free conditions along A'B' and D'E' in the parameter plane are ensured. The singularity is removed from the parameter plane by mapping a unit semi-circle onto the appropriate crack surfaces, Figure 1. A series representation of the stress function is selected, which ensures appropriate symmetry conditions.

An over-determined collocation (least squares) satisfaction of appropriate boundary force and/or displacement conditions if imposed. The stress and displacement boundary conditions applicable to the problem in the physical (z) plane are:

$$\sigma_r = o, \ \tau_{r\theta} = o \qquad \text{over DE and BA}$$

$$u_\theta = o, \ \tau_{r\theta} = o \qquad \text{over EF and AH}$$

$$\sigma_r = o, \ \tau_{r\theta} = o \qquad \text{over FG and HG}$$

$$\sigma_\theta = p(r), \ \tau_{r\theta} = o \qquad \text{over DC and BC}$$

where p(r) is equal and opposite to the loading along the crack line in the unflawed structure for the case of internal pressure, autofrettage or thermal loading, the latter two stress states being essentially equivalent (8).

3. RESULTS

Results for internal pressure in the bore and cracks are presented in Figure 2 for an R_1/R_2 ratio of 0.5. The form of the results at short crack lengths is shown in Figure 3, indicating good convergence to the limiting value. Equivalent results for the case of full (100%) autofrettage and steady-state thermal stressing appear in Figure 4 and Figure 5. Again, the short crack length convergence is good, as is that at longer crack lengths.

By superposition of these results it is possible to determine K for any combination of internal pressure, full autofrettage or steady-state thermal loading. Furthermore, provided the crack tips do not extend beyond the minimum radius to which plastic flow was induced during the autofrettage process, it is also possible to obtain K values for partial autofrettage by a straightforward superposition.

4. ACKNOWLEDGEMENT

This work was funded from a Ministry of Defense research contract, and was written and presented during the attachment of the first author to AMMRC under the aegis of the TTCP.

5. REFERENCES

(1) Goldthorpe B. D. "Fatigue and Fracture of Thick Walled Cylinders and Gun Barrels", 'Case Studies in Fracture Mechanics' AMMRC MS 77-5 (1977).

(2) Pu S. L., Hussain M. A. "Stress Intensity Factors for a Circular Ring with Uniform Array of Radial Cracks Using Cubic Isoparametric Singular Elements", 11th Nat. Symp. on Fracture Mechanics, V.P.I., Blacksburg, VA, June (1978).

(3) Tweed J., Rooke D. P. "The Stress Intensity Factor for a Crack in a Symmetric Array Originating from a Circular Hole in an Infinite Solid" J. Engng. Sci, 13, 653-662 (1975).

(4) Baratta F. I. "Stress Intensity Factors for Internal Multiple Cracks in Thick-Walled Cylinders Stressed by Internal Pressure Using Load Relief Factors" Engng. Frac. Mech., 10, 691-697 (1978).

(5) Tracy P. G. "Elastic Analysis of Radial Cracks Emanating from the Outer and Inner Surfaces of a Circular Ring", Engng. Frac. Mech., 11, 291-300 (1979).

(6) Parker A. P., Farrow J. R. "Stress Intensity Factors for Multiple Radial Cracks Emanating from the Bore of an Autofrettaged or Thermally Stressed, Thick Cylinder". RMCS TN MAT/20, Shrivenham (1979).

(7) Muskhelishvili N. I. "Some Basic Problems of the Mathematical Theory of Elasticity" Noordhoff Ltd. (1953).

(8) Parker A. P., Farrow J. R. "On the Equivalence of Axisymmetric Bending Thermal and Autofrettage Stress Fields" J. Strain Analysis, 15, 1, 51-52 (1980).

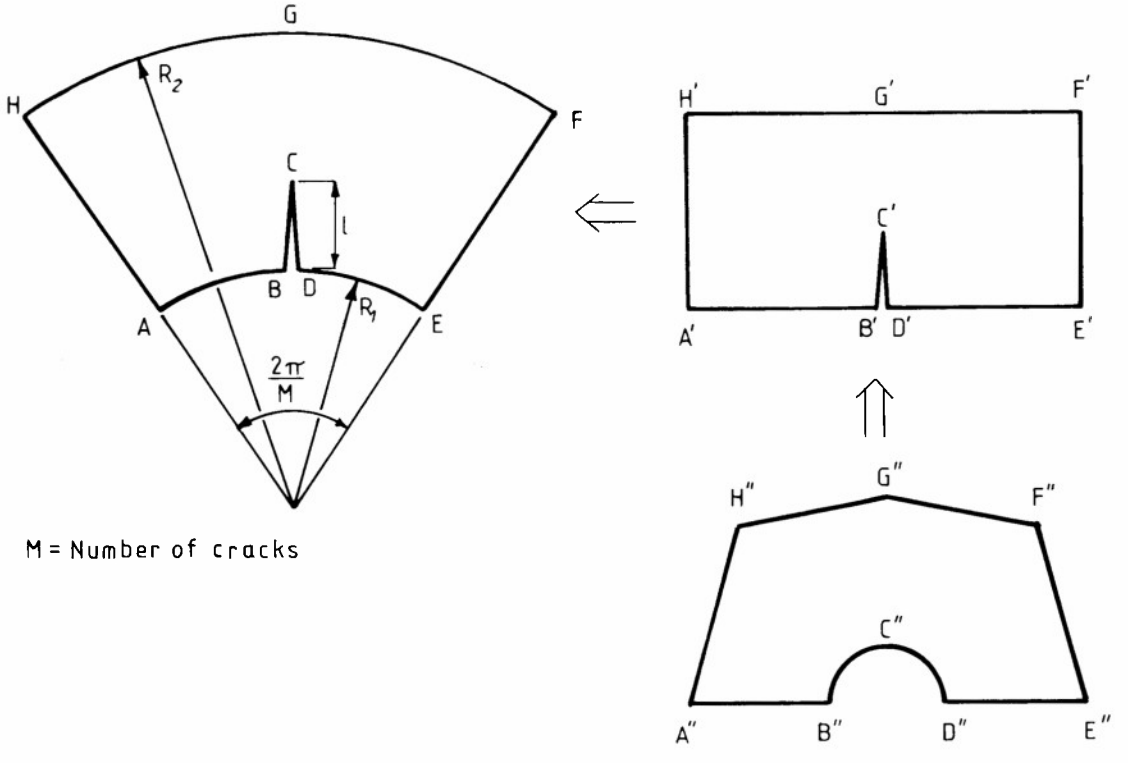

Figure 1: Physical and Mapped Planes.

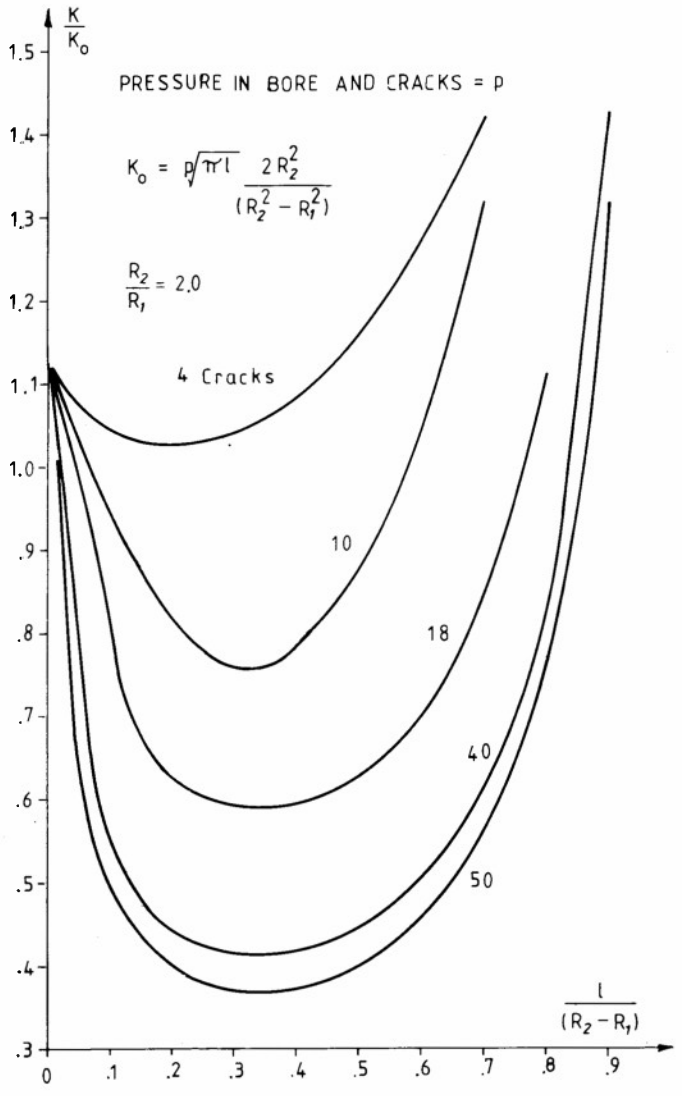

Figure 2: Stress Intensity Factors for Pressurised Thick Cylinder.

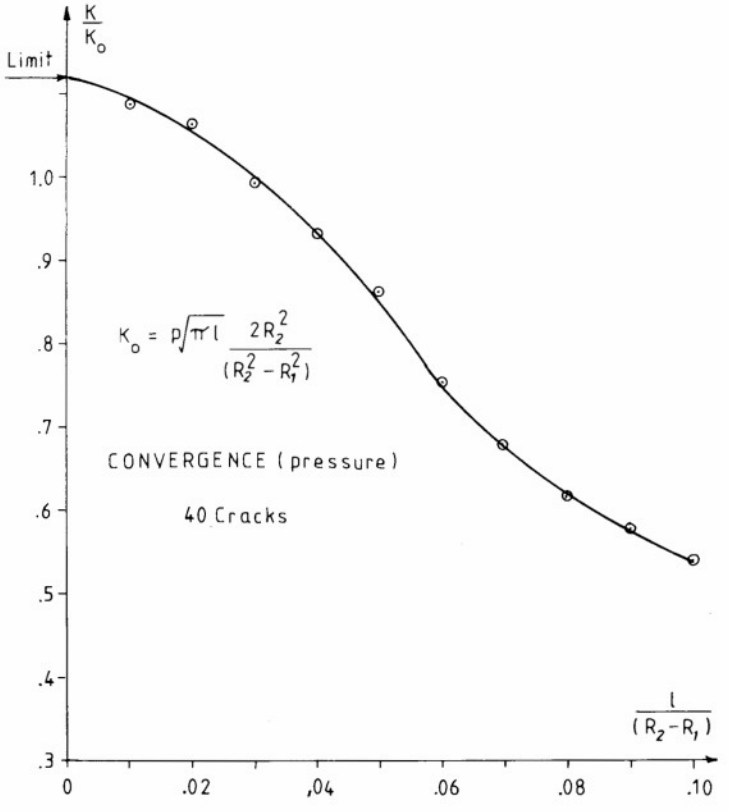

Figure 3: Short Crack Length Convergence Characteristics - Pressurised Thick Cylinder.

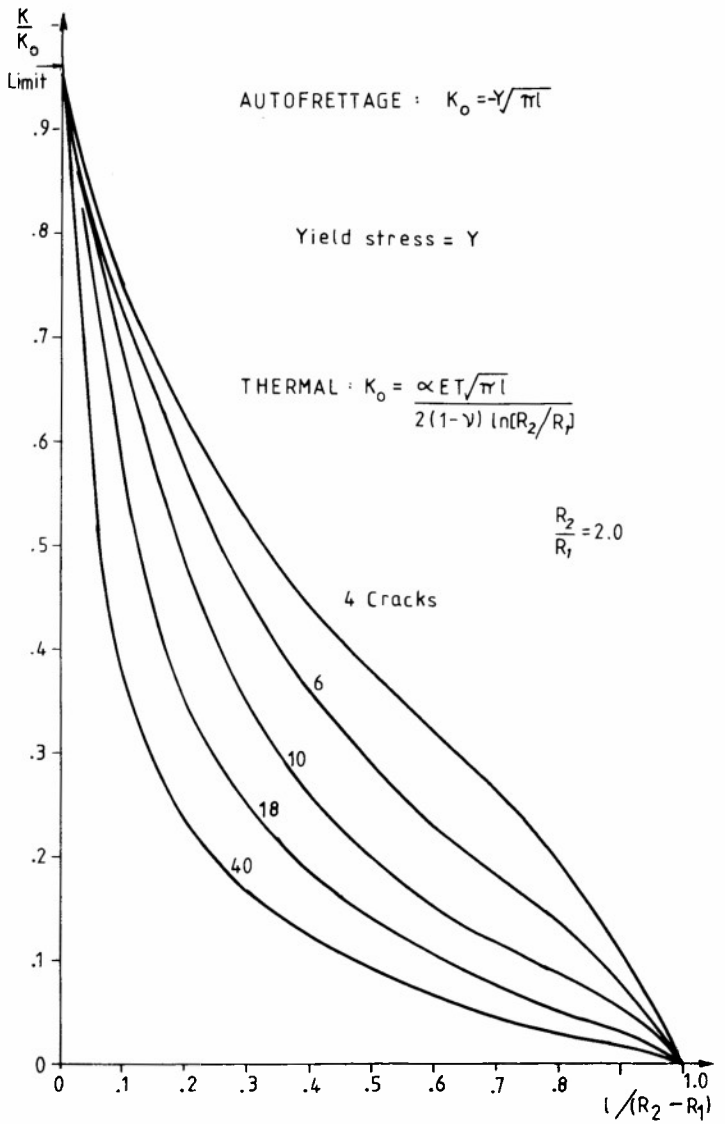

Figure 4: Stress Intensity Factors for Autofrettaged or Thermally Stressed Thick Cylinder.

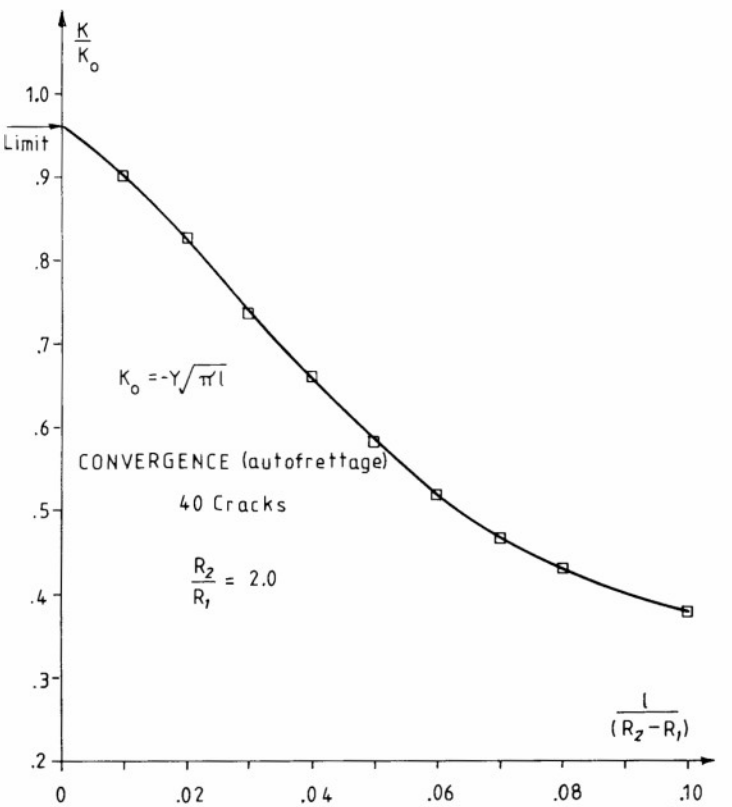

Figure 5: Short Crack Length Convergence Characteristics - Autofrettaged Thick Cylinder.

DIFFUSION BONDED ROTATING BAND ON TITANIUM BASE PROJECTILE

JACOB GREENSPAN
Metallurgist
Army Materials and Mechanics Research Center
Watertown, Massachusetts 02134

EXTENDED ABSTRACT

INTRODUCTION

Traditionally, rotating bands of copper have been attached to steel projectiles mechanically, by swaging. More recently they have been attached to the steel base metallurgically, using weld overlay and also friction welding techniques. The development described in the following however is of attachment to a titanium shell by diffusion bonding. This was performed in support of the XM 785, a 155 mm projectile of advanced design.

The rotating band of a projectile performs the important function of providing spin and also obturating the propellant gases that launch the projectile into flight. In conforming with the rifling geometry of the gun tube the band material must flow plastically, and remain cohesive. At the same time the band must remain securely attached to the projectile. The propellant gas pressures in the gun tube may reach 65 ksi, the linear acceleration 17,800 G's and the radial acceleration 340,000 rad/sec^2.

Though basic feasibility has been demonstrated in firing tests, a number of instances of bands detached have arisen. These are related in part to process inadequacies in the following summary:

PROCESSING

Projectile bodies of Ti-6-6-2 alloy were fabricated by a forge, heat treat, and machining approach, and then rotating bands were diffusion bonded to the bodies by a hot isostatic pressing approach. Table I shows properties of the titanium base for the severe stress environment.

Rotating band material was either copper or copper - 10% Zn alloy ("gild metal"). To produce a bond of required infallibility on the full scale geometry of the XM 785 components a hot isostatic pressing (HIP) approach was selected. This process employs an isostatic pressing medium of hot inert gas, which acts effectively on the configuration. In practice, the band-shell assembly, was thoroughly cleaned, sealed in a jacket impervious to the pressing medium, and was subjected to a temperature - pressure - time cycle of 1200°F and 15,000 psi for one hour in a HIP autoclave chamber. Two essential factors in this process are (1) that the surfaces be clean and free of diffusion barriers, and (2) that the jackets be leak tight to maintain pressure at the band-body interface. In this case, distinct contours form, as in Figure 1, and thus provide an early indication of proper operation.

EVALUATION

Bodies were then separated from the jackets and submitted for non-destructive evaluations of the bond. A conventional ultrasonic pulse echo immersion technique was used. Figure 2 shows typical traces of bonded and unbonded areas.

However, the C scan provides no quantitative information on bond strength. For this a destructive test was used. Cylindrical samples of 3/4" diameter were trepanned from selected areas of test rings and tested in shear. Futher, the entire band was sheared from the ring, ("push test"), to obtain the overall strength of the bond. Figures 3 and 4 illustrate components of the "push test", and also show areas from which small shear test samples were trepanned. Figure 5 shows a photomicrograph of the diffusion bond.

FIRING TESTS

Projectile bodies with C scans indicating no unbond were submitted for firing test. Figure 6 shows the band intact on launch, and Figures 7 and 8 show the band intact on recovery. However, C scans of recovered bodies show various types of damage incurred. One type, observed visually as well as by C scan is the "worm hole", in some cases traversing the entire band seat. This is believed to be the result of concentrated gas jetting, or other propellant gas turbulence. Another type is the "island", apparently the rupture of weak areas, believed related to diffusion barriers.

Figure 9 shows a shattered body, with portions of the band separated on hard impact, again indicating non-uniformity in the diffusion bond.

Figures 10, 11, 12, and 13 show various degrees of erosion, and partial rupture of the diffusion bond, that occured in tests from worn gun tubes. In these cases, rocking on the longitudinal axis appears to have added to the deteriorating effects noted above.

Figure 14 shows a total band separation on launch, where defected bond areas finally exceeded a critical level of tolerance.

REMARKS

The structural behavior of the band is thus seen to be marginal with respect to the relatively extreme load environment in the gun tube.

From the metallurgical and processing point of view, as well as from the tests noted, it is evident that the bond between the rotating band and the body is not yet optimum.

The following corrective actions, to improve the bond are being investigated:

(1) Exclude vapor blast in precleaning operations, and substitute a chemical etch.

(2) Degas band material preliminary to hot isostatic pressing, as a possible source of diffusion barriers.

(3) HIP for longer time and/or higher temperature.

It is believed that these investigations will prove effective.

TABLE I - HEAT TREATMENT AND MECHANICAL PROPERTIES
Ti-6-6-2 BASE SECTION, PROJECTILE XM-785

Identification Number	Heat Treatment	YS 0.1%	T. S.	%EL	%RA	Ft-Lb Charpy-40F
05-51-2-7X	1600°F 1-1/2 hr WC	178,500	189,400	8.5	26.0	7.5
	1075°F 4 hr AC	179,400	189,800	10.6	30.8	6
05-51-2-10X	"	(See Note 1)				
05-72-3-12X		(See Note 1)				
05-72-3-14X	1650°F 1-1/2 hr WQ	164,100	171,200	11.3	43.8	7.8
	1175°F 4 hr AC	163,000	171,300	11.3	49.1	8.4
05-72-3-15X	"	(See Note 2)				
05-72-3-16X		(See Note 2)				
05-72-4-17X	1650°F 1-1/2 hr WQ	177,800	179,800	10.1	30.6	6.7
	1150°F 4 hr AC	177,300	179,300	10.1	34.4	7.8
05-72-4-18X	"	(See Note 3)				
05-72-4-19X	"	(See Note 3)				
05-72-4-20X	"	(See Note 3)				
05-72-4-21X	"	(See Note 3)				

NOTE 1 : Mechanical Properties for 10X x 12X are represented by 7X
NOTE 2 : Mechanical Properties for 15X x 16X are represented by 14X
NOTE 3 : Mechanical Properties for 18X, 19X, 20X and 21X are represented by 17X.

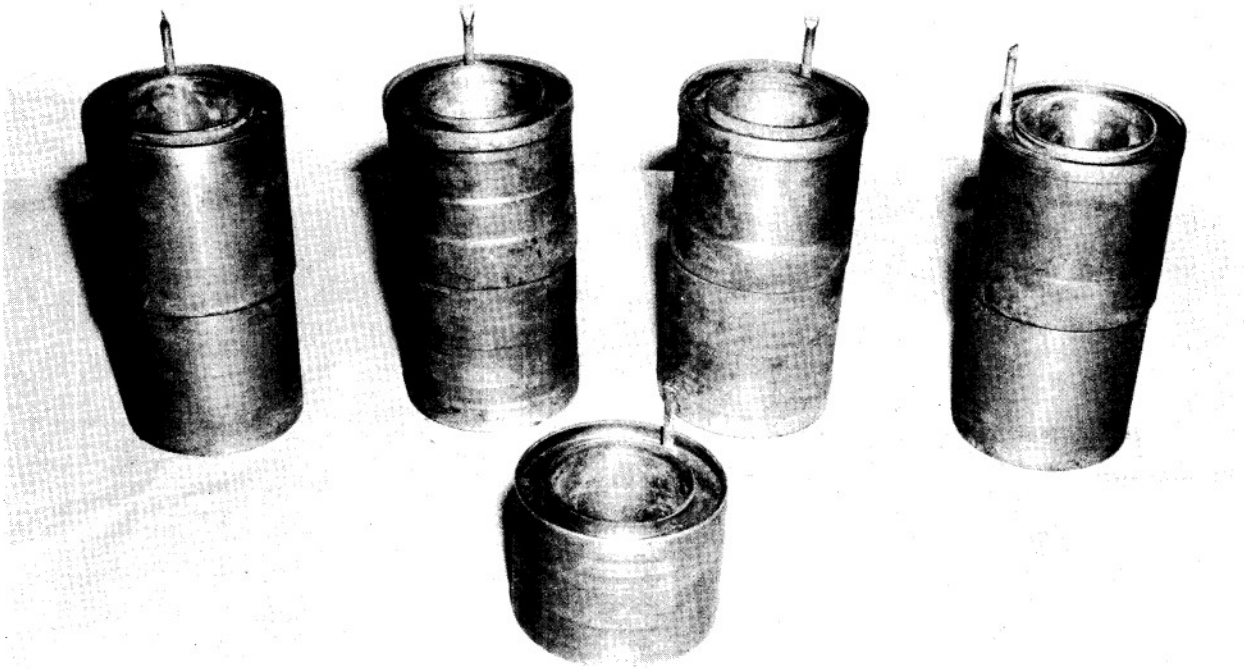

Figure 1. HIP'D UNITS

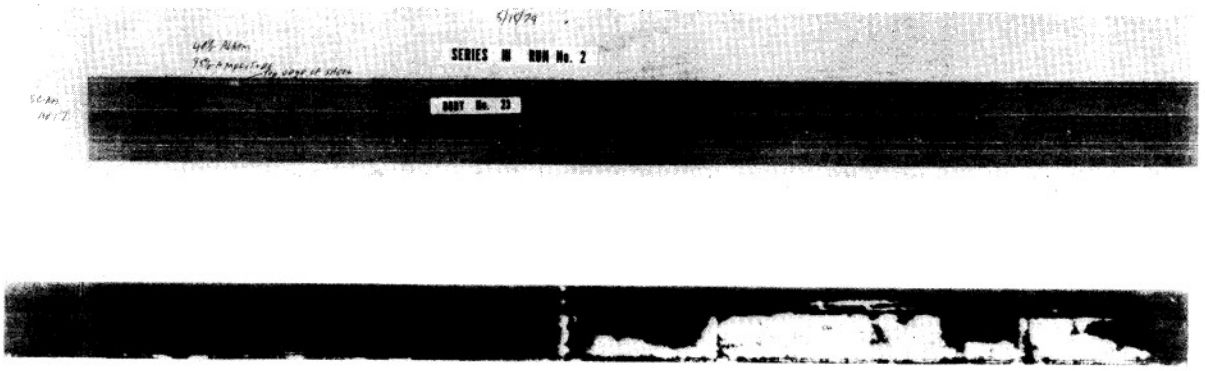

SERIES NO. I
Run No. 3, Sample No. 1
Rocket Body No. 7

25MH$_2$ S-80 Reflectoscope
C-scan after HIPPING scan
from the outside.

SERIES NO. I, Run No. 1, Sample No. 1

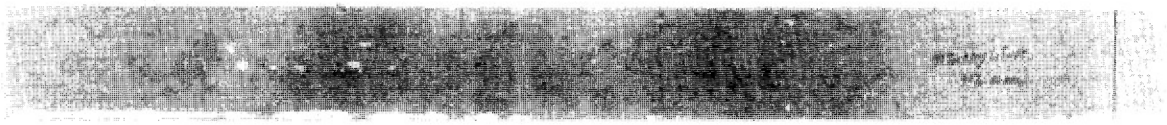

Figure 2. ULTRASONIC SCANS

Figure 3

Figure 4

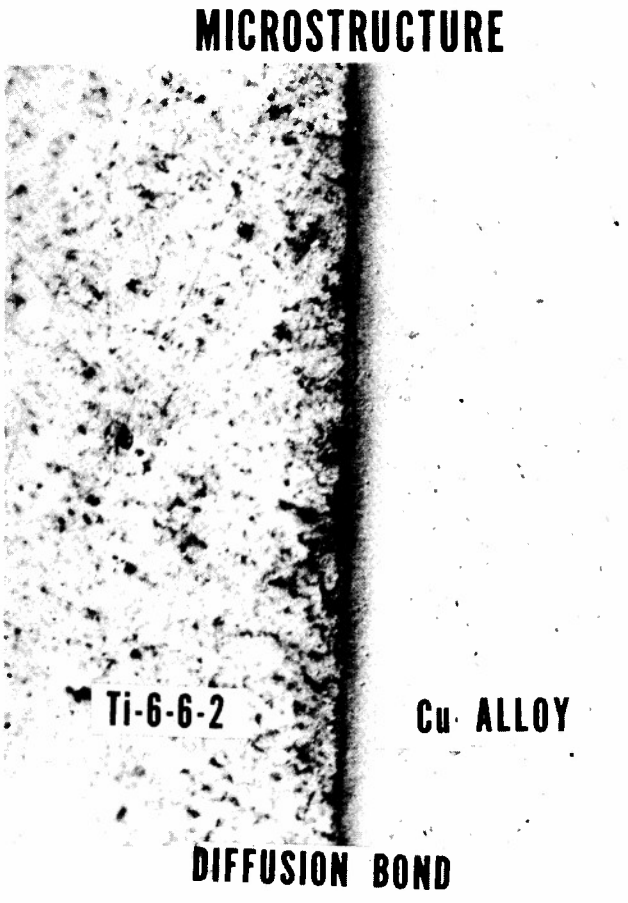

Figure 5. ROTATING BAND - Ti ALLOY BASE

Figure 6. XM 785 BRAZE BANDED SHELL TEST FIRING NO. 1

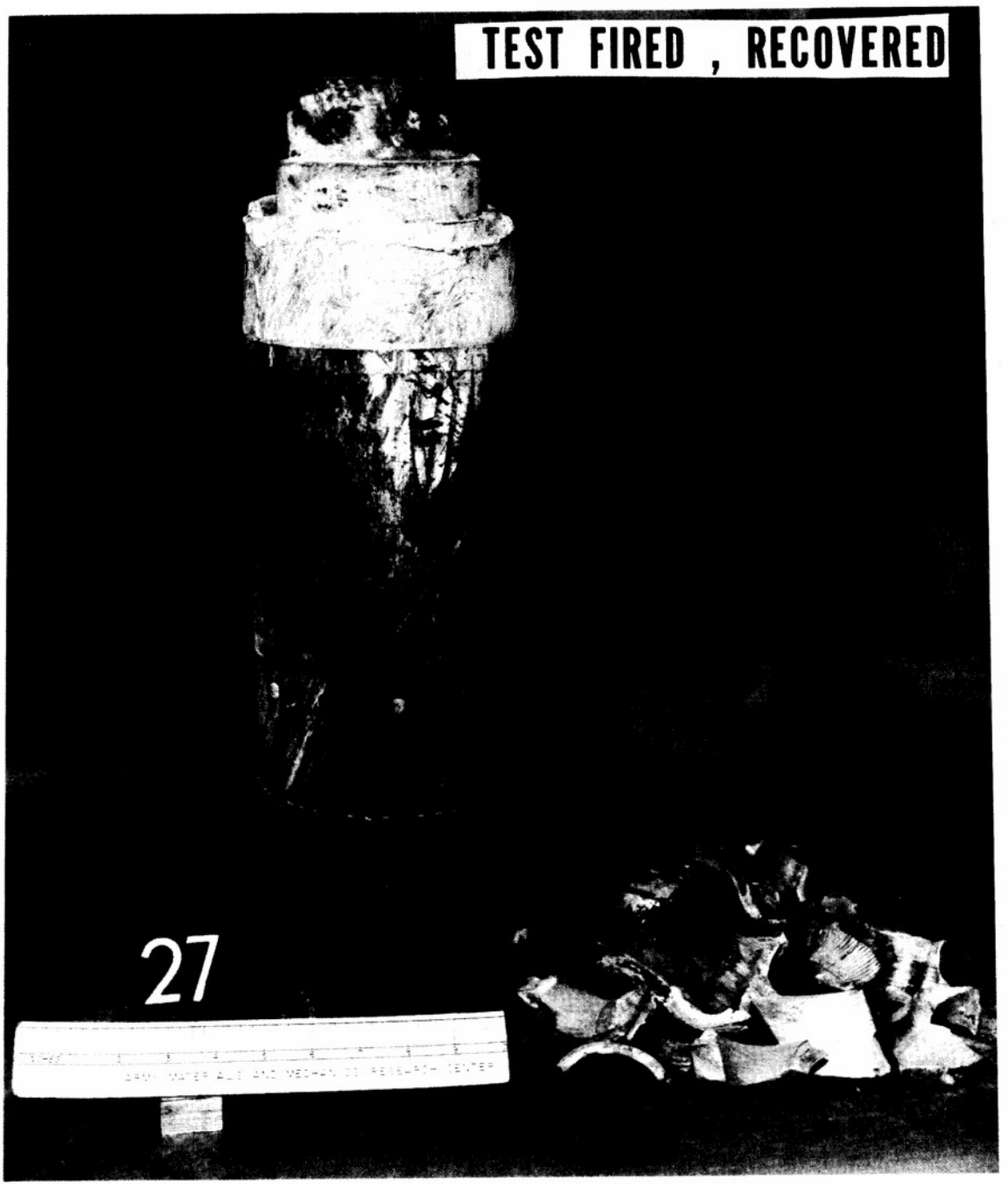

Figure 7

Figure 8

Figure 9

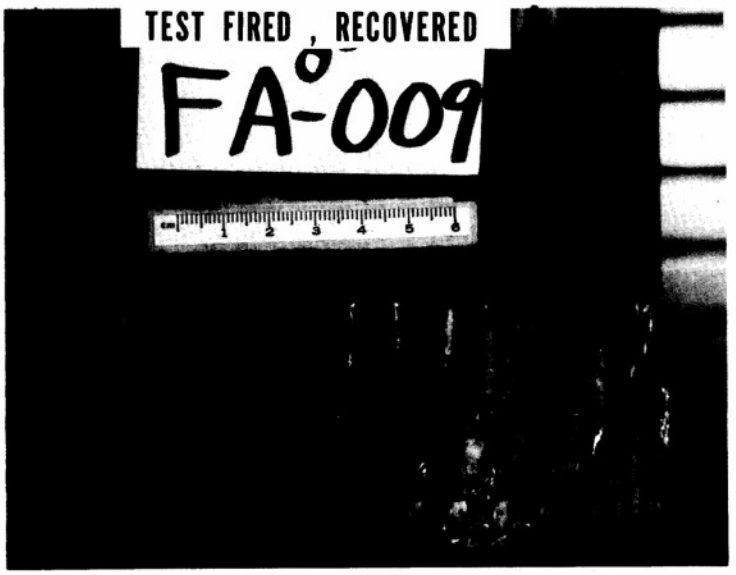

Figure 10

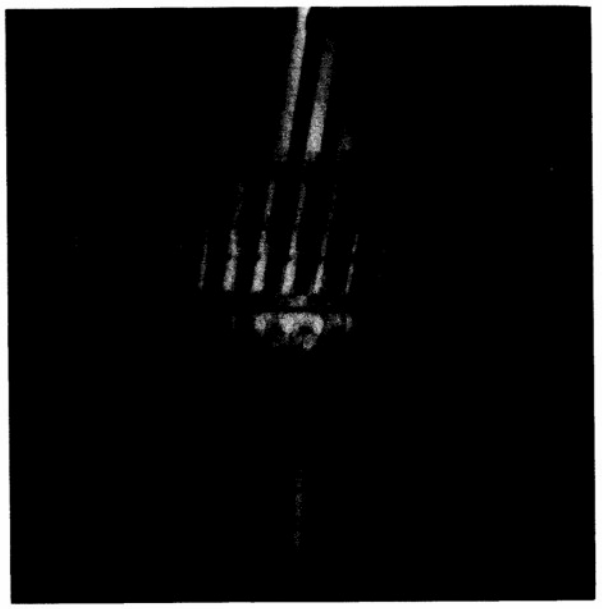

Figure 11. TEST FIRED, RECOVERED

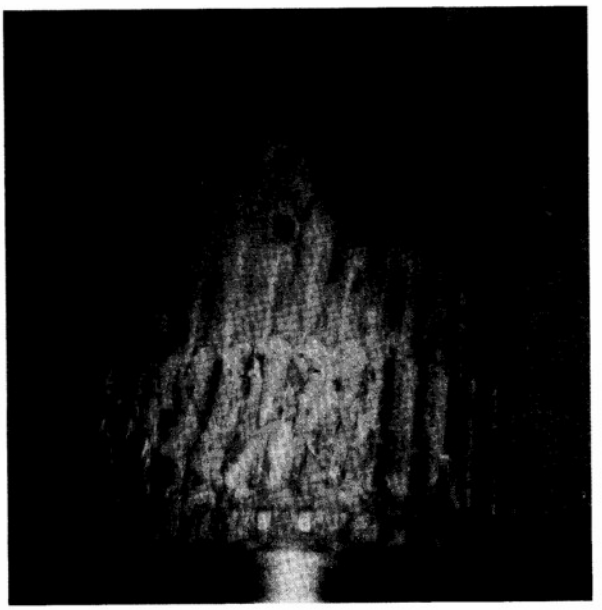

Figure 12. TEST FIRED, RECOVERED

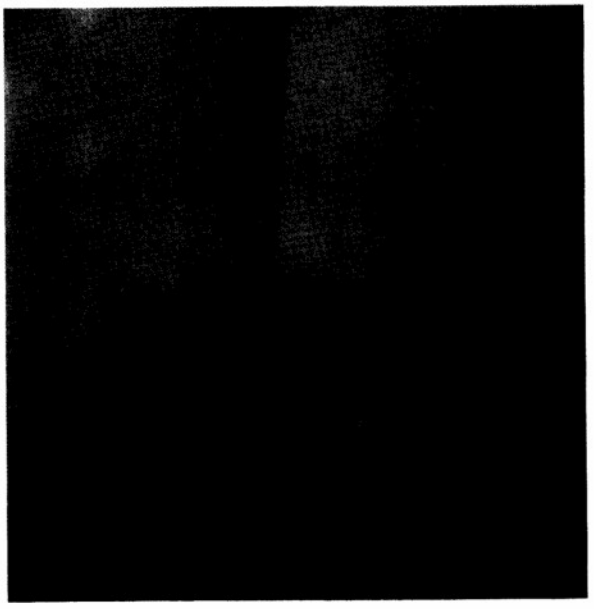

Figure 13. TEST FIRED, RECOVERED

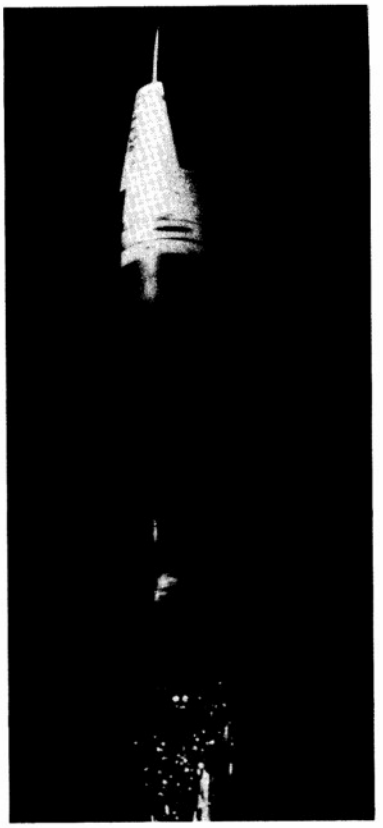

Figure 14. IN LAUNCH

MEASUREMENT OF TORSIONAL IMPULSE AND PROJECTILE BALLOTING FOR ARTILLERY FIRED PROJECTILES USING IN-BORE TELEMETRY*

GERALD A. BENEDETTI
Mechanical Engineer

PAUL E. NIELAN
Mechanical Engineer
Sandia National Laboratories
Livermore, California 94550

EXTENDED ABSTRACT

For a number of years it was assumed the rigid body axial and angular accelerations sustained by an 8-inch diameter projectile during gun firing occur simultaneously and these accelerations result in quasi-static† structural responses of the projectile except during barrel exit. The simultaneity of these accelerations implies the rotating band on the aft end of the projectile is initially engraved (approximately) into the tube rifling. When this is the case, calculations indicate a low coefficient of static friction is required at the joint interface, shown in Figure 1, to transmit the inertia torque resulting from the angular acceleration. The coefficient of friction, μ, is proportional to the ratio of angular ($\ddot{\theta}$) and axial (a_x) accelerations. That is,

$$\tilde{\mu} = \frac{r_{ave}\,\ddot{\theta}}{g\,a_x} \sim \frac{\ddot{\theta}}{a_x} .$$

However, in December 1976, a structural failure of the interface joint lead to the hypothesis that the rigid body axial and angular accelerations are not initially simultaneous. That is, the rotating band is not initially engraved (approximately) into the tube rifling. Subsequent investigation established the rotating band design was such that the forward point on the rotating band contacted the forcing cone one-inch aft of the origin of tube rifling. Further gun testing of the same joint and rotating band resulted in several structural failures of the joint (refer to attached photographs, Figures 2 and 3).

It was concluded the joint failures were caused by the non-simultaneity of the axial and angular accelerations and occur at early times (within the first two to four milliseconds) in the gun launch environment. The rotating

*Work supported by the U. S. Department of Energy under Contract DE-AC04-76DP00789.

†The "load" application times are long relative to the fundamental periods of oscillation for the projectile.

band design allowed the projectile to displace axially (about one-inch) before the rotating band engaged the origin of tube rifling. There is, associated with this axial displacement, an axial velocity and axial acceleration of the projectile. However, since the rotating band is not initially engraved into the tube rifling, there is no corresponding rotational motion associated with the axial motion. Consequently, when the rotating band engages the rifling, the projectile suddenly experiences a torsional impulse which results in an angular velocity. The time rate of change of the torsional impulse results in an angular acceleration which can be very large and depends primarily upon the axial velocity of the projectile and the time history of the impulse. The initial large angular acceleration, which may result in a dynamic torsional response of the projectile, causes a large inertia torque to be generated at a time when the axial acceleration is relatively low (perhaps 2000 to 3000 G's). Consequently, an abnormally large coefficient of friction is required to transmit the inertia torque across the interface joint. If the coefficient of friction for the interface joint is too small, the joint will undergo a rotational slip and failure of the joint occurs.

Decreasing the axial "free run" by reducing the outside diameter of the rotating band does not completely eliminate the torsional impulse and its associated problems. As the tube wears, the most pronounced wear occurs in the region of the origin of tube rifling. This results in conditions analogous to a rotating band with too large an outside diameter. That is, the projectile can attain a significant axial velocity with no corresponding rotational velocity and thus experience a very large torsional impulse when the band engages the "not too worn" tube rifling.

If the interface joint, shown in Figure 1, is simply made "stronger" and the basic problem not addressed, the failure mode may shift to some other area within the projectile. For example, other structural joints and components mounted within the projectile would sustain inertia torques and forces generated by large angular accelerations resulting from the torsional impulse.

A potentially serious problem, particularly at cold temperatures,† may be the explosive charge within the projectile. Consider the case where the axial and angular accelerations are not initially simultaneous. That is, a large angular acceleration occurs which generates a large inertia torque on the explosive charge at an early time in the launch environment (within the first two to four milliseconds), when the axial inertia force on the explosive charge is relatively low. If the design relies on the static coefficient of friction to "spin up" the explosive charge, it is then possible for the projectile case to spin about the charge. This may result in preignition of the charge either in or out of the tube.

Assuming the charge does not ignite, the different angular velocities of the rotating parts may have a pronounced effect on the flight of the projectile. For example, if the explosive charge "clutches up" after barrel exit due to large centrifugal forces, the angular velocity of the projectile will decrease to conserve angular momentum. Hence, the reduced angular speed

†At cold temperatures, the explosive charge contracts away from the cylindrical walls of the projectile case.

of the projectile may affect its gyroscopic stability and subsequently its ballistic flight.

The potential problems described above are by no means complete, but they do serve to illustrate the potential seriousness of a large torsional impulse which is not accounted for in the original projectile design.

Although the above discusses torsional impulse for an 8-inch diameter rifled tube, it is unrealistic to infer that a significant torsional impulse exists only in 8-inch diameter tubes. On the contrary, it is very likely large torsional impulses can occur in worn rifled tubes of various diameters. In addition, if the forward point on the rotating band contacts the forcing cone aft of the origin of tube rifling by one or more inches, large torsional impulses can also occur in new tubes.

Since the angular accelerations associated with a torsional impulse had not yet been measured, a limited testing program was initiated in mid-1978. The primary objectives were to determine the torsional impulse environment and to determine if significant projectile balloting exists for 8-inch and 155 mm projectiles during gun launch.

We have been using telemetry systems on-board projectiles to collect in-bore and free flight data associated with launching them from howitzers. During the past year and a half we have been collecting in-bore data pertaining to torsional impulse and projectile balloting in both new and worn 8-inch and 155 mm gun tubes.

The measured data is continuously transmitted to a down range receiver from the projectile which is subsequently recovered along with the telemetry system by an on-board parachute recovery system. Consequently, most of the projectile and telemetry system is reused.

The measured quantities include base pressure, axial acceleration, tangential acceleration, and axial strains in beams located in the projectile as shown in Figure 4. These strains can be calculated theoretically and from comparing the predicted dynamic beam strain time histories with the measured ones, we have determined that torsional impulse (not projectile balloting) is primarily responsible for initiating the measured dynamic lateral response of the beams.

Some results associated with the testing program will be presented and additional tests associated with the 155 mm projectile will be discussed.

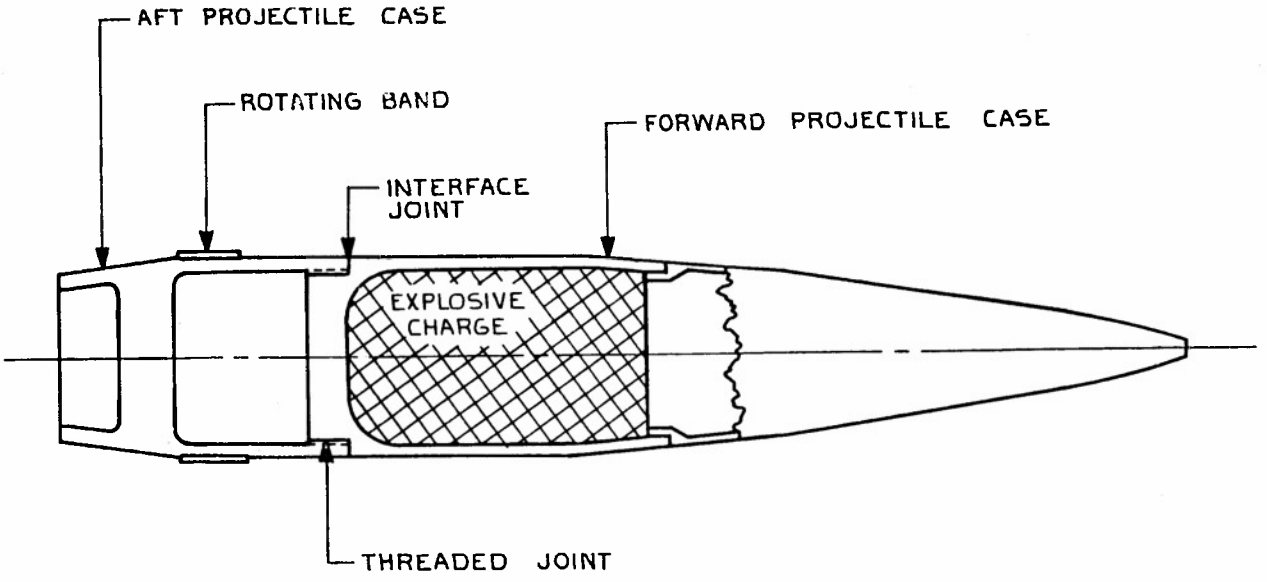

Figure 1. Illustration of Projectile and Threaded Interface Joint

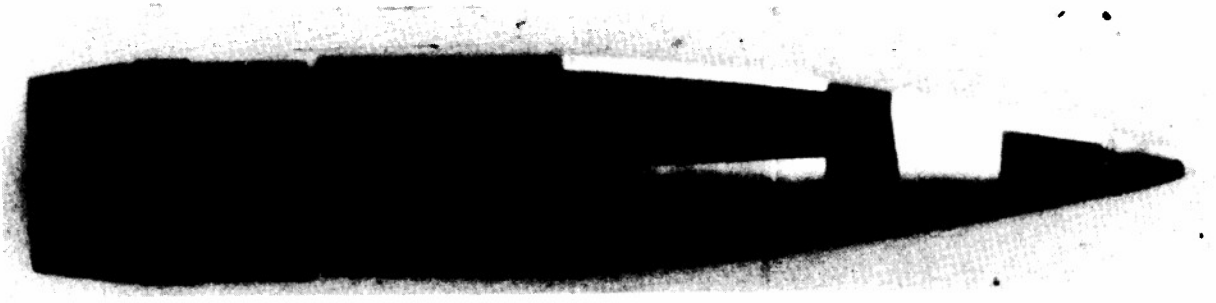

Figure 2. Failure of Interface Joint

Figure 3. Failure of Interface Joint

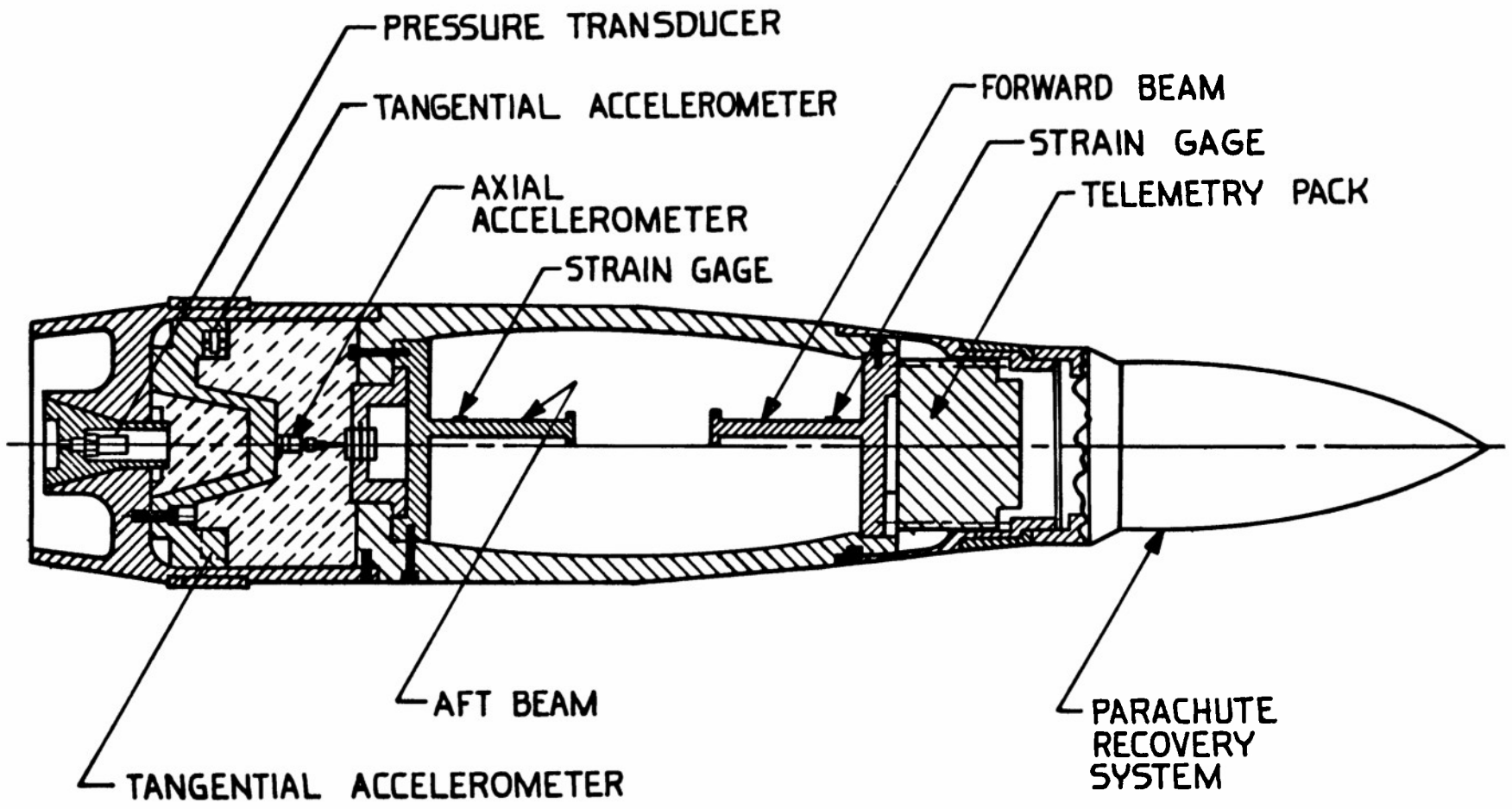

Figure 4. Illustration of the Test Projectile and Instrumentation

THREE-DIMENSIONAL FINITE ELEMENT ANALYSES FOR STRUCTURAL JOINTS OF ARTILLERY PROJECTILES

T. TSUI
Mechanical Engineer
Army Materials and Mechanics Research Center
Watertown, Mass. 02172

The structural joints of artillery projectiles are subjected to extremely high loads during launching. These include axial load due to linear acceleration and tensional load due to angular acceleration as a result of the spin induced by the rifling.

The objective of this work is to exploit and extend as required selected structural analyses and computer codes to advance the state-of-art capability for 3-D analysis of a complex family of structural joint systems. In particular, this study will address structural joint problems of the type being encountered in the nuclear projectiles, XM-753 and XM-785 and conventional counterparts, XM-650 and XM-549; in which threaded joints have uncertain reliability and the need for field disassembly and reassembly of projectiles has become an important requirement. Initially the basic pinned lap-butt joint configuration, commonly used in the design of artillery projectiles, will be addressed.

Since the pinned joint structural problems are contact problems, the interaction between the pins and pinholes becomes nonlinear in nature. In additon, a large number of three-dimensional finite elements must be employed to model the joint in order to adequately determine the stress conditions in the region of the joint. The method of substructure is selected for the analysis in order to reduce the large amount of computing time required by the nonlinearity and the large number of three-dimensional elements encountered in the present problem.

The pinned joint under investigation is divided into three different substructures. Their nodes and finite element meshes have been completely defined and correctly verified with the aid of plots generated by the computer.

Present effort has been focused on the solution of the basic pinned lap-butt joint problem. The results of the solution will be compared with those obtained in the photoelastic study.

RELIABILITY ANALYSIS OF THE XM 753 ROCKET MOTOR PIN JOINT UNDER EXTREME LOADING CONDITIONS

R. VAICAITIS
Professor

M. SHINOZUKA
Renwick Professor of Civil Engineering
Columbia University
New York, N.Y. 10027

EXTENDED ABSTRACT

A multivariate probabilistic reliability model for the XM 753 projectile rocket motor to bulkhead joint under extreme loading conditions is constructed. The reliability assessment is based on the probability of survival for each mission made and is estimated by carrying out a probabilistic failure analysis, which accounts for available statistical data. For those cases where no statistical data are available, calculations are made using several typical dispersion values. The model considers the effects of the gun firing environment, rocket motor-on in the flight environment and interaction of the pin interference with the sealing surface of the joint.

The mathematical assessment of the joint reliability is based on available statistical information of the various system parameters. These parameters include axial and angular accelerations, spin rate, internal pressure due to rocket-on, tolerances of interference fits, local deformations of the sealing surface and gas leakage under high internal pressure during flight. In addition to the inherent randomness of these parameters, the uncertainties such as the errors associated with imperfections in the estimation procedures and the analytical model itself are treated as random variables and included in the reliability formulation. Implicit in this formulation is the Bayesian approach which provides a logical basis on which (subjective) engineering judgement and the information contained in the statistical data can be combined. Furthermore, this approach makes it possible to accomodate a provision to update the data base as more subjective or statistical data become available.

A preliminary estimate of the structural reliability of the rocket motor to bulkhead joint of the XM 753 projectile is approximately 0.99999. This estimate is based on the following conditions: (1) Maximum firing and flight environment; (2) Normal distributions for all the constitutive system variables; (3) 5% statistical variations of the variables for which no statistical data is available at this time; (4) Installation of pins and snap rings according to design specifications; (5) No effect on the ballistic flight stability if some of the pins are lost during the barrel exit stage; (6) No significant amount

---

The work reported herein has been supported by the U.S. Army under Contract No. DAAG-46-80-C-0001.

of additional bulging of the C-seal surface is induced due to high gas pressure during the rocket motor-on; and (7) The maximum allowable bulge height of the seal surface is 0.00025 in. The main findings of this preliminary study include: (1) From the analysis of available experimental data, it is observed that in most cases the statistical dispersions of the constitutive system variables are very small. Such small variations suggest a high degree of tolerance requirements and good quality control during the manufacturing process of the hardware. (2) Usage of worn gun tubes to fire this projectile could induce free-run, increasing the torsional impulse and reducing the survival reliability of the projectile. (3) If the standard pin installation requirements are satisfied for the given design tolerances, the probability of losing even a single pin per projectile during the barrel exit is extremely low. (4) Omission of a snap ring from the pin installation assembly could result in a high probability of losing the corresponding pin. If no snap rings are installed for all sixteen pins (or improperly installed), it would give a high probability of losing several pins per projectile during the barrel exit stage. (5) Pin interference and application of the proof pull test load for each pin after installation increases pin retention reliability. However, this positive effect may be of secondary importance since the snap ring provides the main retention force. (6) If additional bulging of the seal surface is produced due to internal high gas pressure during the rocket motor-on stage, the reliability of the C-seal performance may decrease to unacceptable levels for the present allowable bulge height requirement of 0.00025 in. The effect of additional bulging and leakage criteria of the C-seals under high internal gas pressure needs to be investigated in more detail. It is highly recommended that both experimental and detailed analytical studies of the C-seal performance be conducted.

SHAPED-CHARGE PENETRATION BEHAVIOR ASSOCIATED WITH NON-MONOLITHIC MATERIALS

John N. Majerus
Research Engineer

William P. Walters
Mechanical Engineer

U.S. Army Armament Research and Development Command
Ballistic Research Laboratory
Aberdeen Proving Ground, MD 21005

ABSTRACT

In studies regarding terminal-ballistic effects of shaped-charge warheads, the shaped-charge jet performance along the shot-line into a target must be assessed. This involves calculating the penetration capability of the jet as it passes through two or more materials, one of which may be a gas or liquid. This paper deals with a model developed for predicting the penetration of a stretching hypervelocity jet of solid material which breaks into a series of particles at some time after the formation of the jet.

The basic penetration model is a one-dimensional model called WAM [1]. This model has been shown to yield good predictions of penetration versus time, and penetration versus standoff behavior* for monolithic metallic materials [2]. Figure 1 illustratates the predictive capability of the model for a relatively short copper-jet with a tip velocity of 4.7 km/s impacting a hard steel (BHN 364-377). Figure 2 shows a comparison between experiment and theory for a slightly shorter aluminum-jet with a tip velocity of 8.1 km/s into the same type of steel.

The basic characteristics of the jet used in the model are the tip and rear velocities, average diameter, jet density and strength, virtual origin, and the average time for jet breakup. All of these jet characteristics can be measured using sequential flash-radiographs of the jet. Therefore, in general there are no undetermined jet characteristics for "fitting the data", and the comparisons shown in Figures 1 and 2 involved no attempts to "curve fit" the data.

* *The standoff is the distance from the base of the charge to the top of the target material.*

The required target-material characteristics are density, strength, geometry, and viscosity. The viscosity coefficient is necessary since drag stress terms, or strain-rate effects, are incorporated into the model. This viscosity coefficient may be obtained from separate dynamic tests [3], or determined from monolithic penetration data obtained at a single standoff distance from the base of the shaped-charge liner. Hence, penetration performance of a jet can be determined using a minimal amount of experimental data.

The basic model has been modified for non-monolithic materials, and can consider both layers of different materials and air spaces. The modified model allows one to predict penetration versus time behavior, jet tip-velocity at any axial location within the material, and the final depth of penetration into the material. The modified model was applied to a variety of non-monolithic materials which include air spaces, and the velocities of the exiting jet in the air space are compared with radiographically measured velocities. Also, the depths of penetration into the last layer of material are calculated and compared with experimental results.

To date, the comparison between the experimental data and the predictions for non-monolithic targets exhibit good agreement both in terms of exit-velocities and final penetration depths. However, further comparisons with a broader experimental data base are necessary before the full utilization of the model will be established.

---

[1] *W. Walters and J. Majerus, "Hypervelocity Impact Models for Hole Growth and Geometry", Proceedings of the Third Annual Vulnerability Survivalibility Symposium, Naval Amphibious Base Coronado, San Diego, CA, November 1977.*

[2] *W. Walters and J. Majerus, "Shaped-Charge Penetration Model, Part I. "Monolithic Penetration and Comparison With Experimental Data", Technical Report ARBRL-TR-02184, August 1979.*

[3] *W. Walters, "Influence of Material Viscosity on the Theory of Shaped-Charge Jet Formation", Memorandum Report, ARBRL-MR-02941, August 1979.*

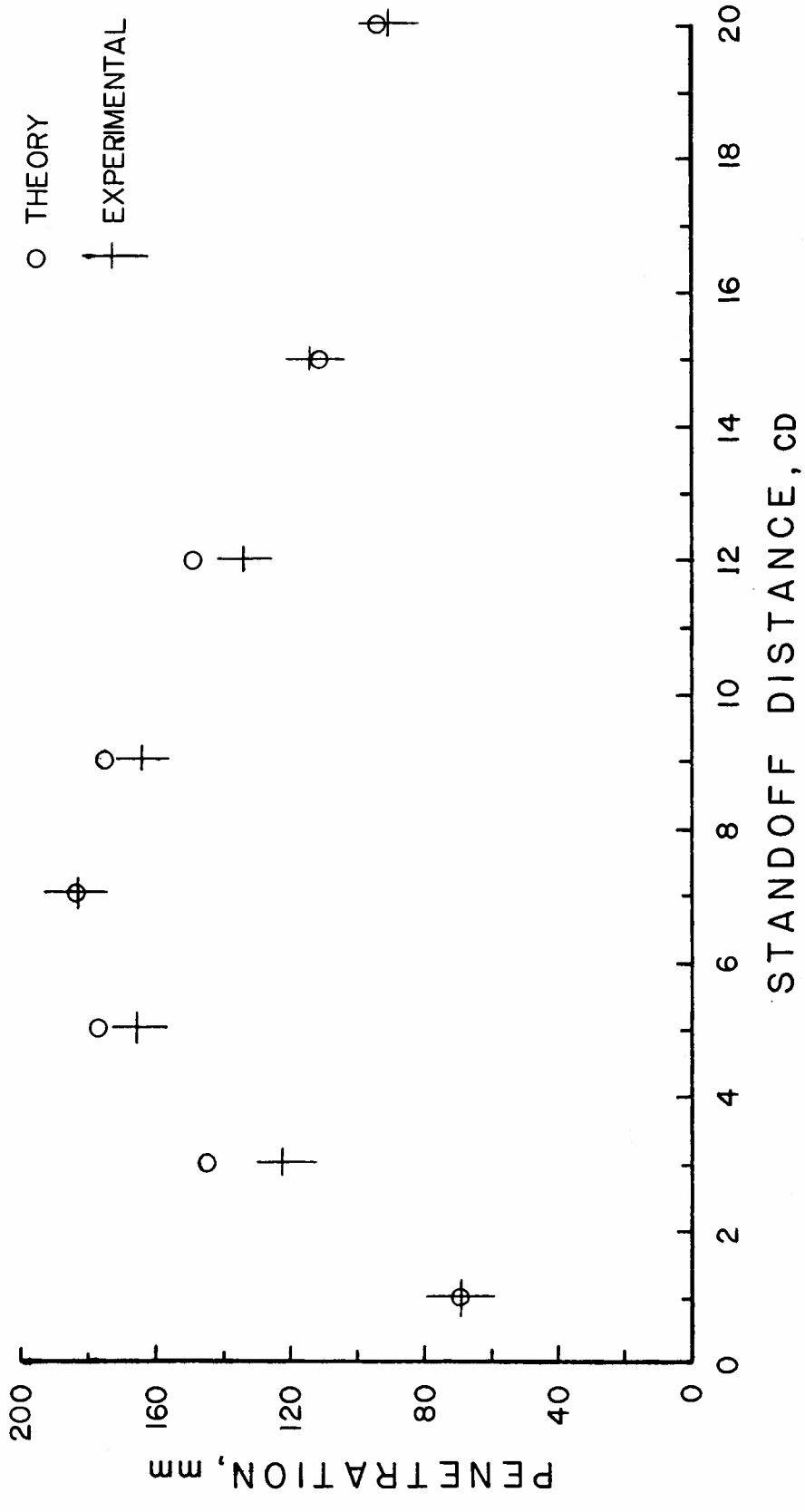

Figure 1. Analytical and experimental penetration versus standoff curve for a copper jet impacting a steel target.

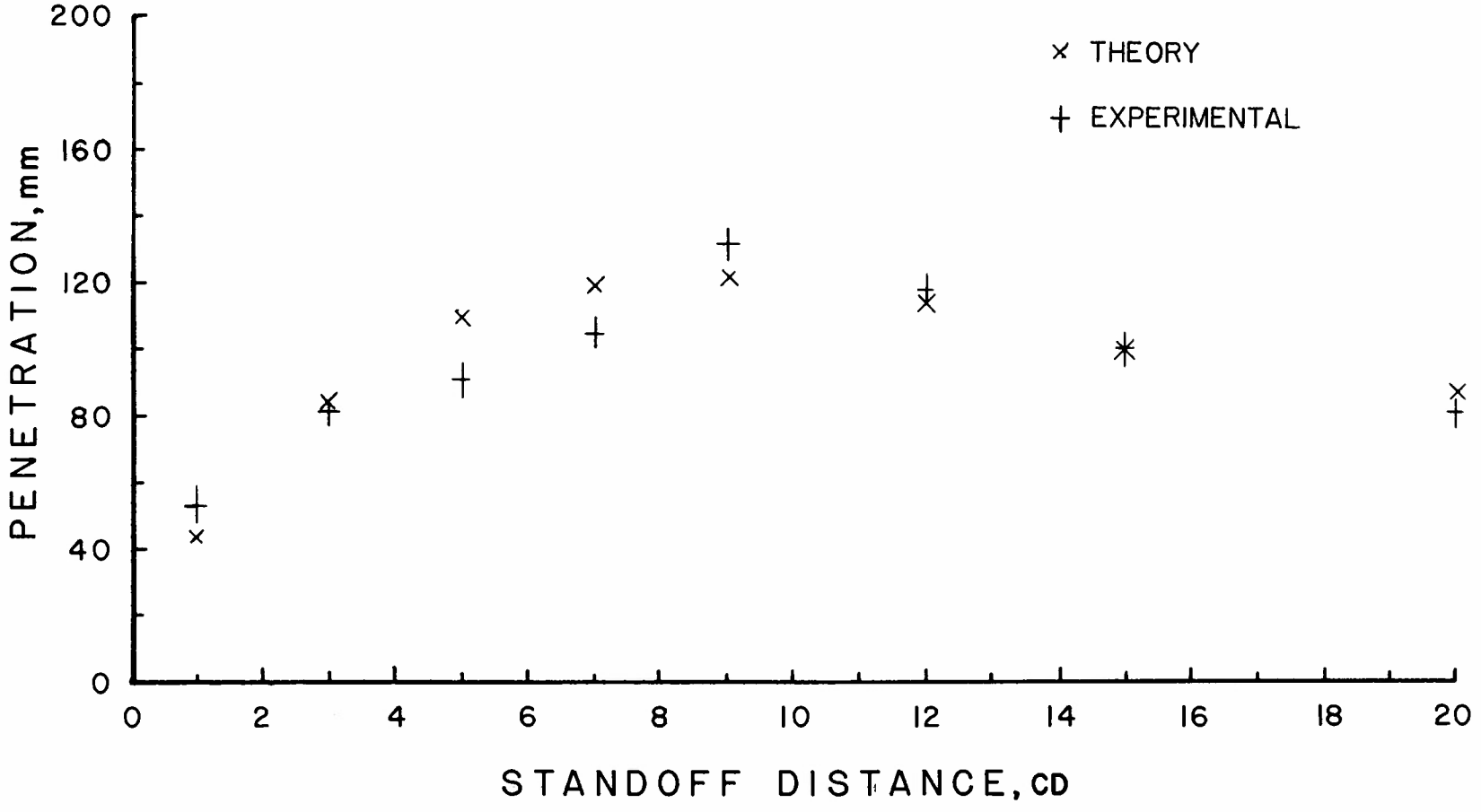

Figure 2. Analytical and experimental penetration versus standoff curve for an aluminum jet impacting a steel target.

MATERIALS CHARACTERIZATION FOR COMPUTATIONS INVOLVING SEVERE DYNAMIC LOADING

GORDON R. JOHNSON
Engineering Fellow
Honeywell Defense Systems Division
Hopkins, Minnesota 55343

EXTENDED ABSTRACT

Numerical simulations are being used more frequently for severe dynamic loading conditions such as impact and explosive detonation. An example of an EPIC-3 simulation is shown in Figure 1, where an explosive device accelerates a metal self-forging fragment. Although there are many computer codes available to perform various simulations, in many instances the material models and associated input data are not adequate.

In distinguishing "dynamic" material properties from "static" material properties, the strain rate is often assumed to be the most important variable. Often associated with high strain rates, however, are large strains, high temperatures and high pressures, as is the situation in Figure 1. Therefore, it is important that the effects of each variable be properly assessed, rather than assuming all distinguishing characteristics are due to the strain rate alone.

The objective of the ongoing investigation is to better define the strength and failure characteristics of various metals such that more accurate numerical simulations can be performed. Specifically, it is to define their characteristics as functions of strain, strain rate, temperature, pressure and stress, since these are the important variables commonly used in the computer codes. This work is being accomplished through a program of testing and analysis. Included herein are some results involving strength characteristics at large strains and high strain rates, and a proposed damage model for failure.

STRENGTH RESULTS

Figures 2 and 3 show shear stress-strain relationships at various strain rates, for OFHC copper and 2024-T3 aluminum. These data were obtained from a dynamic torsion test facility developed by U.S. Lindholm at Southwest Research Institute and funded by Honeywell. Some desirable features of this testing technique are that the state of stress in the specimen is well defined, large shear strains can be achieved without geometric instabilities, and a wide range of strain rates can be obtained with the same testing technique (quasi-static to about 500 s^{-1}).

For the aluminum data, neither the strength nor the failure strain appear to be strongly influenced by the strain rate. The copper data show positive strain

hardening and strain rate hardening for strain rates up to 9.6 s^{-1}. For the higher strain rates, the stresses actually decrease at large strains; this is due to a thermal softening instability. Heat conduction computations indicate the tests involving strain rates up to 9.6 s^{-1} are essentially isothermal; the heat generated by the plastic flow is conducted into the massive portion of the specimen. These data are used to generate the analytic expression for the shear stress as shown in Figure 4. The extrapolated data for the higher strain rates are for an assumed isothermal condition. Since material response at high strain rates is generally not isothermal, but adiabatic, it is necessary to include the effect of thermal softening. The resulting adiabatic behavior for two assumed thermal softening relationships is also shown in Figure 4. The temperature is obtained from the work done by the plastic flow stresses. The maximum stresses are indicated to identify the strain at which the thermal softening overtakes the strain hardening. Under adiabatic conditions, it as at these strains that instabilities would probably begin to occur.

Figure 5 shows EPIC-2 computed results for the high strain rate test (330 s^{-1}), and it is clear that a thermal instability has indeed formed. This is further verified by metallographic analysis. These computed results include both plastic flow and heat conduction. Other materials being tested include RHA (rolled homogeneous armor), S-7 tool steel, 1006 steel, high purity iron, tungsten base alloy, 7039 aluminum and cartridge brass. The addition of high temperature torsion testing is anticipated such that thermal softening effects can be better defined.

Another item of importance concerns the von Mises flow rule for large plastic deformations, as shown in Figure 6. Curve A represents true stress-strain copper data obtained from a quasi-static tensile test. The equivalent tensile flow stress of curve B is slightly reduced since the true tensile stress contains a component of hydrostatic tension in the necked tensile region. Curve C represents shear stress-strain data from Figure 2 ($\dot{\gamma}$ = .009 s^{-1}), and curve D is the equivalent tensile flow stress obtained by using the von Mises flow rule. Since there is a considerable discrepancy between curves B and D, the von Mises flow rule may not be adequate for very large strains.

FAILURE MODEL

A simplified damage model for ductile failure has been defined and will be evaluated. It is summarized in Figure 7. It has the capability to take into account the effects of strain, strain rate, temperature, pressure and stress. It is path-dependent and requires only one storage variable per element. It can be applied to cases from the simplest, where failure is dependent only on strain, to the most complicated, where failure is a path-dependent function of many variables.

Referring to Figure 7, the first step is to define the failure strain, ε^f, as a function of strain rate, $\dot{\varepsilon}$, temperature, T, pressure, P, and flow stress, σ. This should be done for constant values of the variables. It is recognized that these relationships are not well-defined for most materials, but more data are being generated to better define these relationships. The damage to an element during an integration cycle is then $\Delta D = \Delta\varepsilon / \varepsilon^f$, where $\Delta\varepsilon$ is the

equivalent plastic strain during that cycle and ε^f is the failure strain under the current conditions of $\dot{\varepsilon}$, T, P, σ . The total damage is then $D = \Sigma \Delta\varepsilon / \varepsilon^f$ and failure occurs when D = 1.0.

As an example, it is assumed that the failure strain is a function of only the ratio, P/σ , as shown in Figure 7. This relationship indicates the material can be more severely strained if it is under hydrostatic compression. This trend is demonstrated by the copper data of Figure 6 where the tensile test caused failure at ε = 1.3 (hydrostatic tension), and the torsion test did not yet fail at ε = 4.0. An example shows how damage is accumulated when the strain takes place under hydrostatic compression. When the pressure is released to P = 0, D = 0.75 even though the plastic strain, ε , is greater than ε^f at P = 0.

Since this failure model is based on failure strains at constant $\dot{\varepsilon}$, T, P, σ , it is, of course, accurate under constant conditions. It is not yet known how well this model will predict failure for complicated loading paths. Although simple, the model is rational, and should provide a significant improvement over other failure models based only on plastic strain or current conditions of other variables.

ACKNOWLEDGEMENTS

This work is currently being funded by a Honeywell Independent Development Program and the Ballistic Research Laboratories. The other participants are J.H. Hoegfeldt and S.R. Nelson (Honeywell), and U.S. Lindholm and A. Nagy (Southwest Research Institute).

FIGURES

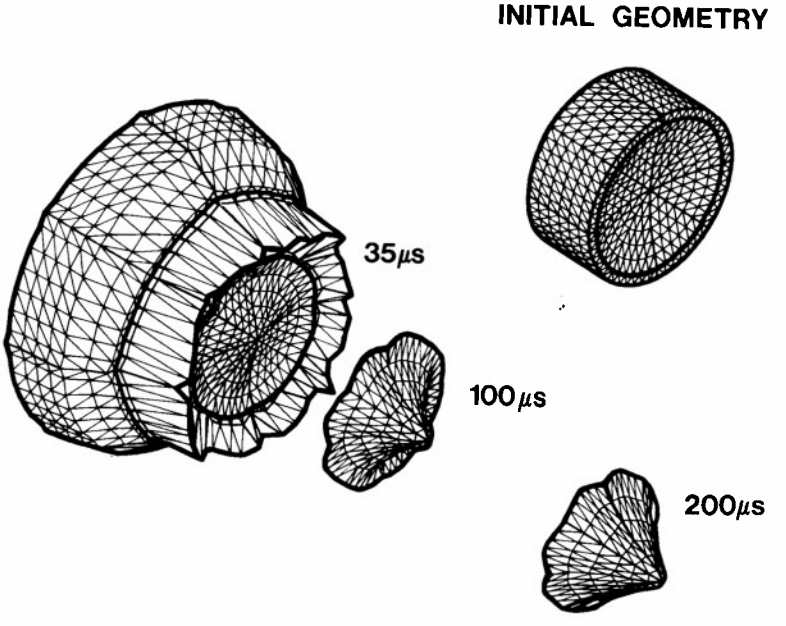

Figure 1. Explosive Detonation and Formation of a Self-Forging Fragment

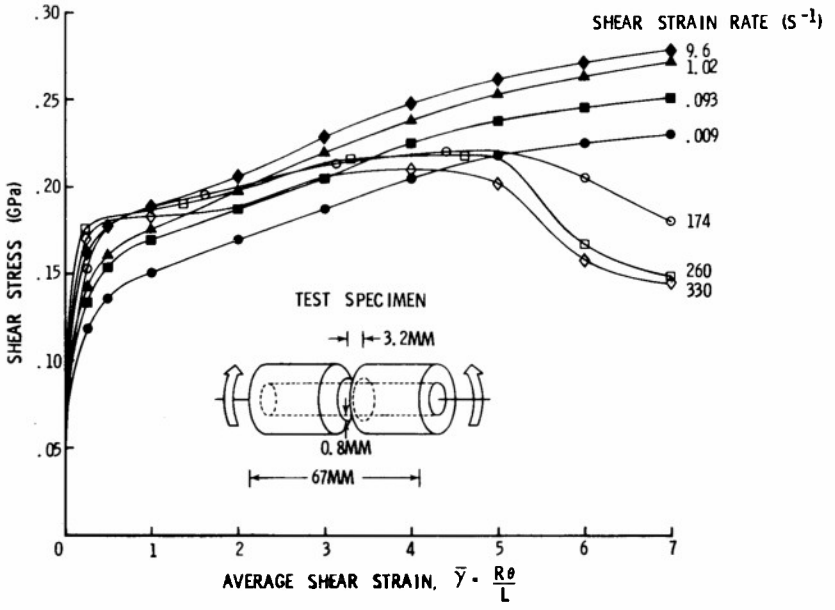

Figure 2. Shear Stress-Strain Relationships for OFHC Copper

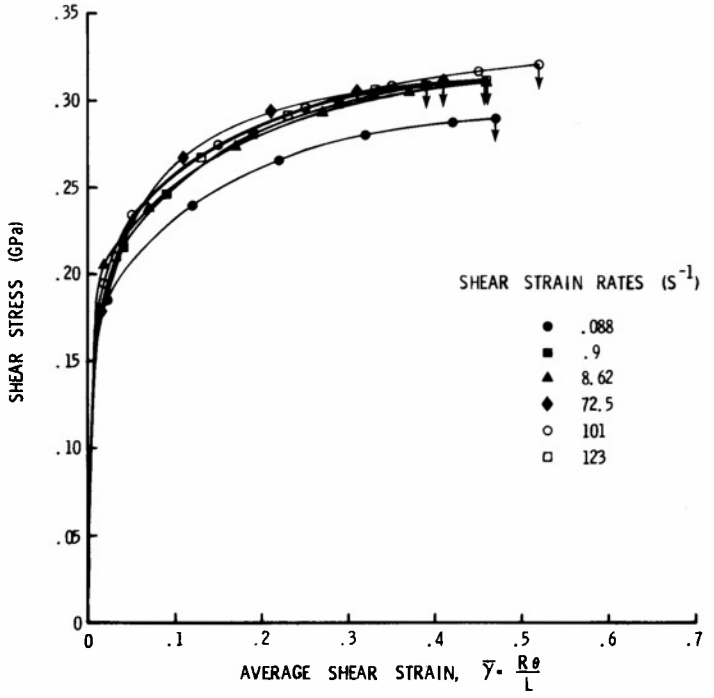

Figure 3. Shear Stress-Strain Relationships for 2024-T3 Aluminum

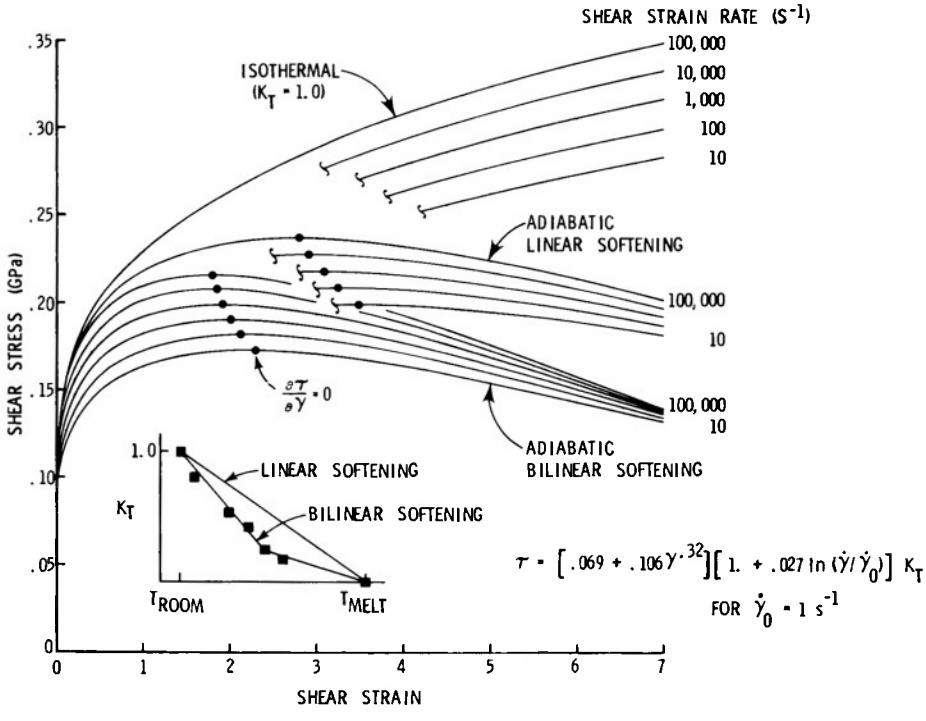

Figure 4. Adiabatic Stress-Strain Relationships for OFHC Copper

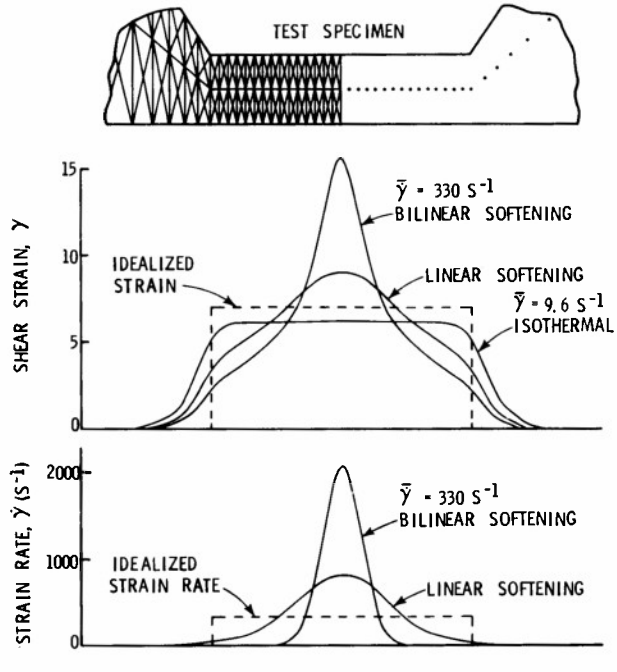

Figure 5. Computed Strain and Strain Rate in Specimen at $\bar{\gamma} = 7$

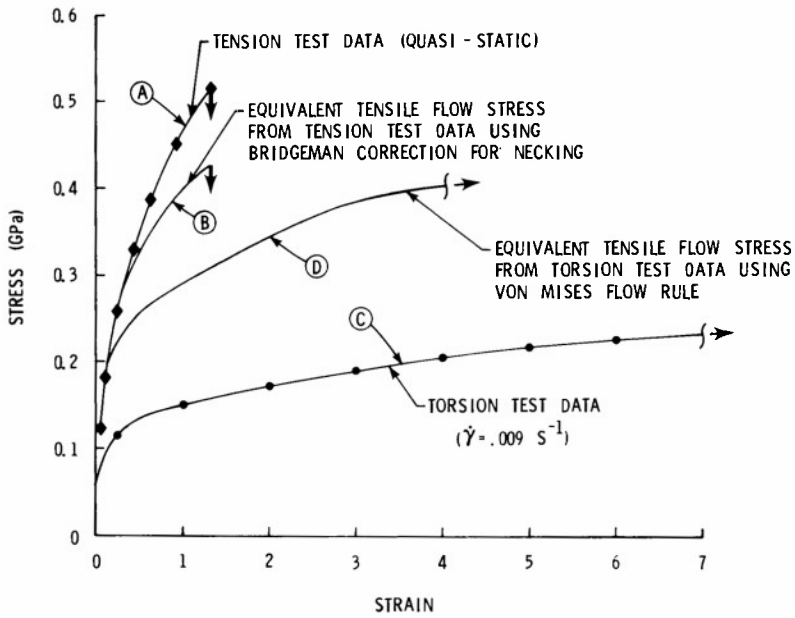

Figure 6. Comparison of Tension and Torsion Data for OFHC Copper

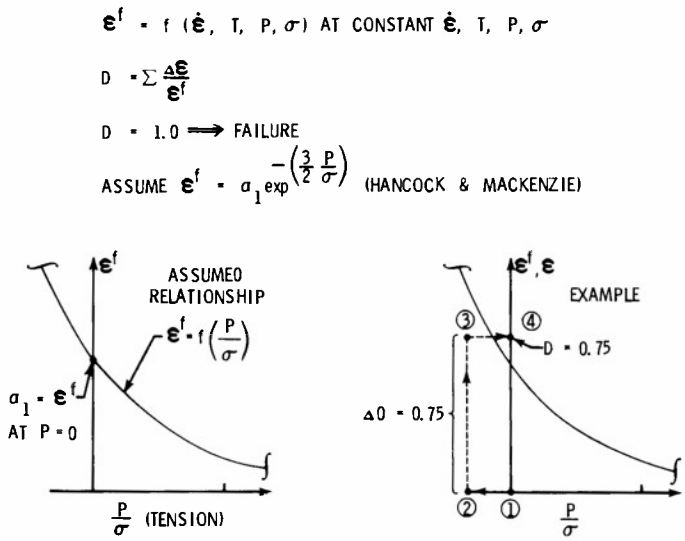

Figure 7. Summary of Damage Model for Material Failure

A SHEAR BAND MODEL FOR 4340 STEEL*

L. SEAMAN
D. R. CURRAN
D. A. SHOCKEY
D. C. ERLICH

Poulter Laboratory
SRI International
333 Ravenswood Avenue
Menlo Park, CA 94025

A microdamage model describing the evolution of shear bands has been developed to represent data from fragmenting cylinders of 4340 steel. The cylinders were exploded by a new technique allowing an observation of the gradual development of damage. These data led to a model for nucleation, growth, and coalescence of shear bands to form fragment size distributions. The procedure for fitting the model to the data and relative precision of the fit obtained with 4340 steel are illustrated.

The shear band data were obtained by counting and measuring bands observed on the surfaces of eight cylinders after contained-fragmenting-cylinder experiments. The experimental configuration (Fig. 1) shows a low density PETN core inside and an acrylic tube and heavy steel and lead tubes outside. The explosive expands the test cylinder, extending the acrylic tube, but the steel and lead tubes halt the expansion before complete separation of the test tube. The acrylic thickness and explosive density were varied to provide ranges of strain rates, peak strain, peak pressures, and levels of shear banding.

After the bands were counted the cumulative numbers of bands N_g larger than a given radius R were assembled into size distributions. The distributions were fitted to the exponential relation

$$N_g = N_o \exp(-R/R_1) \qquad (1)$$

where N_o and R_1 are parameters of the distribution.

The shear band model derived from these data contains nucleation, growth, and coalescence processes. Nucleation occurs when the plastic shear strain in any orientation (currently three coordinate directions and three 45° directions are considered) exceeds a threshold level. Then a distribution of bands with a total of ΔN are initiated:

*This work was sponsored by Army Materials and Mechanics Research Center and Ballistic Research Laboratory.

$$\Delta N = N \exp (A_n \Delta\varepsilon^n) \qquad (2)$$

where N is the current number/cm^3, A_n is a material constant, and $\Delta\varepsilon^n$ is the plastic strain increment. Growth occurs according to the rate law

$$dR/dt = C_G R \, d\varepsilon/dt \qquad (3)$$

where C_G is a material constant and $d\varepsilon/dt$ is the strain rate. Coalescence and fragmentation occur when the fragments whose surfaces are defined by shear bands completely fill the volume of material. As the damage increases the strength decreases so that an anisotropic stress-relaxation process is in the model. This model is incorporated into a computer subroutine SHEAR3.

Simulations of the contained-fragmenting-cylinder experiments were made with a two-dimensional wave propagation code that calls SHEAR3 to compute stress and damage. Appropriate shear banding parameters (e.g., A_n and C_G) were derived from multiple simulations and comparisons with the data. The final calculations for cylinders with the most and least damage (Tests 8 and 2) led to the comparisons shown in Fig. 2. The correspondence with all aspects of the data indicate that shear banding in the fragmenting cylinders is well represented by the SHEAR3 model.

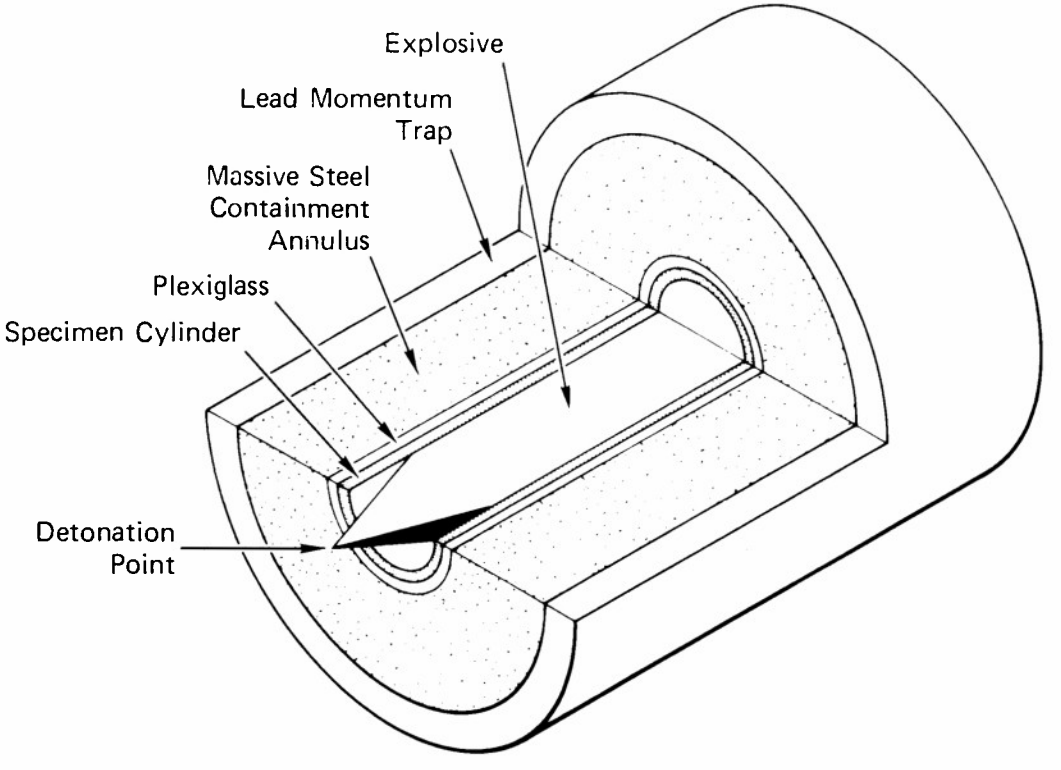

FIGURE 1 CONTAINED EXPLODING CYLINDER EXPERIMENT FOR STUDYING SHEAR BAND BEHAVIOR

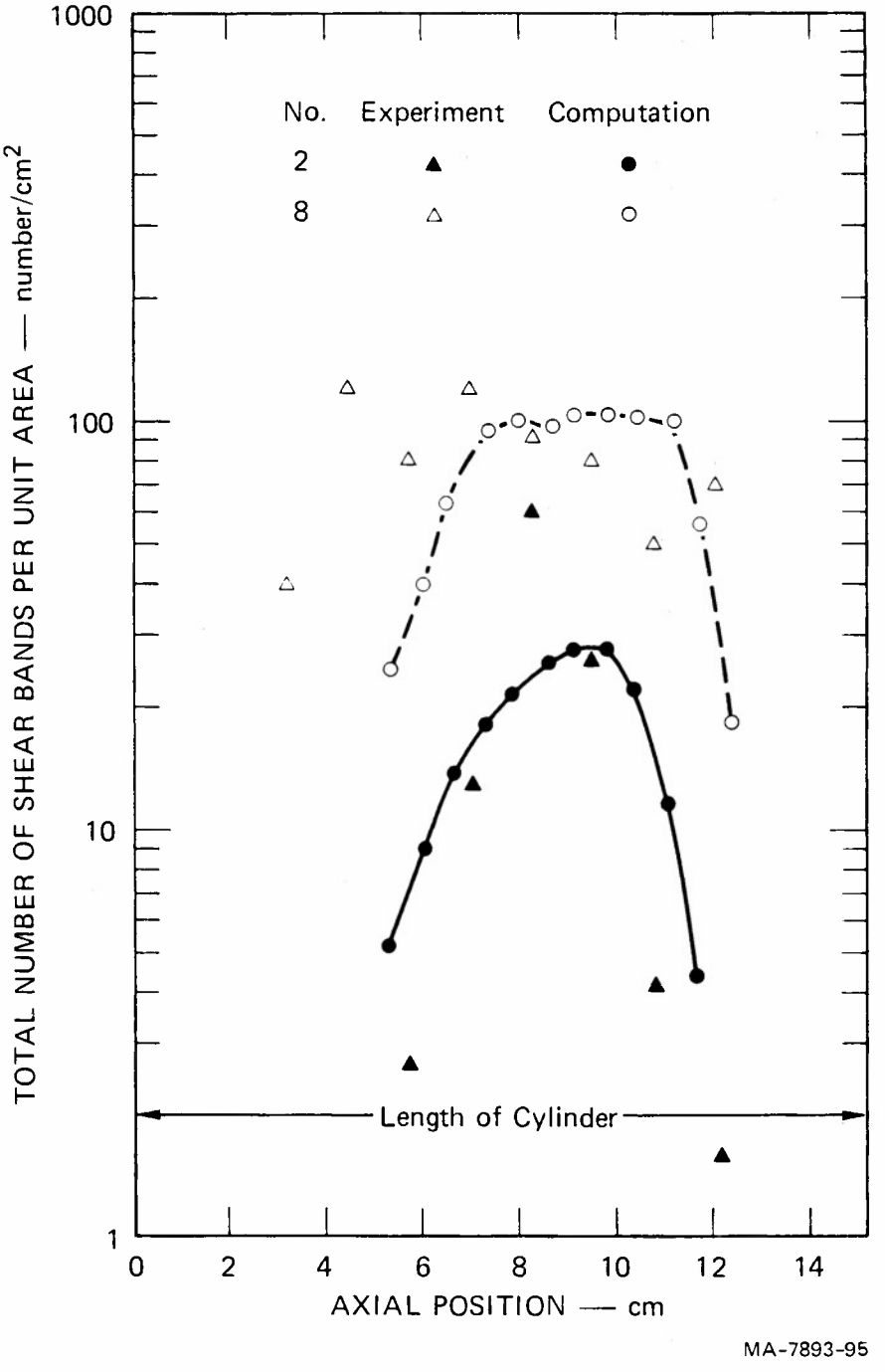

FIGURE 2 COMPARISON OF THE VARIATION OF THE NUMBER OF SHEAR BANDS n_0 WITH AXIAL POSITION FOR CONTAINED-FRAGMENTING-CYLINDER EXPERIMENTS IN 4340 STEEL

ANALYSIS AND SIMULATION OF NONSTATIONARY GUNFIRE ENVIRONMENTS

RONALD G. MERRITT
Mechanical Engineer

WILLIAM N. JONES
Mechanical Engineer
Naval Weapons Center
China Lake, California 93555

EXTENDED ABSTRACT

To assess the potential for damage to sensitive missile components from extreme transient shock/vibration environments, statistically based analysis and simulation models for such environments are being developed at the Naval Weapons Center. The initial models utilize environmental data from a missile carried aboard an aircraft during captive flight. Gunfire bursts of two seconds duration at twenty rounds per second provide some forty well defined pressure impact pulses transverse to the lightly damped missile. The impact of the pulses is a function of the aircraft speed and is measured at varying positions along the missile by a piezoelectric accelerometer installation. Acceleration measurements from this configuration provide a measure of the vibration/shock environment for the missile.

In order to assess the impact of severe transient environments on sensitive missile components, a combined analysis of the data and subsequent simulation of the environment in the laboratory must be performed. The accelerometer data is characteristically nonstationary and capable of being analyzed as a series of pulses. Each pulse is decomposed into a varying mean time history (low frequency) and a zero mean, varying mean-square time history (high frequency). The entire gunfire burst is considered a series of independent nonstationary pulses composed of a superposition of these two characteristic time histories.

In order to analyze and simulate the environment a series of input/output models is used to define the environment. The basic analysis model is provided in Figure 1. The model consists of a measured input at a particular structural hard point of the missile, a measured output at a particular point of interest of the missile, and a system transfer function between the two points. During analysis of the missile system the coherence between the system input and the system output is determined. This defines a relationship of input to output and provides the basic information for the simulation of the environment.

During laboratory simulation, the input to the missile system is sustantially different than that of the captive carry flight input. Simulation only provides input through a shaker system at two or three hard points on the missile/launcher configuration whereas captive flight input is not only through these points but from transfer of air pressure pulses to the missile skin and into the missile. Figure 2 provides the basic simulation model. If such an input can be adjusted such that the relationship between the missile system measured input/output is maintained then the simulation is adequate. The criteria for adequate simulation is the matching in a statistically acceptable manner of coherence functions obtained from measured flight data and the laboratory simulation.

For stationary vibration data, the statistics of such analysis/simulation are based upon well known averaging techniques. For nonstationary records the statistics of such an analysis/simulation are based upon ensemble averaging techniques.

Extensions beyond the basic model provided in Figure 1 and Figure 2 require consideration of multiple inputs. Development of these more advanced models will provide for more refined simulations of nonstationary environments.

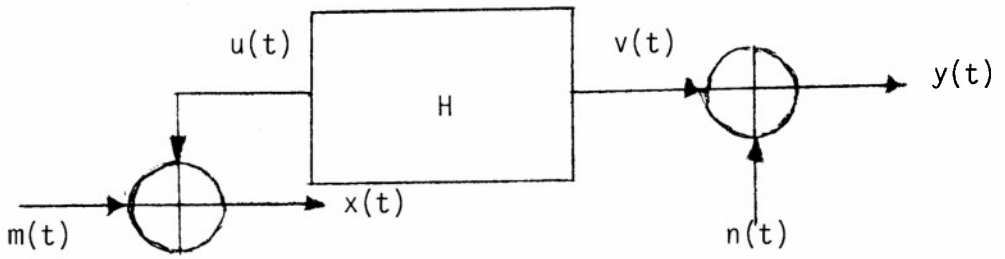

x(t) - measured system input
y(t) - measured system output
m(t) - measured system input noise
n(t) - measured system output noise
u(t) - system input
v(t) - system output
H - system transfer function

γ_{xy} - computed system coherence function relating x and y

Figure 1: Basic Flight Data Analysis Model

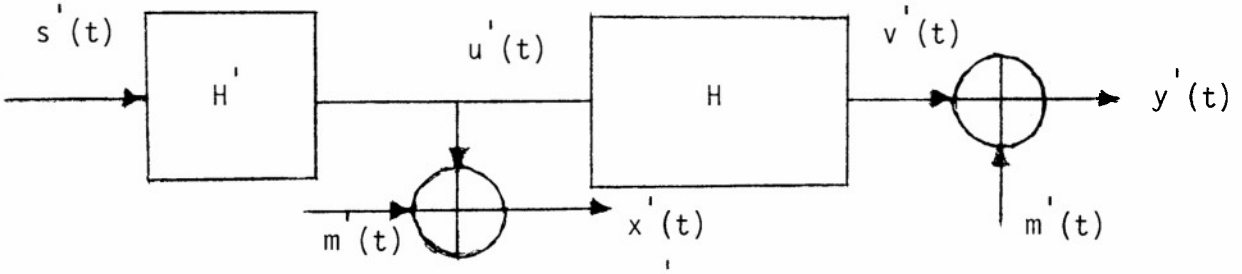

$s'_i(t)$ - simulated shaker system input
$x'_i(t)$ - measured system input
$y'_i(t)$ - measured system output
$m'_i(t)$ - measured system input noise
$n'_i(t)$ - measured system output noise
$u'_i(t)$ - system input
$v'(t)$ - system output
H'_i - system transfer function
H - shaker system transfer function

$\gamma_{x'y'}$ - computed system coherence function relating x' and y'

Figure 2: Basic Laboratory Simulation Model

COMPARISON OF COMPUTED AND MEASURED ACCELERATIONS IN A DYNAMICALLY LOADED TACTICAL SHELTER

ARTHUR R. JOHNSON
General Engineer
US Army Natick R&D Command
Natick, MA 01760

ABSTRACT

The Army is currently developing a family of rigid wall tactical shelters. Prototype 8' by 8' by 20' (2.4 m by 2.4 m by 6.1 m) one-side expandable shelters have been designed and fabricated. These shelters are undergoing environmental and transportation testing. Tactical shelters are fabricated from aluminum extrusions and paper honeycomb core/aluminum skin sandwich panels. The transportation tests consist of a number of dynamic tests which simulate the extreme loads expected when the shelter is shipped. The comparison of computed and measured accelerations for two of the dynamic tests is the topic of this ongoing effort. The first test is the rotational end drop test in which one end of the shelter is placed on a block and the other end is lifted and allowed to drop. The second test is called a Belgian block test in which the shelter is mounted on a mobilizer and towed over a specially prepared road surface. The experiments were conducted by contractors and the analysis work was done at the US Army Natick R&D Command.

The shelter was outfitted with accelerometers and acceleration versus time data was obtained for each test. For the end drop test there were 11 accelerometers attached to the floor, one on the center of the roof, and two on the center of the expandable floor. For the mobilizer test 12 accelerometers were located at four corners of the shelter and three accelerometers were located on the roof.

A finite element model of the shelter was made for use with the COSMIC*NASTRAN program on NARADCOM's UNIVAC 1106 computer system. The model includes beam elements, plate elements with transverse shear, and multipoint constraint equations to represent door and wall hinge and latch connections. To determine an approximate representation of the dynamic loads acting on the shelter in the end drop test the shelter was modeled as a rigid body impacting a flat elastic surface. The equations of motion were solved numerically. The properties of the elastic impact surface were changed until the computed acceleration profiles were similar to the measured profiles at the end of the shelter. The time dependent force which the elastic surface applied to the rigid shelter was then used for input to a dynamic analysis of the shelter using the NASTRAN program. The finite element equations of motion were integrated by the Newmark method. The distribution of accelerations predicted by the finite element analysis agree well with the measured distribution of accelerations. Currently the case when the impact surface becomes infinitely rigid is being considered for analysis. The data obtained in the Belgian block test is being analyzed and the shelter free-body, low frequency, natural modes of vibration are being determined by the finite element method.

EVALUATION OF THE EFFECTS OF VOIDS IN THE IMPROVED MAIN ROTOR BLADE (IMRB)

DREW G. ORLINO
Aerospace Engineer
Applied Technology Laboratory
US Army Research and Technology Laboratories (AVRADCOM)
Ft Eustis, VA 23604

WILLIAM W. HOUGHTON
Research Mechanical Engineer
Composites Development Division
US Army Materials and Mechanics Research Center
Watertown, MA 02172

EXTENDED ABSTRACT

With the introduction of the Improved Main Rotor Blade (IMRB) to the Army's inventory as the first production composite main rotor blade (flown on the AH-1S helicopter), quality assurance personnel were questioning the impact that typical manufacturing flaws might have on a composite rotor blade's service life. Since little data was available regarding the propagation rate of "voids" when subjected to flight loads for an extended number of flight hours, an investigation was initiated by the Applied Technology Laboratory (ATL) of the US Army Research and Technology Laboratories (AVRADCOM). The objectives of this program were twofold: (1) To study the propagation rate of known voids as they appear in composite rotor blades under fatigue loading. (2) To establish confidence in the K-747 blade's service life by subjecting high void content R&D blades to an extended number of simulated flight hours.

Reliable Nondestructive Inspection (NDI) techniques were needed to aid in the investigation of the propagation characteristics of voids in composite structures. The following NDI techniques were used: ultrasonics, x-radiography, borescope, acoustic emission, visual analysis, cointapping, and thermography. While cointapping and visual analysis were used to establish blade surface flaws, the other techniques established a firm baseline within the blade spar.

Design and fabrication of the IMRB, a replacement of the Model 540 production Cobra blade, evolved through mission requirements necessitating higher armament payloads, and thus a need to improve its lifting capacity. The necessary six percent increase in hover gross weight appeared obtainable by direct replacement of the main rotor blades with blades of increased aerodynamic efficiency. Improved ballistic damage tolerance and a longer fatigue life were also considered as desirable improvements. The blade configuration is shown in Figure 1. The design fatigue life of the K-747 blade was based on fatigue tests and analysis.

To accomplish the objective of this program, four (R&D) blades were to be fatigue tested to 28 million cycles based on the AH-1S flight spectrum (Figure 2). These blades were from the first lot of R&D blades manufactured and consequently had considerable manufacturing defects. Spectrum testing was chosen because it is considered to be more representative of actual flight loads. If no sign of degradation or void growth occurred at this point, a good level of confidence could be established. A block diagram outlining the test approach taken is presented in Figure 3. As is apparent from Figure 4, the construction of the K-747 blade is relatively complex and this combined with the relatively infant state-of-the-art application of NDI to composite spars makes clear definition of these voids difficult, especially for a completely assembled blade.

The flight spectrum used during testing was based on the Bell Helicopter Textron (BHT) flight spectrum for the AH-1S Cobra. The loads applied to the blade were generated from a flight-load survey previously conducted. The spectrum consisted of at least 100 maneuvers for three gross weights and density attitudes. The spectrum was developed for station 120 which was an area of considerable delamination in addition to being the maximum deflection point of the blade (midspan).

Fatigue testing was conducted in the Rotor Blade Resonant Fatigue Test Machine (Figure 5). The fatigue test machine is approximately 44 feet long, 10 feet wide, 12 feet high, and can accept specimens up to 24 feet in length. It consists of a frame, a centrifugal loading system, hydraulic actuator subsystems, and specimen attachment fittings. The first blade of this program was mounted in the machine at the tip through a doubler arrangement while the blade root end attached through its root fitting adapter to an AH-1G hub yoke which contains a pitch horn and an attachment point for the drag brace.

During testing, the blade was periodically stopped and ultrasonically inspected for void growth. After approximately 700 simulated flight hours, the blade was removed from the test fixture, with NDI performed in the form of x-ray ultrasonics, and borescope. After reinstallation of the blade in the test fixture was completed, acoustic emission testing was conducted, with fatigue testing resuming thereafter. Fatigue testing continued for an additional 14 million cycles with NDI occurring daily. Throughout the program there was no noticeable change in strain levels at the test section.

Based on the results of the K-747 Rotor Blade Fatigue Test Program to date, it is concluded that:

(1) Ultrasonic inspection, acoustic emission, and vibrothermography appear to have the potential for being viable NDI techniques for monitoring voids in composite rotor blades; however, there is a need to develop a technique for inspection in the field.

(2) A 50-60 percent increase in void area occurred in the test section. (Figures 6 and 7)

(3) Confidence is established in the blade's service life after completing 28 million cycles (1440 flight hours) of spectrum loading with an early R&D quality blade.

K-747 COMPOSITE BLADE

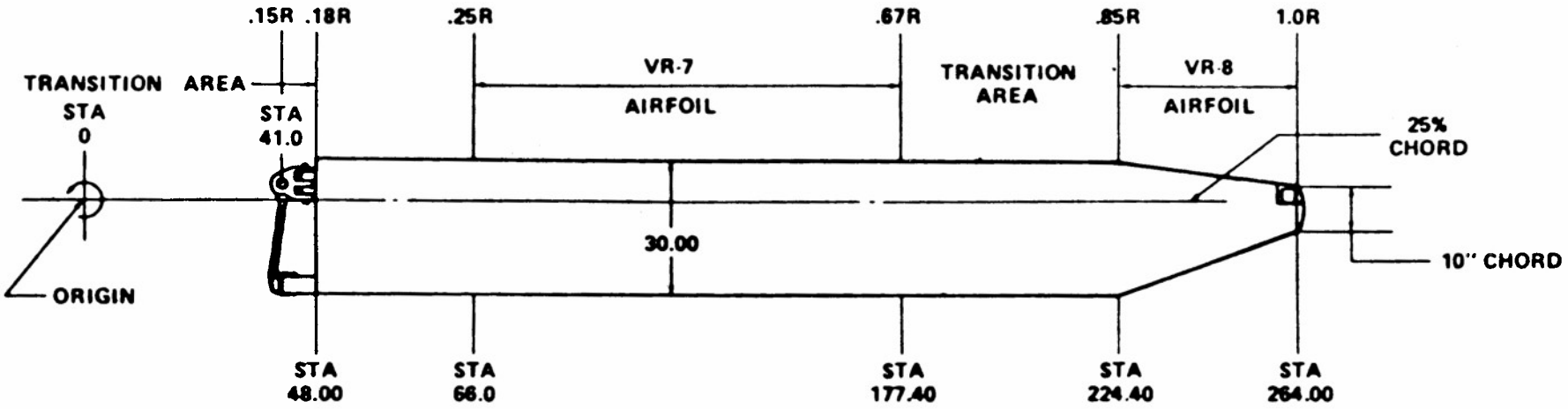

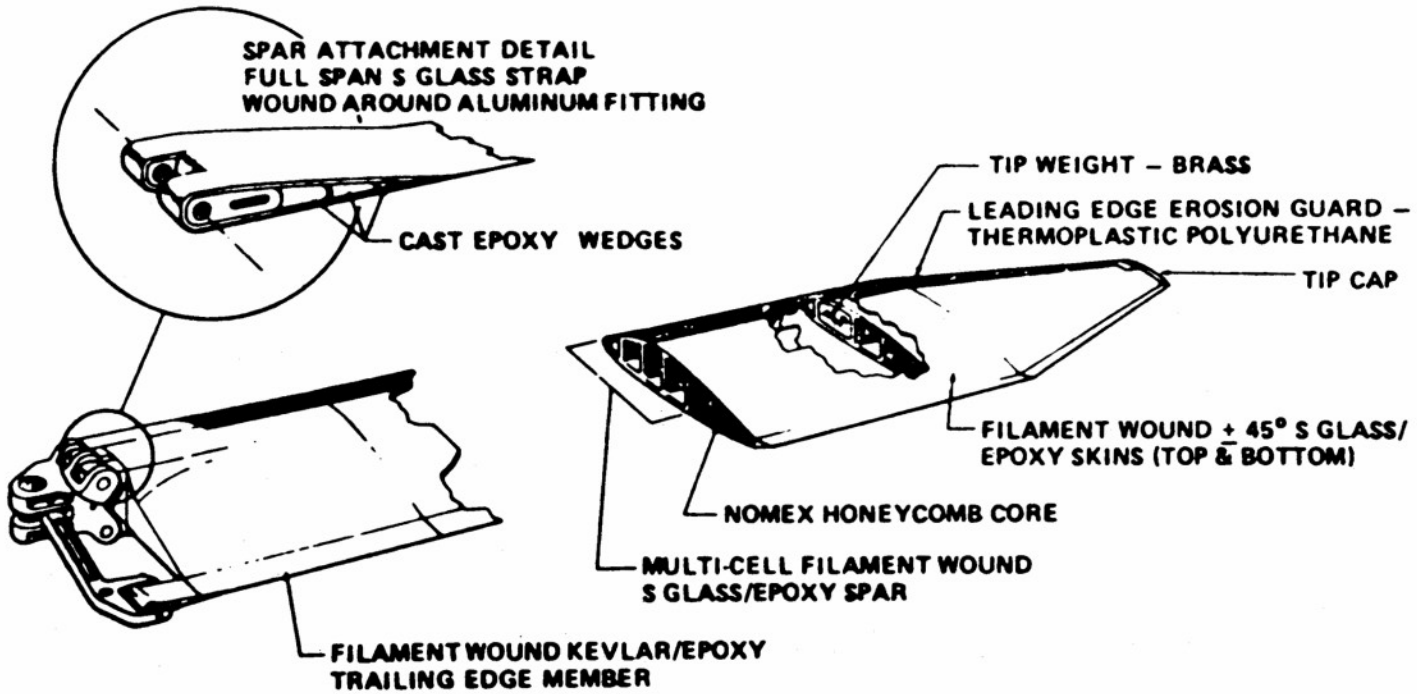

FIGURE 1

SEQUENCE	BLOCK #	ALTERNATING BENDING(IN-LB)	*ALTERNATING CHORD(IN-LB)	ALTERNATING TORSION(IN-LB)	MEAN TORSION (IN-LB)	% TIME	**CYCLES/ 100 HRS	**CYCLES/ 2 HRS
9	1	3101	16094	1320	-7230	2.5125	48843	977
3	2	4652	24144	2410	-5740	3.985	77468	1549
1	3	5858	30403	2460	-5090	1.9109	37148	743
7	4	6892	35770	3140	-6910	8.7761	170607	3412
4	5	7237	37560	3923	-7164	18.302	355791	7116
11	6	8960	46503	5654	-8814	14.7001	285770	5715
5	7	11207	58165	5136	-6652	28.5274	554573	11091
2	8	11400	59166	6400	-8700	14.6014	283851	5677
6	9	12586	65322	4588	-2151	4.8843	94951	1899
10	10	14138	73376	7326	-8841	1.1298	21963	439
8	11	15862	82324	9487	-9267	.6784	13188	264
						100 %	1944153	38882

*Based on a .1926 flap-to-chord ratio.

**Based on a 1/rev and 324 rotor RPM.

C.F. = 82000 lb

FIGURE 2

TEST PROGRAM APPROACH

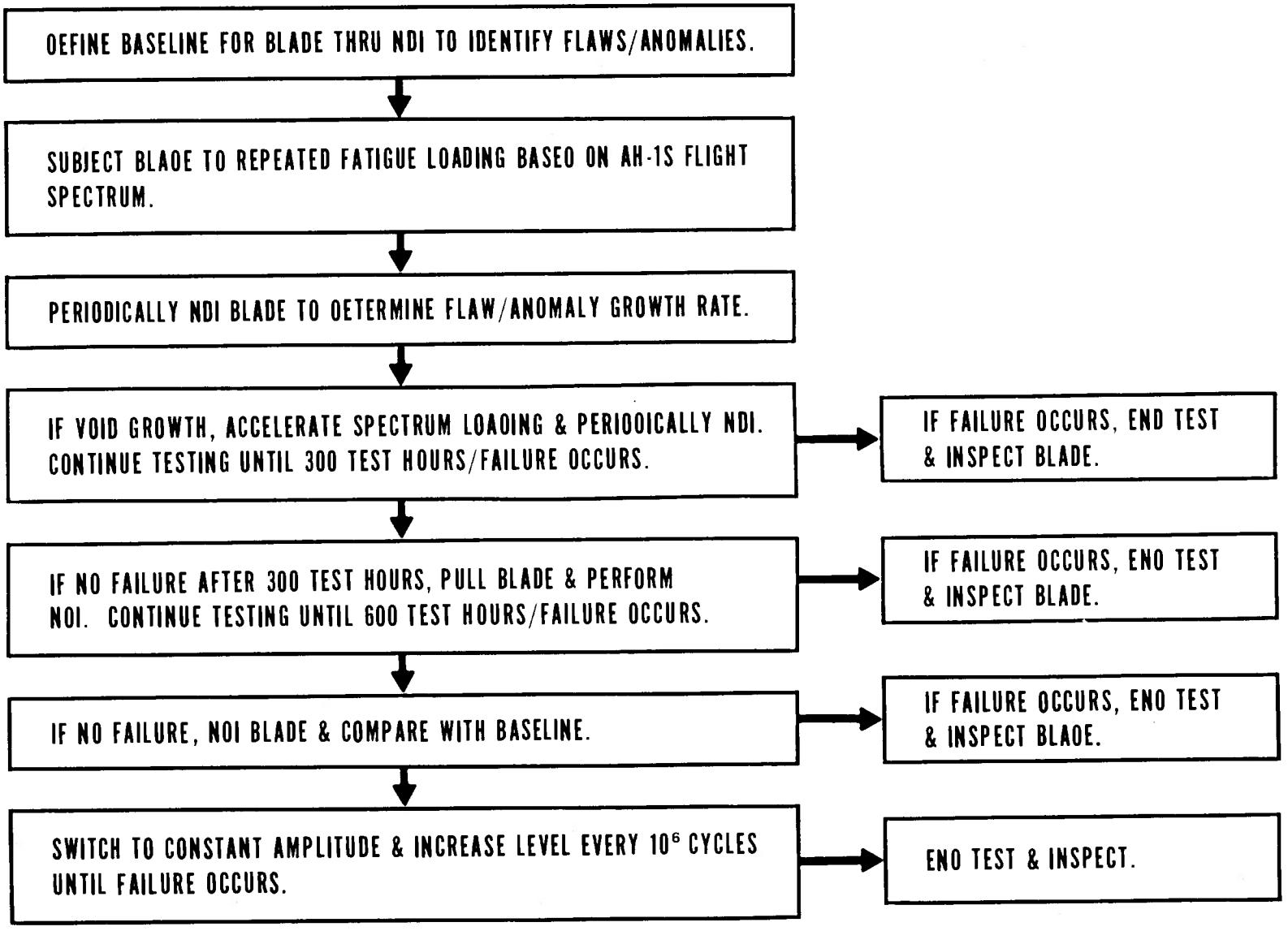

FIGURE 3

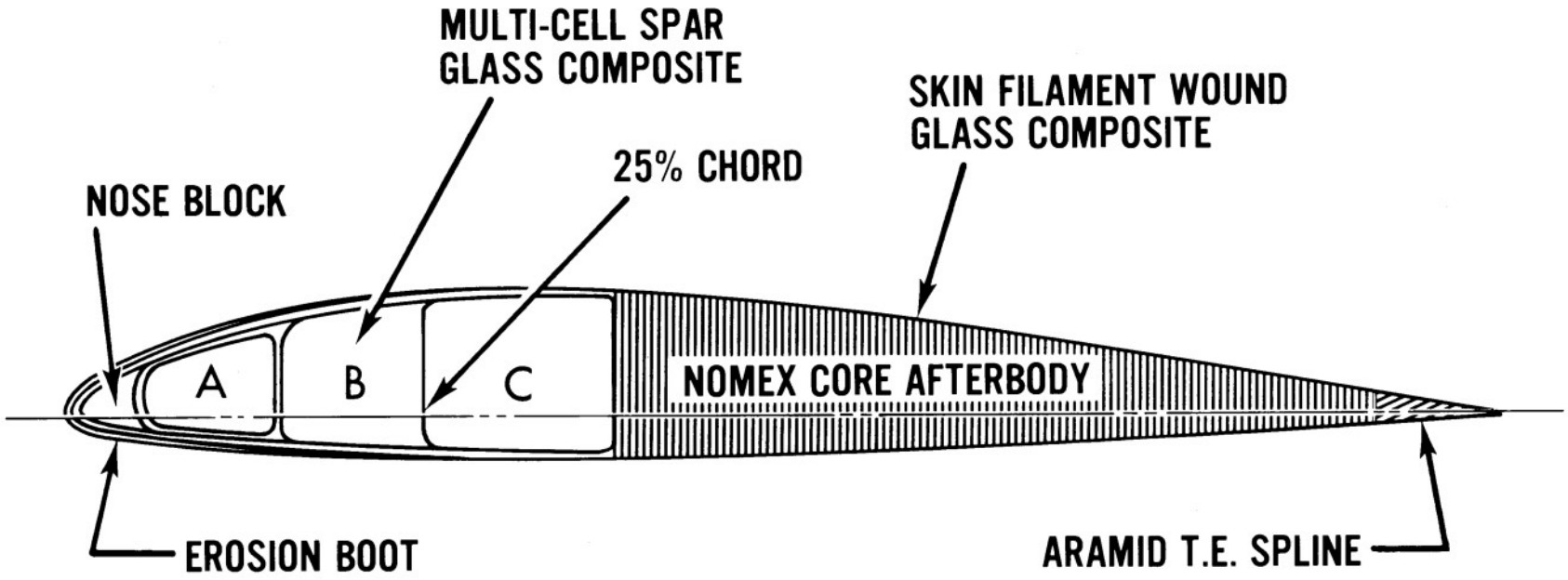

STA. 86.000 THRU STA. 177.400

K-747 BLADE CROSS-SECTION
STRUCTURAL ARRANGEMENT

FIGURE 4

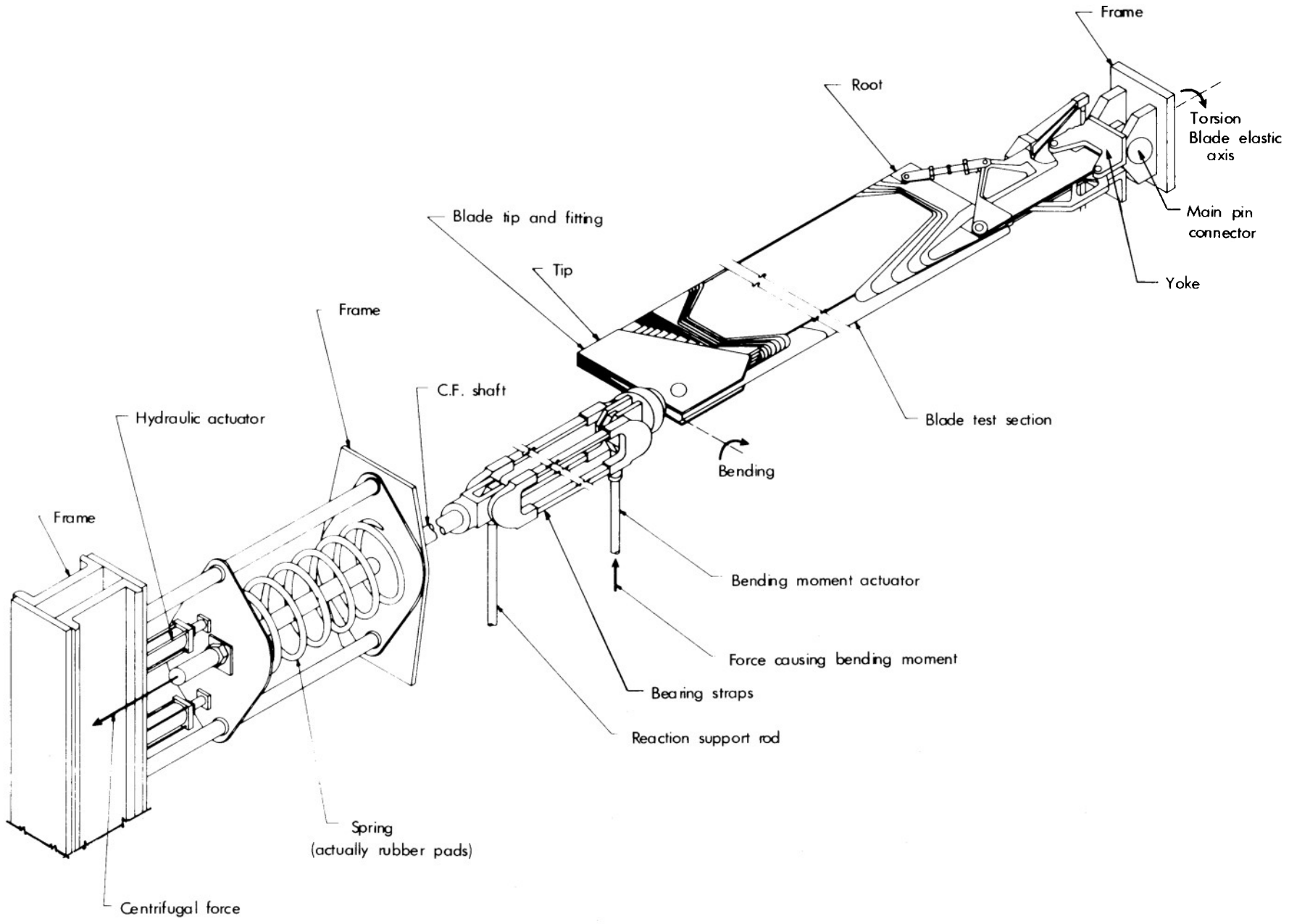
Frame
Root
Torsion
Blade elastic
axis
Main pin
connector
Yoke
Blade tip and fitting
Tip
Frame
C.F. shaft
Hydraulic actuator
Blade test section
Bending
Frame
Bending moment actuator
Force causing bending moment
Bearing straps
Reaction support rod
Spring
(actually rubber pads)
Centrifugal force

FIGURE 5

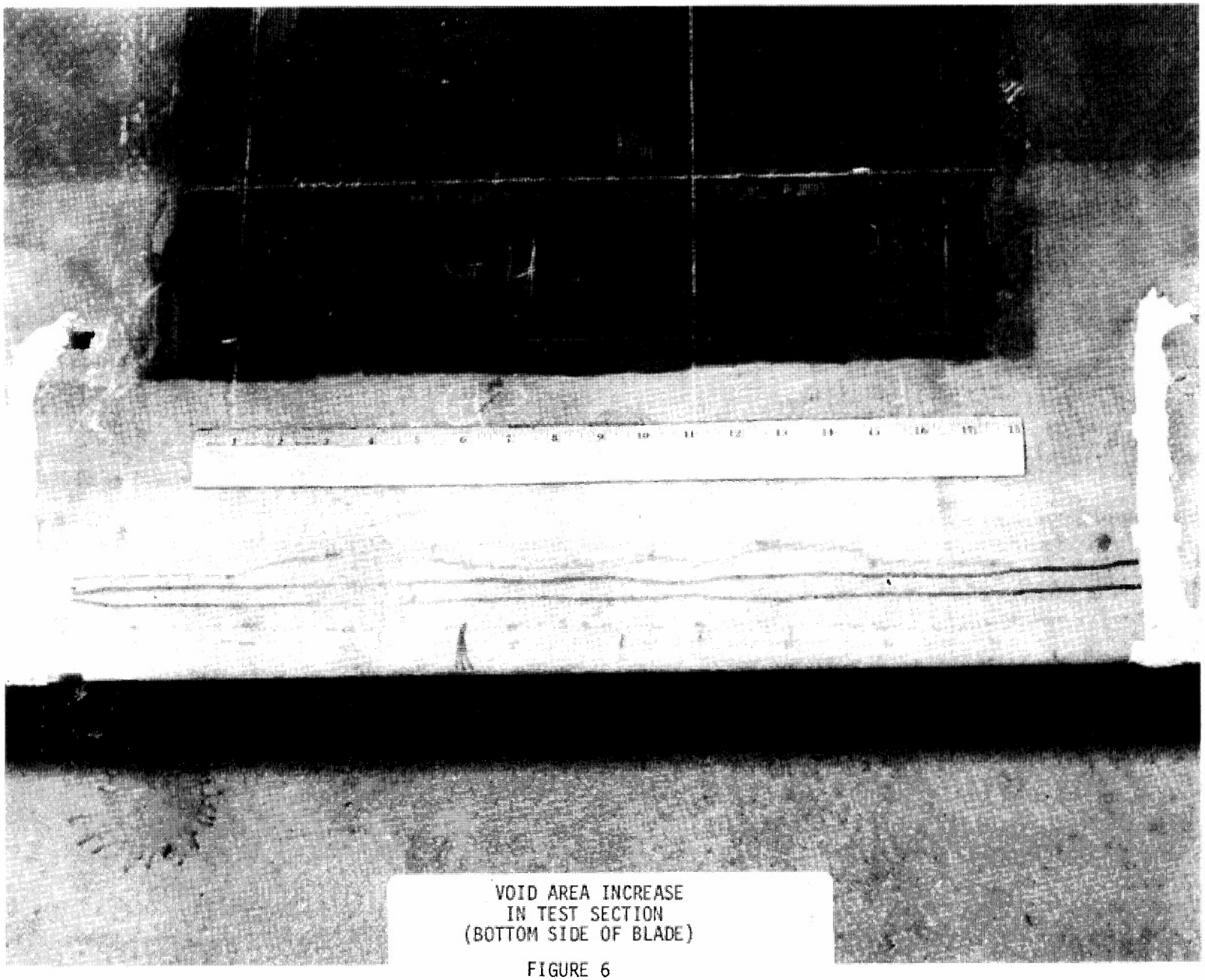

VOID AREA INCREASE
IN TEST SECTION
(BOTTOM SIDE OF BLADE)

FIGURE 6

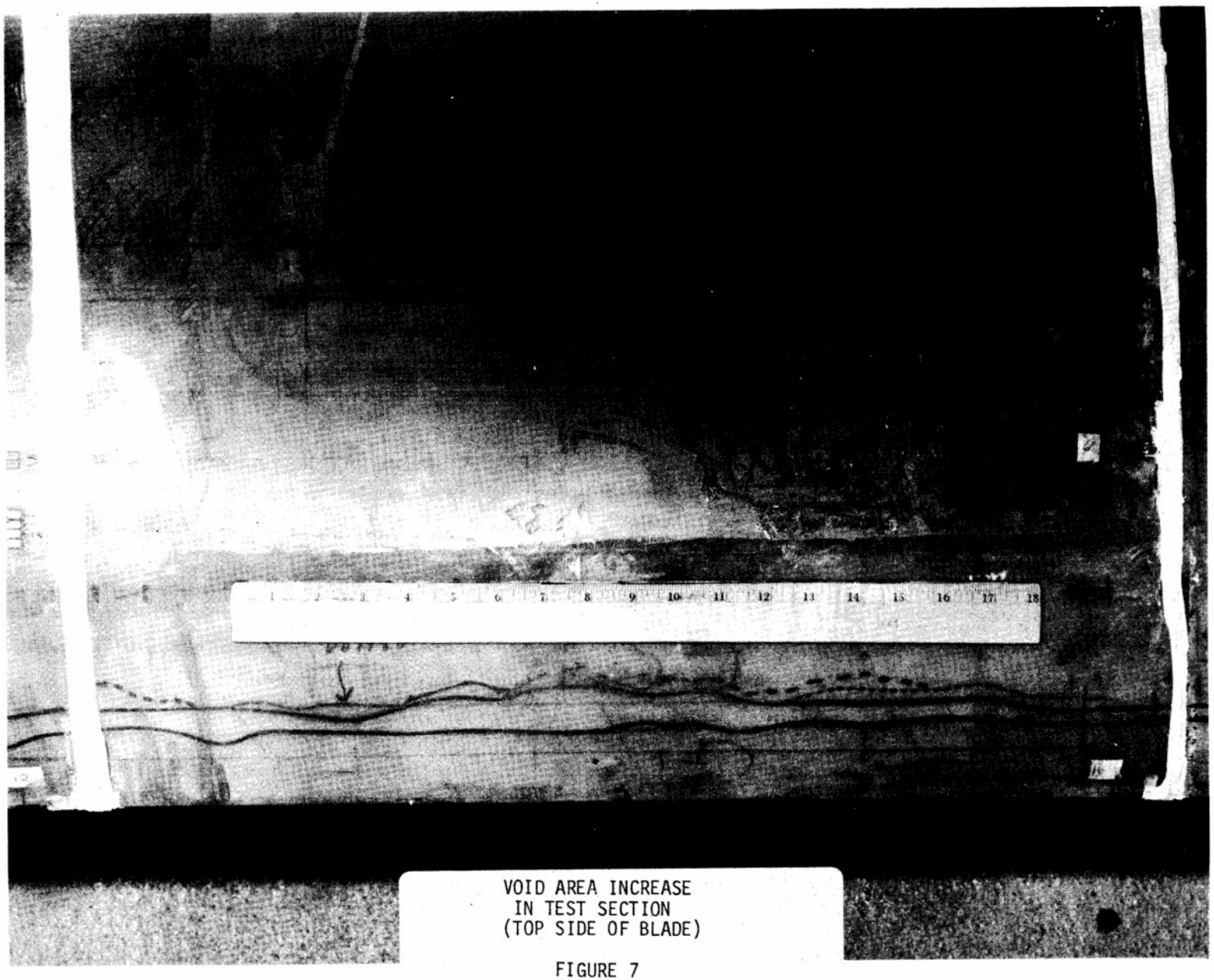

VOID AREA INCREASE
IN TEST SECTION
(TOP SIDE OF BLADE)

FIGURE 7

EXPERIMENTAL INVESTIGATION OF LONG, FLAT, RECTANGULAR AS/3501-6 GRAPHITE/EPOXY PLATES UNDER UNIFORM PRESSURE LOADING

RICHARD W. GEHRING
Member of Technical Staff
North American Aircraft Division
Rockwell International Corporation
Columbus, Ohio

EXTENDED ABSTRACT

The program described herein represents an initial experimental effort for the definition of stresses, ultimate strength, deflections, and permanent set in long orthotropic plates subjected to lateral pressures as typified by fuel pressure, aerodynamic pressure, cabin pressurization, and hammershock in engine inlet ducts. Initial theoretical analyses utilized state-of-the-art classical methods for membranes and plates subjected to uniform pressure using minor modifications to account for orthotropic properties.

For the initial experimental program a series of four AS/3501-6 graphite/epoxy plates were subjected to uniform lateral pressure loadings to determine ultimate strength, deflections, and bending moments and axial loads at selected locations. Plate dimensions inside the fixture frame were 6 inches (15.24 cm) by 24 inches (60.96 cm) which gave a minimum geometric aspect ratio of a/b = 4.0. For three of the four panels the "effective" aspect ratio would be much greater due to the higher flexural rigidity and axial stiffness in the short direction. Therefore, all plates were considered to be long for purposes of evaluation; i.e., an elemental strip across the plate is sufficient for evaluation. Basic ply orientations were $[\pm 45_2]_T$, $[0_2/\pm 45_2]_T$, $[0_4/\pm 45_4]_T$, and $[0_{12}/\pm 45_8]_T$ to encompass a practical range of laminates and stiffness and geometric parameters. Figure I illustrates the basic panel geometry, laminate stacking sequence, and nominal thickness for each panel. Aluminum doublers were used to obtain higher bearing strength and reduce in-plane movement caused by excessive bearing deformations. Doublers were bonded to the panels using a room temperature cure adhesive (EC 2216).

The basic test setup and instrumentation are shown in Figure II where strain gages and the deflection transducer were located at points which could be compared directly with calculations. All strain gages were back-to-back and wired separately to obtain both axial load and bending moments. A 200 psi (1.379 MPa) capacity compressor was used for the basic air supply with a nitrogen bottle utilized to fail one panel which exceeded the compressor capacity. Only panels 101, 102, and 104 were tested to destruction with tests planned for panel 103 incomplete at this time.

Panel 101 failed at 112 psi (0.772 MPa) which was considerably higher than predicted by present elastic methods assuming no in-plane or out-of-plane initial deflections. This was partially due to a severe buckle which formed after installation in the test fixture. This buckle produced an out-of-plane deflection which was estimated to be 0.350 inch (0.889 cm). Allowing for this deflection an approximate inelastic analysis gave a predicted failure of 100 psi (0.689 MPa) which showed better agreement with the test failure at 112 psi (0.772 MPa). The failure criteria used in the theoretical analysis was the failure strain for $[\pm 45]$ laminates obtained from the Advanced Composites Design Guide. Visual inspection of the panel after 90 psi (0.620 MPa) showed severe permanent set.

Evaluation of panel 102 was more extensive and included investigations at both relatively low pressures and ultimate load. This panel was initially flat with no measureable eccentricities and represents a practical laminate with both $[0]$ and $[45]$ plies. Analyses were performed using classical elastic methods for plates at a pressure of 20 psi (0.138 MPa) in order to evaluate strain gage data. Table I summarizes the results of the theoretical investigation and includes the test data for comparison. Initial analyses for simply supported plates, plates with fixed edges, and membranes did not agree with the test data obtained which indicated the presence of other factors which influenced the test results. Since no measureable out-of-plane deflection was noted prior to testing, the two most important factors were in-plane displacements and edge elasticity; i.e., edge conditions between simply supported and fixed. Although neither of these factors can be numerically defined it was possible to estimate values which could be used in the analysis. For example, the in-plane displacements were assumed to be a function of the bolt and hole tolerances for drilled holes. These tolerances can accumulate to .010 inch (.0254 cm) for bolts allowing for both sides. Therefore, the estimated in-plane displacement was taken as .010 inch (.0254 cm) for purposes of analysis. The edge elasticity was more difficult to estimate since the effects of the sealing compound were unknown. Therefore, two reasonable values of the edge elasticity factor, γ , were assumed, $\gamma = 0.7$ and 0.9. It is also important to note that the in-plane displacements and edge elasticity are a function of the applied pressure since bearing deformation and local bending at the edge of the fixture are influenced by the pressure. Reference to Table I indicates reasonably good agreement between test and theory when in-plane displacements and edge elasticity factors are considered in the analysis for the applied pressure of 20 psi (0.138 MPa). Although the bending in the plate appears to be a significant factor at rather low pressures, these effects disappear at the extremely high applied pressures which cause failure of the panel. Panel 102 failed catastrophically at 275 psi (1.896 MPa) in tension at the long side of the panel. Elastic analysis indicated failure as a membrane at 265 psi (1.827 MPa) which indicated that the bending effects had virtually disappeared at the higher loads and larger deflections. The failure criterion used in the analysis was the failure strain for the $[0]$ plies which was obtained from the Advanced Design Guide. For analysis purposes the modulus of elasticity was obtained from tensile coupon data

based on NAAD tests where these data indicated essentially linear stress-strain curves. A photograph of the catastrophic failure is shown in Figure III which is typical of the failures for panels 101 and 104.

Panel 103 was tested to 100 psi (0.689 MPa) without failure and indicated a high degree of bending due to the high flexural rigidity present. At this pressure level the panel elemental strip acted very much like a fixed end beam and had not reverted to membrane action as had the thinner panels. However, this panel was not tested to failure and has not been fully analyzed. With a high degree of bending present it may be necessary to utilize inelastic strain procedures for analysis to predict failure since the bending moments will induce inelastic stress-strain relationships in the $[\pm 45]$ plies.

Panel 104 was investigated prior to testing and indicated an out-of-plane displacement of approximately .065 inch (0.165 cm). Strain gage data for this panel are shown in Figure IV for the center of the panel and the edge [0.18 inch (0.457 cm) from the edge]. These data indicate initial bending which rapidly reverts to membrane action at relatively low pressures. The bending moment at the center becomes nearly constant and the tension gage at the edge rapidly went off scale. At failure this panel acted more as a membrane and failure prediction was based on membrane analysis. Deflection data for this panel are shown in Figure V in addition to permanent set data and comparison with theoretical calculations based on membrane analysis which allowed for the .065 inch (0.165 cm) initial deflection. The difference has tentatively been attributed to in-plane displacements which were not clearly identified. Although the permanent set shown in Figure V is small, the in-plane displacements may also explain the apparent slight increase in permanent set as the pressure is increased. This in-plane displacement is probably a function of the bolt hole tolerances but has not been fully evaluated.

A summary of experimental and theoretical failure data is presented in Table II. Failures were all very similar with clean tension failures at the long side of the panel and all were catastrophic.

In summary it is clear that initial imperfections have a significant influence on the behavior and ultimate strength of composite panels under pressure loading. In addition, the failure analyses tend to indicate the failures to be a function of the allowable tensile strain of the most critical element or lamina in the laminate. The results to date indicate extremely high panel strengths which are impractical since substructure strength and other potential failure modes would preclude attaining these strengths. Additional testing of more realistic airframe panels and further investigation of analysis methods are required. Since only long panels were investigated in this program, further investigation of the influence of effective aspect ratio is also warranted where geometry and axial and flexural rigidites would define the necessary parameter for use with the classical theories for plates which cannot be classified as long.

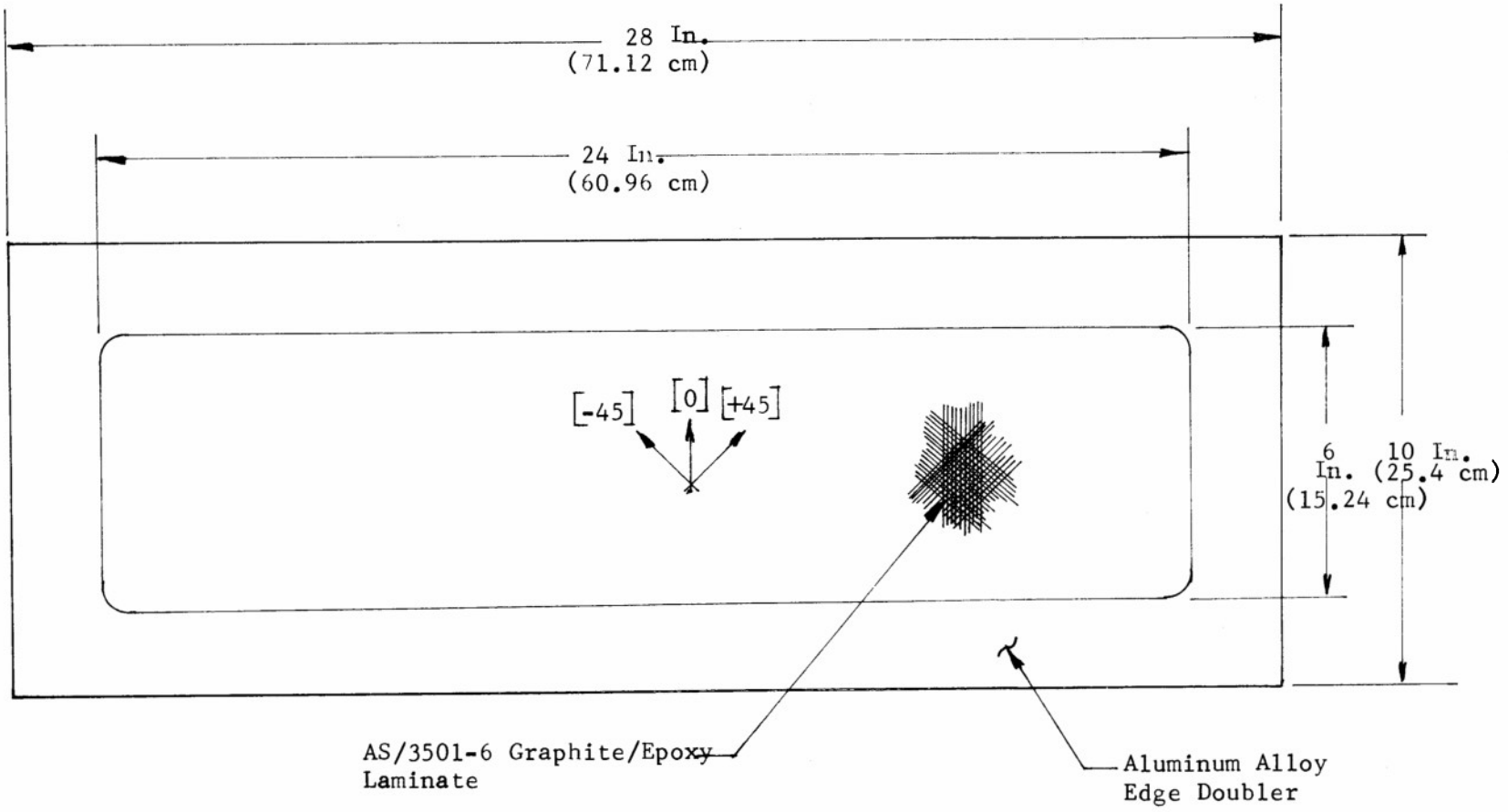

Specimen No.	Laminate	Stacking Sequence	Nominal Thickness, in.
101	$[\pm 45_2]_T$	$[+45, -45 \not\mathbb{C}]$	.021 inch (.053 cm)
102	$[0_4/\pm 45_4]_T$	$[+45, -45, 0, 0, -45, +45 \not\mathbb{C}]$	.062 inch (.157 cm)
103	$[0_{12}/\pm 45_8]_T$	$[+45, -45, 0, 0, -45, +45, 0, 0, +45, -45, 0, 0, -45, +45 \not\mathbb{C}]$	.145 inch (.368 cm)
104	$[0_2/\pm 45_2]_T$	$[+45, -45, 0 \not\mathbb{C}]$	.031 inch (.078 cm)

FIGURE I GRAPHITE/EPOXY PANELS FOR PRESSURE TEST

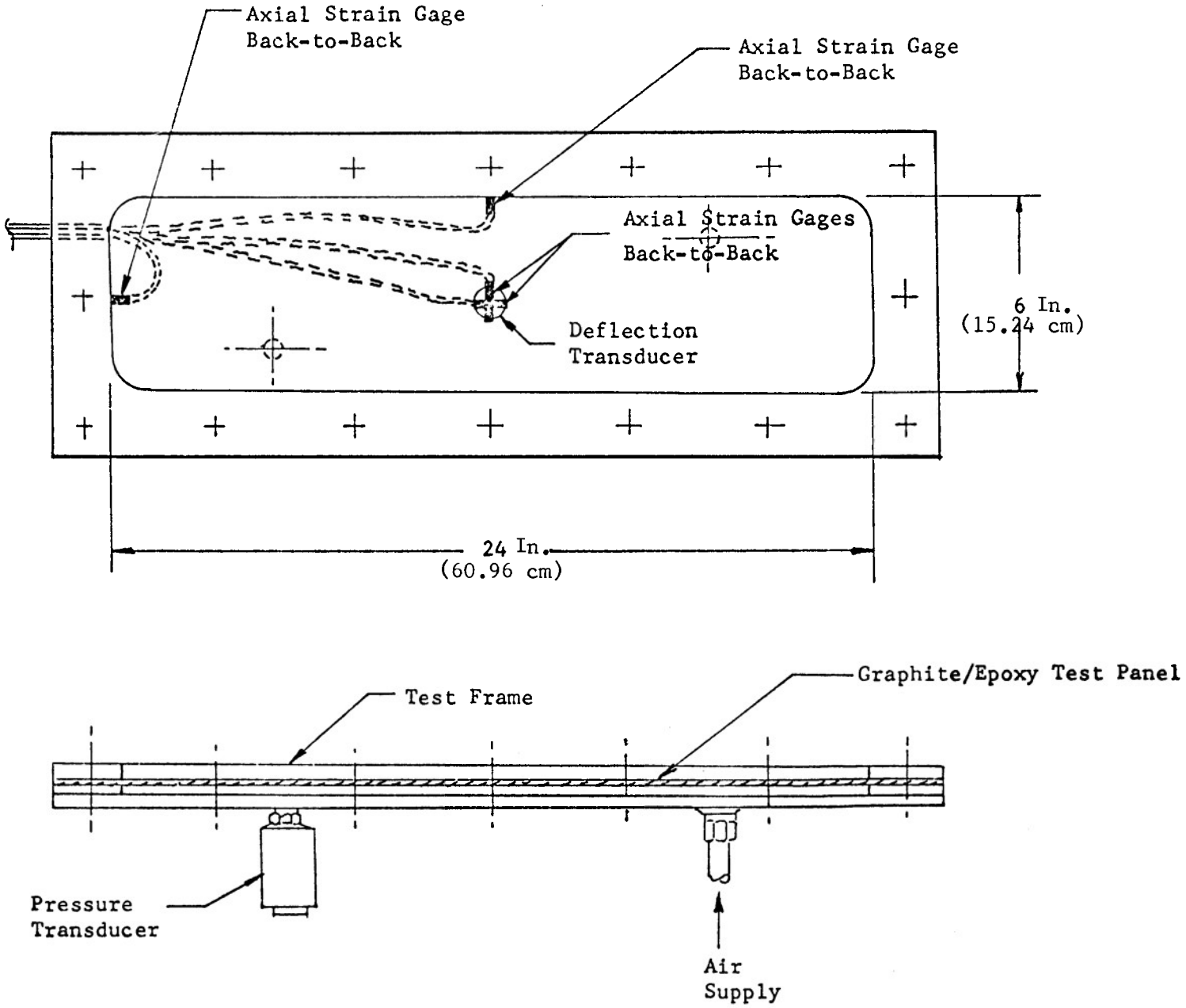

FIGURE II GRAPHITE/EPOXY PRESSURE PANEL TEST SETUP AND INSTRUMENTATION

TABLE I. TEST-THEORY COMPARISON FOR PANEL -102, $[0_4/\pm45_4]_T$, AT 20 psi (0.138 MPa) UNIFORM PRESSURE

Edge Condition	End Moment	Bending Moment @ Center	Center Deflection	Membrane Tensile Force	In-Plane Displacement, Δ	Edge Elasticity Factor, γ
Simply Supported	0	6.37 in.-lbs. (0.719 N-m)	0.119 inch (.302 cm)	704.5 lbs. (3133 N)	0	0
Membrane	0	0	0.120 inch (.304 cm)	745 lbs. (3313 N)	0	0
Fixed	-31.37 in.-lbs. (-3.54 N-m)	8.17 in.-lbs. (0.923 N-m)	0.102 inch (.259 cm)	496.7 lbs. (2209 N)	0	0
In-Plane Displacement Only	-41.57 in.-lbs. (-4.696 N-m)	14.89 in.-lbs. (1.682 N-m)	0.167 inch (.424 cm)	200.8 lbs. (893.1 N)	.010 inch* (.0254 cm)	0
In-Plane Displacement Plus Edge Elasticity	-26.3 in.-lbs. (-2.971 N-m)	12.82 in.-lbs. (1.448 N-m)	0.177 inch (.449 cm)	287.4 lbs. (1278 N)	.010 inch* (.0254 cm)	0.7*
	-36.17 in.-lbs. (-4.086 N-m)	14.39 in.-lbs. (1.626 N-m)	0.174 inch (.442 cm)	228 lbs. (1014 N)	.010 inch* (.0254 cm)	0.9*
Test Data	-29.5 in.-lbs.▲ (-3.33 N-m)	15.47 in.-lbs. (1.747 N-m)	0.185 inch (.470 cm)	161 lbs.(Max) (716 N)	Unknown	Unknown

* Assumed values; ▲ 0.18 inch (.457 cm) from edge

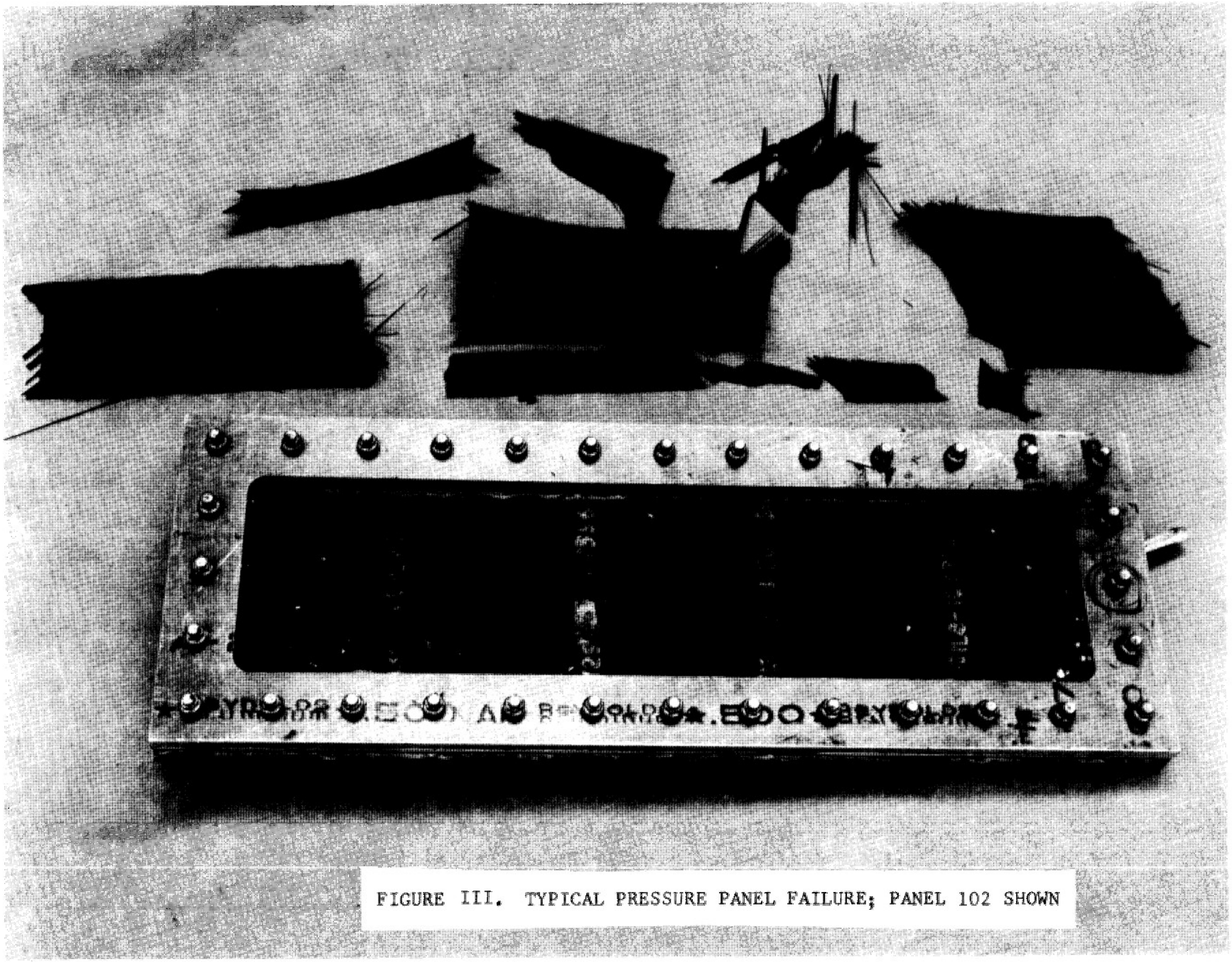

FIGURE III. TYPICAL PRESSURE PANEL FAILURE; PANEL 102 SHOWN

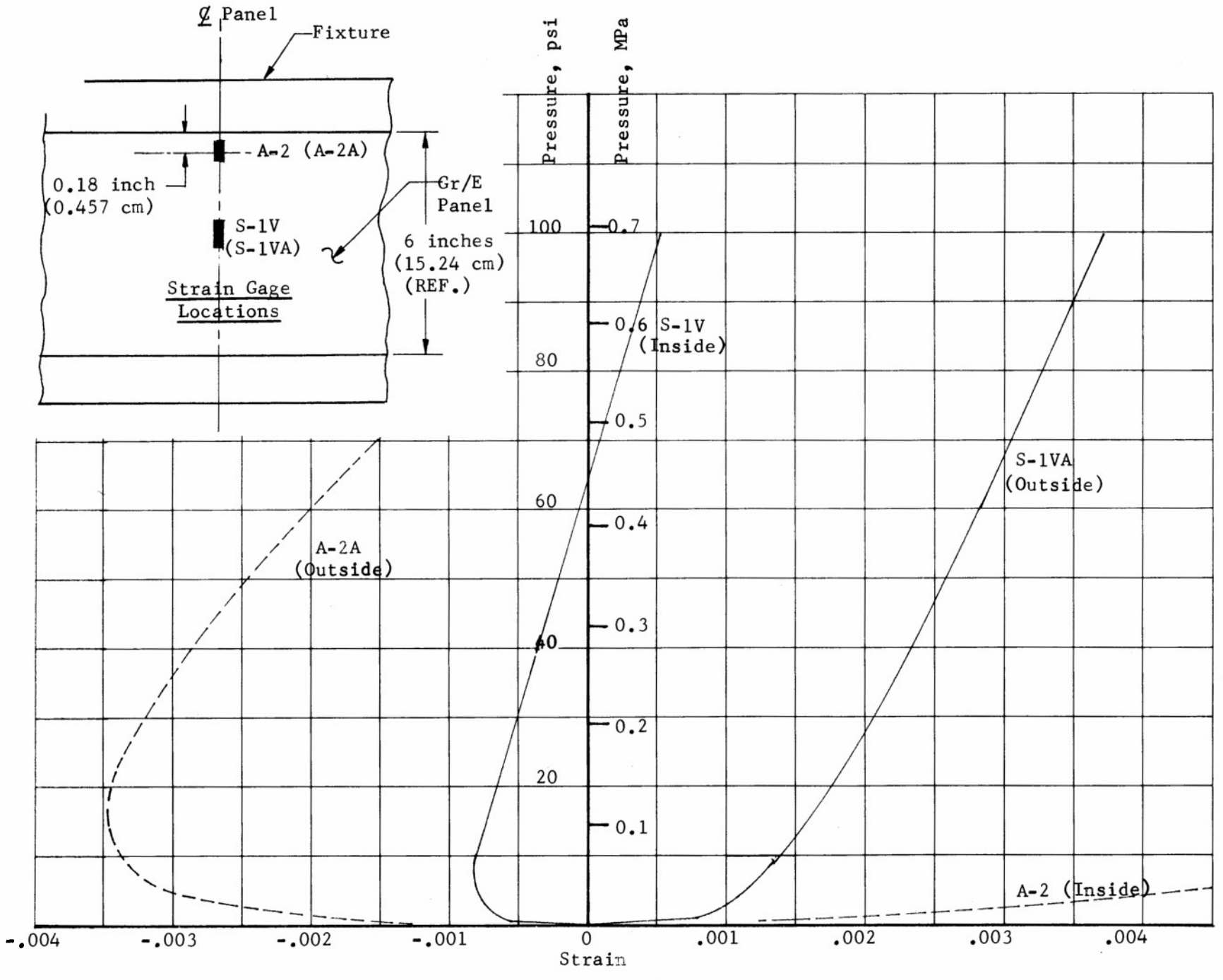

FIGURE IV STRAIN GAGE DATA, PANEL 104

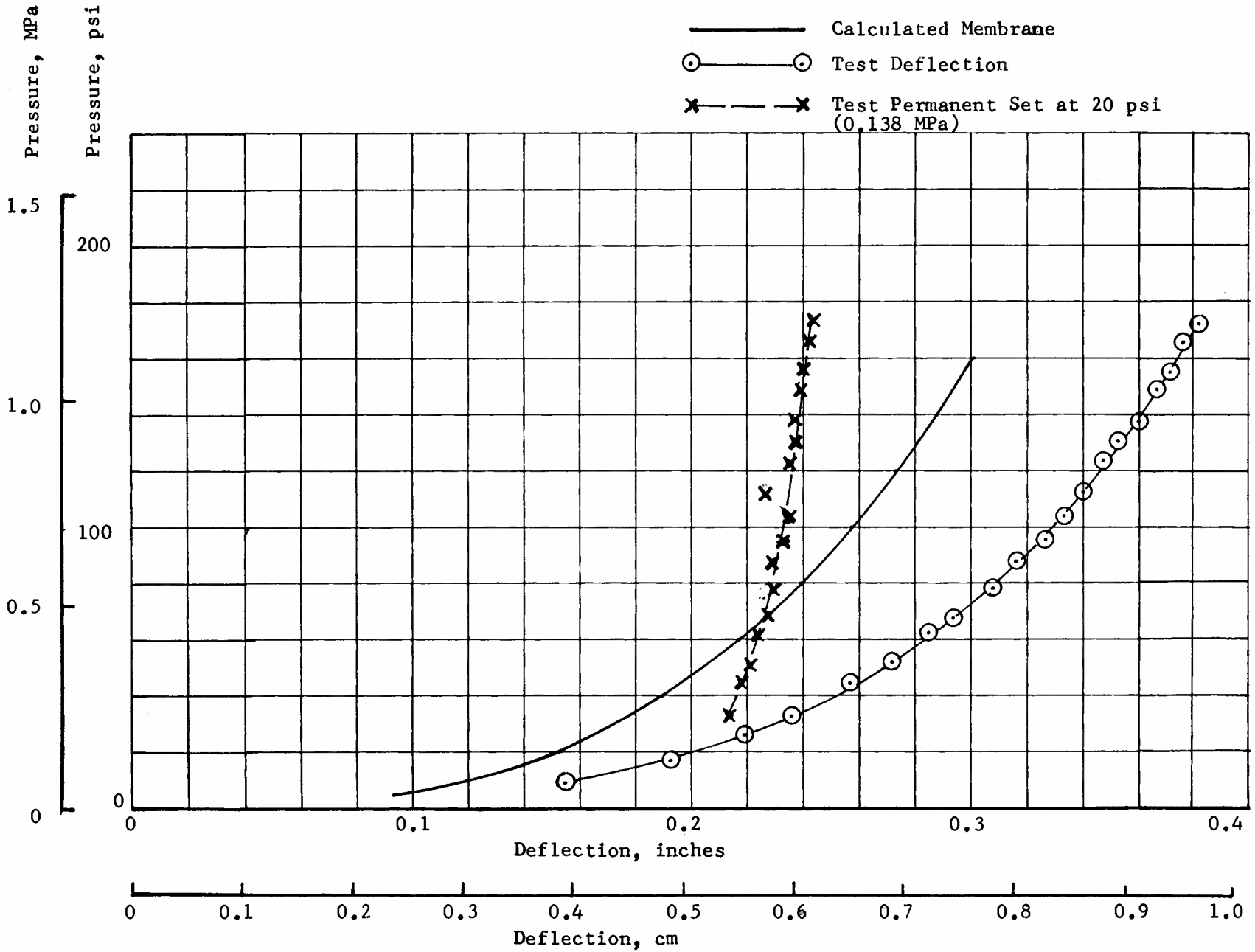

FIGURE V TYPICAL MEMBRANE DEFLECTION AND PERMANENT SET CURVES, PANEL 104

TABLE II FAILING LOAD SUMMARY

Panel No.	Laminate (Ref.)	Pressure at Failure	Estimated Pressure ■ @ Failure	Type of Failure	Remarks
-101	$[\pm 45_2]_T$	112 psi (0.772 MPa)	100 psi ▲ (0.689 MPa)	Inelastic Membrane Tension @ Edges	Buckled prior to testing †
-102	$[0_4/\pm 45_4]_T$	275 psi (1.896 MPa)	265 psi ◆ (1.827 MPa)	Elastic Membrane Tension @ Edges	No known eccentricities
-103	$[0_{12}/\pm 45_8]_T$	No Failure	Not Predicted	None	Test to be performed
-104	$[0_2/\pm 45_2]_T$	182 psi (1.255 MPa)	160 psi (1.103 MPa)	Elastic Membrane Tension @ Edges	.065 inch (0.165 cm) initial deflection prior to failure test

† Buckle assumed equivalent to initial deflection of 0.350 inch (0.889 cm)

▲ Approximate inelastic analysis using secant modulus

■ Failures based on critical element strain using Advanced Composite Design Guide values for [0] or [45] plies.

◆ Modulus of elasticity from NAAD tensile coupon data.

INVESTIGATIONS OF THE EFFECTS OF MOISTURE AND TEMPERATURE IN COMPOSITE MATERIALS ACCOUNTING FOR TIME-DEPENDENT MATERIALS BEHAVIOR

B. Harper
Graduate Student

R. Lott
Graduate Student

Y. Weitsman
Professor
Civil Engineering Department
Texas A&M University
College Station, Texas 77843

EXTENDED ABSTRACT

This work concerns analytical and experimental investigations to predict the effects of temperature and moisture on the mechanical response of graphite-epoxy laminates, accounting for the temperature and moisture enhanced creep which occurs in directions transverse to the fibers and in shear.

The analysis is based upon creep data [1,2] for AS-3502 and 5208-T300 graphite-epoxy laminas which was approximated by a linear, rheologically simple, viscoelastic constitutive law. The viscoelastic expression for the transverse compliance S_T is given in "power law" forms

$$S_T = D_o + D_1 t^q \quad \text{or} \quad S_T = D_0(\tau_0 + t)^q$$

and the effects of moisture and temperature on the compliance are given by means of a single, horizontal, shift factor function

$$a_{TM} = a_M(m)a_T(T) \quad \text{where } a_T = \exp(-T/A + B) \text{ and } a_M = a_1 m^{b_1}$$

In the above expressions D_0, D_1, τ_0, q, A, B, a_1, and b_1 are material constants, t is time, T is temperature and m is moisture content in % weight gain.

We consider the in-plane extensions and anti-clastic bending of a $(0^o)_n/(90^o)_n$ non-symmetric, square laminates undergoing various, prescribed, time-temperature cooling paths from cure down to room-temperature. In addition some of those plates are then exposed to moisture at 98% at 140^oF.

In the absence of external loads we require that all net moments and forces vanish at all times. This requirement provides the necessary equations to determine the strains and curvatures of the non-symmetric plates. The viscoelastic solution is obtained from the elastic results

by means of the approximate "quasi-elastic" analogy[3]. This analogy combines the correspondence principle with an approximate Laplace inversion technique and was shown to provide very good accuracy[4]. Actual computations are performed with the aid of a digital computer, upon discretizing both the time domain t and the coordinate z across the thickness of the plate.

In order to test the validity of the analytical predictions twenty plate specimens, each 6" square and made of $0^{o}_{12}/90^{o}_{12}$ AS-3502 graphite/epoxy pre-preg material, were manufactured and cured according to manufacturer's specification. These specimens were divided into five groups and each group was cooled-down along its own time-temperature path. Cooling times varied between 10 minutes (path "A") and 24 hours (path "E"). Upon cool-down the plates were placed in a specially designed rig and their deflections measured at 17 separate locations thus providing information about the anti-clastic curvatures in all plates. These curvatures provide the necessary experimental basis for comparison.

Similarly, deflection measurements are taken at discrete time intervals of four plates that are exposed to a constant state of 98% R.H. at 140^{o}F thus obtaining a time-curvature relationship. In the latter case all plates come from a single cool-down group.

At the present time we obtained a comparison between "Measured and Adjusted" curvatures and "Theoretically Predicted Curvatures" for the various cool-down paths. Those cool-down paths, marked "A" to "E", are ranked according to length of time, "A" being the shortest and "E" the longest.

Table 1: Comparison Between "Measured and Adjusted" Curvatures and Theoretically Predicted Values.

Cooldown Path	Measured and Adjusted hK_x (in/in)	Theoretical hK_x (in/in)	
		Viscoelastic	Elastic
A	.00167 ± .00004	.00169	.00186
B	.00162 ± .00013	.00163	.00186
C	.00160 ± .00002	.00162	.00186
D	.00167 ± .00011	.00160	.00186
E	.00156 ± .00004	.00159	.00186

Note the good correlation between experimental values and viscoelastic predictions with an average discrepancy of about 0.1% and maximal descrepancy of 4%. This agreement is far better than with the elastic predictions where the discrepancy is about 15%. Nevertheless the viscoelastic predictions deviate from the elastic results by only 15% and consequently may be of limited technical significance except in those cases where a highly accurate predictive capability is required, as may be the case in high-precision structures.

Although no results are yet available for the effects of moisture we expect in this case a significant difference between elastic and viscoelastic predictions. Our expectation is based upon a previous analysis of a symmetric cross-ply laminate[5] where discrepancies of several hundreds percent occurred between elastic calculations and viscoelastic predictions.

ACKNOWLEDGMENT

This research was sponsored by the Air Force Office of Scientific Research under Contract Number F49620-78-C-0034 with Texas A&M University.

REFERENCES

1. "Time Dependent Environmental Behavior of Graphite/Epoxy Composites," Quarterly Progress Reports Nos. 1-9, General Dynamics, Fort Worth Division.

2. W. J. Renton and T. Ho, "The Effect of Environment on the Mechanical Behavior of AS/3501-6 Graphite-Epoxy Material," Vought Corp., Dallas, Texas. Report No. B-92100/80R-105, pp. 57-63.

3. R. A. Schapery, "Viscoelastic Behavior and Analysis of Composite Materials," Vol. 2, Mechanics of Composite Materials, G. P. Sendeckj, ed., Academic Press (1974).

4. Y. Weitsman, "Interfacial Stresses in Viscoelastic Adhesive-Layers Due to Moisture Sorption," Int. J. Solids Structures, Vol. 15, pp. 701-713 (1978).

5. D. A. Douglass, Y. Weitsman, "Stresses Due to Environmental Conditioning of Cross-Ply Graphite/Epoxy Laminates," 3rd International Conference on Composite Materials, August 1980 (forthcoming).

AUTHOR INDEX